

UCSF

UC San Francisco Electronic Theses and Dissertations

Title

“Shining a light” on ciliary signaling: Vertebrate cells differentially interpret ciliary and extraciliary cAMP

Permalink

<https://escholarship.org/uc/item/4fs2t31f>

Author

Truong, Melissa Elizabeth

Publication Date

2021

Peer reviewed|Thesis/dissertation

“Shining a light” on ciliary signaling: Vertebrate cells differentially interpret ciliary and extraciliary cAMP

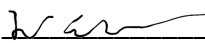
by
Melissa Elizabeth Truong

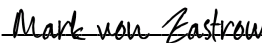
DISSERTATION
Submitted in partial satisfaction of the requirements for degree of
DOCTOR OF PHILOSOPHY


in
Developmental and Stem Cell Biology

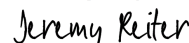
in the
GRADUATE DIVISION
of the
UNIVERSITY OF CALIFORNIA, SAN FRANCISCO

Approved:

DocuSigned by:

68DD18512B3C4D9... Wallace Marshall
Chair

DocuSigned by:

DocuSigned by: 7043C... Mark von Zastrow


DocuSigned by: 0416... Orion Weiner

DocuSigned by:

F07C889D1B164B3... Jeremy Reiter

Committee Members

DEDICATION AND ACKNOWLEDGEMENTS

The saying “It takes a village” is absolutely spot-on when I think about my journey to the PhD. This work would not have been possible without the support of many individuals.

First, I would like to thank the incredible people that make up the Reiter lab. Jeremy, I could not have asked for a better PI. If you weren’t kicking me out, I would stick around for another PhD if I could. Your boundless enthusiasm for science and your uncanny ability to ask exactly the right question is inspiring. Thank you for listening to me vent about failed experiments or technical challenges. Thank you for knowing when I’m missing the forest for the trees and helping me refocus on the big picture. Perhaps most importantly, thank you for cloning most of my constructs. I will miss your whiteboard drawings during lab meetings, our weekly meetings over Spruce cappuccinos, and your encyclopedic knowledge of all things ciliary biology. Most of all, I will miss your guidance and scientific mentorship. My time in your lab has fundamentally changed the way I approach new scientific questions, ideas, and challenges. Thank you.

Nobody enjoys every second of their PhD, but this was close. I’ve had a blast doing exciting and impactful science with the Reiter lab. My lab mates challenge and inspire me to become a better scientist. They also let me pester them with naïve questions and are some of my biggest cheerleaders. There are a couple of lab members that I would like to thank in particular. Elle, thank you for being my molecular biology guru and taking me under your wing when I first joined the lab. Dhivya, thank you for answering my unending western blot questions and sitting down to troubleshoot with me when I inevitably storm over with my botched transfer. Lauren, thank you for being there since the first day of graduate school. We’ve gone through classes and quals together and have more recently been attempting to navigate the crazy world of Hedgehog signaling together. Thank you for the western blot commiserations, the endless coffee runs, and for introducing me to Ethiopian food day at the hospital cafeteria. Lastly, Semil, you had the unfortunate luck of sitting across from me during my time in the Reiter lab. I don’t know anyone who I pestered more than you. Thank you for teaching me everything I know about zebrafish, for

nerding out about cool seminars with me, and for answering my endless questions about all things data analysis, cloning, and imaging. You pushed me to think deeply about science, and perhaps most importantly, you taught me to sequence the hell out of every plasmid.

I've been lucky to have fantastic mentors outside of the Reiter lab. Leanne Jones was my first PI. After hearing her give the keynote talk at a high school science outreach event at the Salk Institute, my mind was blown. That was the first time I had ever heard what a stem cell was and was the first time I had ever met a scientist. Leanne was the person who set me on the path to graduate school and basic science. To Leanne, thank you for empowering me, even as a 19-year-old freshman in college, to think critically and take ownership of my own project. Your ongoing mentorship even after I've left your lab, has been invaluable.

My time at UCSF has given me the opportunity to pursue my PhD in a truly supportive environment surrounded by some of the smartest people I've ever met. My support network is vast and spans both campuses. The UCSF Cilia community has been incredibly generous with both reagents and ideas. My thesis committee of Wallace Marshall, Mark von Zastrow, and Orion Weiner have challenged me to think about biology in new and unexpected ways. Wallace pushed me to think about my project with a 30,000-foot view. Mark was my GPCR guru and continual source of reagents. Work from his lab tremendously inspired our study. Orion always provided a fresh perspective during my committee meetings, encouraging me to think about signaling not as a geneticist, but with an engineer's eye.

Outside of my thesis committee, Roshanak Irannejad's lab was my second lab "home". Quinn is the ELISA expert and continually bails me out when I run out of drug aliquots. Ting-Yu has fielded all my questions about blotting for phosphorylated proteins with unending patience. To Roshanak, thank you for your cheerleading and encouragement. I have deeply appreciated being able to bounce ideas about GPCR signaling and PKA localization off you. I will miss our hallway chats and unintentional outfit matching and am so excited to see what you and your lab accomplish in the future.

The Developmental and Stem Cell Biology community at UCSF is such a special group to be a part of. I thoroughly enjoyed my interactions with faculty and other community members at yearly retreats and happy hours. Thank you to Demian Sainz for shepherding me through the grad school and for being the absolute linchpin of the DSCB program. For me, the best part of the DSCB community was the students. My cohort of Lauren, Steven, Jacob, Nate, Arpana, and Sung were some of my first friends in San Francisco. From late nights in the RMB boardroom working on Cell Bio problem sets, to our first Thanksgiving at my old apartment, to collectively scratching our heads at the immunology jargon at the BMS retreat, my cohort helped make San Francisco feel like home. Beyond my cohort, the DSCB community is tight-knit, supportive, and incredibly fun to be around. I will miss grabbing oysters at Tomales Bay before retreats and catching up with everyone during recruitment events. Lazing around with a beer at Cathedral Lakes, trekking out to the Meadow to stare at the stars, and cursing Jake out for his “easy” hikes during our yearly camping trips to Yosemite are some of my fondest memories of grad school.

I would also like to thank those that kept me going outside of lab and UCSF. Grad school is a marathon, not a sprint. The people who helped remind me that there is life outside of the bench kept me sane and picked me up when science just was not working. Finishing up grad school in the middle of a pandemic was isolating and stressful. Zoom hangouts with Amy and Charlie provided much-needed human interaction and made me laugh until my sides hurt. I cannot wait to finally hang out in 3D again. Semil and Pervin are nearly family at this point. Thank you for feeding me delicious Singaporean delicacies, being the entirety of our “Pandemic Bubble”, and most importantly, for letting me use Kaya as my grad school doggie therapist.

Finally, I would like to thank my family. To my partner Saurabh, thank you for being my anchor throughout this journey. Thank you for being my personal tech support to troubleshoot my Arduino and MATLAB code, for knowing when I need a hug and glass of wine when science isn't working, and for being my biggest cheerleader. Lastly, thank you to my parents and brother. My parents came to the U.S. as refugees following the Vietnam War. They taught themselves English,

worked minimum wage jobs to pay for college, and sacrificed much to give me and my brother a comfortable life growing up. Through family vacations to National Parks and trips to the Zoo, they inspired and encouraged my love of biology. You guys have been rooting for me since the very beginning. This work is dedicated to you.

CONTRIBUTIONS

This dissertation is adapted from work originally published in *Cell* entitled “Vertebrate cells differentially interpret ciliary and extraciliary cAMP”. The co-author listed in this publication directed and supervised the research that forms the basis for this dissertation.

“Shining a light” on ciliary signaling:

Vertebrate cells differentially interpret ciliary and extraciliary cAMP

Melissa Elizabeth Truong

ABSTRACT

Hedgehog pathway components and select GPCRs localize to the primary cilium, an organelle specialized for signal transduction. How cells distinguish cAMP produced by different GPCRs is poorly understood. To test whether ciliary and extraciliary cAMP convey different information, we engineered optogenetic and chemogenetic tools to control the subcellular site of cAMP generation. Generating equal amounts of ciliary and cytoplasmic cAMP in zebrafish and mammalian cells revealed that ciliary cAMP, but not cytoplasmic cAMP, inhibited Hedgehog signaling. Modeling suggested that the distinct geometries of the cilium and cell body differentially activate local effectors. The search for effectors identified a ciliary pool of Protein Kinase A (PKA). Blocking the function of ciliary PKA, but not extraciliary PKA, activated Hedgehog signal transduction and reversed the effects of ciliary cAMP. Therefore, cells distinguish ciliary and extraciliary cAMP using functionally and spatially distinct pools of PKA, and different subcellular pools of cAMP convey different information.

TABLE OF CONTENTS

INTRODUCTION	1
Subcellular localization of GPCRs	2
Primary cilia as a cellular antenna	3
Hedgehog and primary cilia	4
cAMP components and cilia.....	5
PKA and Hedgehog signaling	6
cAMP in cilia	8
Hedgehog-dependent cell fates during development	10
Zebrafish slow muscle	11
Optogenetics to manipulate development	12
Spatial and temporal control of cAMP	14
Contribution to the field.....	15
Vertebrate cells differentially interpret ciliary and extraciliary cAMP	17
INTRODUCTION	17
RESULTS	19
Ciliary cAMP specifically modulates HH signal transduction	21
Ciliary GPCRs regulate HH pathway output	33
Ciliary PKA regulates HH signal transduction.....	38
Ciliary PKA interprets ciliary cAMP	48
DISCUSSION	50
Limitations of the Study.....	54
MATERIALS AND METHODS.....	55
ACKNOWLEDGEMENTS.....	73
AUTHOR CONTRIBUTIONS.....	74
FUTURE DIRECTIONS AND CONSIDERATIONS	75

REFERENCES 79

LIST OF FIGURES

Figure 1. An optogenetic system for inducing cAMP <i>in vivo</i> at specific subcellular locations	20
Figure 2. Light activation of Cilia-bPAC and Cyto-bPAC does not morphologically perturb development	21
Figure 3. Cilium-generated cAMP specifically inhibits HH signal transduction	22
Figure 4. Cilium-generated cAMP specifically inhibits HH signal transduction	24
Figure 5. Cilium-generated cAMP specifically inhibits HH-dependent neural tube cell fates	25
Figure 6. Cilium-generated cAMP inhibits HH signal transduction in mammalian cells.....	27
Figure 7. Ciliary targeted Pink Flamindo reports ciliary cAMP	30
Figure 8. cAMP does not affect SMO or GPR161 trafficking to or from cilia	31
Figure 9. Ciliary GPCR activity specifically modulates HH signal transduction	34
Figure 10. Ciliary targeted DREADD activates G α s in cilia	36
Figure 11. PKA acts at cilia to regulate HH signal transduction <i>in vivo</i>	39
Figure 12. Modeling of PKA at the ciliary and plasma membrane upon ciliary and plasma membrane cAMP generation	41
Figure 13. Modeling of PKA at the ciliary and plasma membrane upon supraphysiological levels of ciliary and plasma membrane cAMP generation	43
Figure 14. PKA localizes to cilia	45
Figure 15. RAB23 misexpression does not expand zebrafish somite HH signaling or HH-dependent fates	47
Figure 16. Ciliary PKA interprets ciliary cAMP to inhibit HH signal transduction	49
Figure 17. Summary figure	53

LIST OF TABLES

Table 1. Key Resource Table 55

INTRODUCTION

Cells use a surprisingly small number of signaling intermediates in order to both sense and respond to environmental perturbations. These signaling intermediates, also called “second messengers” act as chemical messengers in order to relay signals into the cell. However, a single second messenger may have multiple downstream effectors and regulate a variety of physiological processes. How signal specificity is achieved despite the use of common second messengers is poorly understood.

Subcellular compartmentalization of signaling pathways allows cells to deploy the same molecule to elicit discrete outcomes. This strategy of restricting signaling to discrete spatial domains allows cells to multiplex signaling (McCormick and Baillie, 2014). For example, compartmentalization of calcium ions within dendritic spines is distinctly regulated from the cell body and thought to mediate synaptic plasticity (Adrian et al., 2014; Yuste et al., 2000). Additionally, localized nitric oxide production ensures that activation of a protein called Ras is limited to the plasma membrane (Batista et al., 2013).

In the 1950s, Early Sutherland discovered that hormones communicate to cells through a molecule called 3',5'-Cyclic adenosine monophosphate (cAMP) (Rall and Sutherland, 1958). cAMP became the first second messenger discovered. Seminal work on this molecule is largely the basis for our understanding of compartmentalization of signal effectors. This was all despite strong initial criticism that it was impossible that a single substance could lead to distinct effects caused by different hormones. We now realize that diverse proteins called G protein-coupled receptors (GPCRs) communicate through cAMP and elicit distinct cellular outcomes. However, on the eve of the fiftieth anniversary of Sutherland's Nobel Prize, how cells distinguish cAMP produced by different GPCRs remains an area of active investigation.

Subcellular localization of GPCRs

GPCRs are encoded by approximately 800 different genes in humans (Pierce et al., 2002). Over 30% of drugs approved by the U.S. Food and Drug Administration act on GPCRs. Drugs that target GPCRs also account for 27% of the global market share of therapeutic drugs (Hauser et al., 2017). Therefore, understanding how cells interpret and organize signals from different GPCRs is vitally important. In particular, we know very little about how GPCRs translate extracellular signals into a well-orchestrated biological response in the vast complexity of a developing organism.

GPCRs initiate canonical signaling via activation of heterotrimeric G proteins, such as $G_{\alpha s}$ and $G_{\alpha i}$. Activating $G_{\alpha s}$ stimulates adenylyl cyclases to produce cAMP whereas activating $G_{\alpha i}$ inhibits cAMP production (Pierce et al., 2002). cAMP binds and activates downstream effectors, such as Protein Kinase A (PKA), which phosphorylates downstream targets (Taylor et al., 2012, 2013). Early work on GPCRs was crucial to describing the biochemical mechanisms of GPCR signaling (Beavo and Brunton, 2002). However, active GPCR signaling was previously assumed to be confined to the plasma membrane. Thus, there was limited interest in the subcellular localization of ligand-dependent GPCR signaling.

However, a model where GPCR activity was uniformly activated across the plasma membrane to generate cAMP and uniformly activate downstream effectors was perplexing. This hypothesis would seem to indicate that a GPCR signaling event should activate all cAMP responses within the cell at once. In 1975, Ted Rall, the co-discoverer of cAMP, noted that this hypothesis presented an "...unsatisfying picture of the catalytic subunit of protein kinase swimming about, happily phosphorylating a variety of cellular constituents whether they need it or not" (Beavo and Brunton, 2002). This initial hypothesis was unable to explain data observed in living cells. For example, epinephrine and prostaglandin E1 induce similar increases in cAMP and PKA activity in cardiomyocytes, but only epinephrine induces Troponin I phosphorylation and

increases contractility (Brunton et al., 1979; Keely, 1979). This and similar studies led to the hypothesis that cAMP signaling proteins may not be randomly distributed on biological membranes.

With innovations in imaging techniques and the development of reporters for receptor signaling in cells, additional sites of GPCR localization and ligand-induced activation have been recognized (Calebiro and Maiellaro, 2014; Patel and Gold, 2015). Recent studies have demonstrated that various GPCRs can initiate signaling from more than one subcellular location, including the endosomes and Golgi membrane (Calebiro and Koszegi, 2019; Irannejad et al., 2013, 2017; Mullershausen et al., 2009). These findings revealed that GPCRs are spatially and temporally regulated to enable signaling fidelity, despite the use of a common and otherwise freely diffusible, second messenger.

Primary cilia as a cellular antenna

A subset of GPCRs localize not to the plasma membrane, but to the membrane of the primary cilium. The primary cilium is found on most vertebrate cells and functions as a sensory organelle. Unlike motile cilia, such as those found on cells in the airway and the oviduct that beat in order to move fluid, primary cilia are immotile and act as a cellular antenna (Ishikawa and Marshall, 2011). Ciliary machinery is evolutionarily highly conserved, even between humans and a ciliated unicellular green algae called *Chlamydomonas reinhardtii* (Avidor-Reiss et al., 2004; Pazour et al., 2000). However, most vertebrate cells have solitary, non-motile cilia. After years of disregard as a vestigial structure, cilia are now appreciated in having fundamental roles in cellular communication (Goetz and Anderson, 2010). Disruption of ciliary cause a wide range of developmental and physiological phenotypes that are collectively known as ciliopathies (Reiter and Leroux, 2017).

The primary cilium shares a membrane that is contiguous with the plasma membrane and is open to the cytosol. Despite this, a distinct set of proteins are enriched within the cilium. This

subcellular compartmentalization is achieved through a distinct lipid and protein composition within the cilium (Garcia et al., 2018). All of this is maintained by a proteinaceous structure at the ciliary base called the transition zone, which regulates cargo in and out of the cilium (Garcia-Gonzalo and Reiter, 2017; Gonçalves and Pelletier, 2017). In addition, the volume of the primary cilium has been estimated to be between 1/4,000 to 1/10,000 the volume of the cell body (Gigante and Caspary, 2020). This privileged microenvironment and exceedingly small volume within cilia allows signaling proteins and their downstream effectors to come together in close spatial proximity (Nachury, 2014).

A subset of these signaling proteins are GPCRs. Over 30 different GPCRs have been shown to localize to cilia, including SSTR3, MC4R, and FFAR4 (Hilgendorf et al., 2016, 2019; Schou et al., 2015; Siljee et al., 2018). This list will undoubtedly grow, as future and ongoing proteomics studies will likely uncover additional ciliary GPCRs (Mick et al., 2015; Sigg et al., 2017).

Hedgehog and primary cilia

Notably, the $G\alpha_s$ -coupled GPCR GPR161 and the GPCR-related protein Smoothed (SMO) also localize to cilia (Corbit et al., 2005; Mukhopadhyay et al., 2013). These two proteins play central roles in the vertebrate Hedgehog (HH) pathway. The HH pathway is a key developmental pathway that is crucial for development of nearly every organ in mammals (Briscoe and Théron, 2013). HH signaling plays roles in homeostasis and regeneration and is disrupted in several types of cancer. Seminal work in *Drosophila* identified core pathway components, including HH ligand, the HH receptor Patched (PTCH), SMO, and the key transcription factor Cubitus interruptus (Ingham, 1998; Nusslein-Volhard and Wieschaus, 1980).

As core HH pathway components are conserved between vertebrates and *Drosophila*, it was a complete surprise when a forward mouse genetics screen identified HH pathway defects in mutants for ciliary machinery proteins (Huangfu and Anderson, 2005; Huangfu et al., 2003).

Intense study over the past two decades has revealed that the primary cilium is crucial for vertebrate HH signaling. Indeed, nearly all events in HH signaling have been linked to ciliary mechanisms. HH signal transduction in vertebrates is driven by a highly choreographed set of protein trafficking events in and out of cilia (Bangs and Anderson, 2017). GPCRs play key roles in HH signal transduction.

Upon HH ligand addition, the GPCR-related protein and key HH pathway effector SMO accumulates within cilia within minutes (Corbit et al., 2005). Simultaneously, the HH receptor PTCH and the GPCR GPR161 are trafficked out from the cilium (Mukhopadhyay et al., 2013; Pal et al., 2016; Rohatgi et al., 2007). This coordinated trafficking event results in the activation of the GLI family of transcription factors (Cubitus interruptus in *Drosophila*). GPR161 is a negative regulator of the HH pathway (Mukhopadhyay et al., 2013). Apart from GPR161, both cAMP and PKA negatively regulate HH signal transduction (Hammerschmidt et al., 1996; Jiang and Struhl, 1995; Kong et al., 2019; Li et al., 1995; Wang et al., 1999).

cAMP components and cilia

A subset of proteins that stimulate, sense, and degrade cAMP localize to cilia (Mukhopadhyay and Rohatgi, 2014). Mutations in these proteins profoundly disrupt HH signaling.

GPR161 is a $G_{\alpha s}$ -coupled GPCR that, at least in cultured cells, is thought to constitutively couple to $G_{\alpha s}$ to stimulate cAMP production. Loss of GPR161 results in an expansion of HH-dependent cell fates within the developing neural tube (Mukhopadhyay et al., 2013). Loss of a protein called Tulp3, which promotes trafficking of GPR161 to cilia, also causes aberrant HH activation (Norman et al., 2009). As the role and expression of GPR161 in HH signaling seems to be tissue-specific, other ciliary GPCRs likely impinge on HH signaling as well (Pusapati et al., 2018; Singh et al., 2015).

The G-protein $G_{\alpha s}$, as well as various adenylyl cyclases (AC3, AC5/6) that generate are also enriched in cilia (Bishop et al., 2007; He et al., 2014; Vuolo et al., 2015). Loss of $G_{\alpha s}$ and

knockdown of ADCY3, 5, and 6 activate HH signaling in bone formation in mice and neuronal precursors in chick, respectively (Regard et al., 2013; Vuolo et al., 2015). Pharmacological activation of adenylyl cyclases via the drug forskolin potently inhibits HH signaling *in vivo* (Barresi et al., 2000). Additionally, mutations in $G\alpha s$ underlie some forms of HH-driven medulloblastoma and basal cell carcinoma (He et al., 2014; Iglesias-Bartolome et al., 2015). A protein called ANKMY2 has recently been reported to be important in maturation and trafficking adenylyl cyclases to cilia. Cells mutant for ANKMY2 have defective ciliary adenylyl cyclase localization. In mouse embryos, ANKMY2 is one of the strongest identified negative regulators of HH signaling and displays phenotypes similar to loss of PTCH1 (Bandarigoda Nipunika Somatilaka et al., 2020).

A family of proteins called phosphodiesterases (PDEs) degrade cAMP (Baillie, 2009; Conti et al., 2014; Maurice et al., 2014). Broad spectrum inhibition of phosphodiesterases prevents HH pathway activation (Wang et al., 2000). In particular, PDE4D inhibits the HH pathway and can suppress HH-dependent medulloblastoma growth (Ge et al., 2015; Williams et al., 2015). Recent proteomics studies suggest select isoforms of PDEs localize to cilia (Mick et al., 2015; Sigg et al., 2017). PDE4C localizes to cilia in renal epithelial cells, but further characterization of PDE localization is necessary (Choi et al., 2011).

The actions of cAMP are mediated by three different effector proteins: Protein Kinase A, cyclic nucleotide-gated channels, and EPACs (Edwards et al., 2011). Of these proteins, PKA plays a central role in HH signal transduction.

PKA and Hedgehog signaling

In its inactive state, PKA exists as an auto-inhibited tetramer consisting of two regulatory and two catalytic subunits. Binding of four cAMP molecules to the regulatory subunits triggers the release of active catalytic subunits and downstream phosphorylation of downstream targets (Taylor et al., 2013). PKA is an evolutionarily conserved negative regulator of the HH pathway

(Hammerschmidt et al., 1996; Jiang and Struhl, 1995; Li et al., 1995; Wang et al., 1999). Loss of PKA activity leads to mid-gestation lethality and an expansion of HH-dependent cell types in the mouse neural tube (Tuson et al., 2011).

The GLI proteins are transcriptional effectors of the HH pathway. In the absence of HH ligand, proteolytically processed forms of the GLI transcription factors repress HH target genes (Chen et al., 1998; Wang et al., 1999). This proteolytic processing into GLI2 and GLI3 repressor forms depends on direct phosphorylation of six conserved phosphorylation sites on GLI2 and GLI3 by PKA (Aza-Blanc et al., 1997; Price and Kalderon, 1999). PKA also seems to play an additional role in preventing the formation of GLI2 activator (Niewiadowski et al., 2014).

Loss of both PKA catalytic subunits in mice causes strong activation of the HH pathway. In these mice, cells within the neural tube that are specified by the highest levels of HH signaling are expanded at the expense of non-HH-dependent cell fates (Tuson et al., 2011). Embryos mutant for both PKA catalytic subunits and cilia show phenotypes similar to loss of PKA catalytic subunits alone. Therefore, cilia are important for the function of PKA (Bangs and Anderson, 2017; Tuson et al., 2011).

Both the catalytic and regulatory subunits of PKA are highly enriched at the base of cilia by antibody staining (Barzi et al., 2009; Tuson et al., 2011). However, recent ciliary proteomics studies have identified PKA regulatory and catalytic subunits within cilia (May et al., 2020; Mick et al., 2015). Stably expressed PKA Regulatory Subunit 1 α (PKA-R1 α) can localize to the primary cilium, raising the possibility that a small pool of PKA may reside within the cilium (Mick et al., 2015). PKA-R1 α may be targeted to the cilium via GPR161. PKA is anchored within the cell by A-Kinase Anchoring Proteins (AKAPs) (Wong and Scott, 2004). A recent study identified GPR161 as an AKAP for PKA-R1 α , functioning to recruit PKA to the cilium (Bachmann et al., 2016). A recent time-resolved proteomics study reported that PKA-R1 α exits the cilium with similar kinetics

as GPR161 upon HH stimulation. Though PKA-R1 α is able to localize to the cilium, PKA-C α had yet to be detected within cilia until this present study.

As both catalytic and regulatory subunits show high levels of antibody staining at the ciliary base, cAMP generated in or near cilia was proposed to activate pools of PKA at the ciliary base, which would subsequently phosphorylate GLI proteins trafficking in and out of the cilium (Tuson et al., 2011). However, the presence of ciliary PKA-R1 α suggested that PKA may sense cAMP levels within the cilium proper. Targeting a PKA inhibitory peptide to the cilium specifically resulted in defective GLI3 repressor formation (Mick et al., 2015). These data suggested that the sensing of cAMP by PKA may take place within cilia. However, whether ciliary PKA regulates HH transcriptional output and whether this was relevant *in vivo* remained unclear.

cAMP in cilia

Though PKA may localize to the cilium, cAMP is thought to be a freely diffusible molecule (Agarwal et al., 2016; Irannejad et al., 2017). The diffusibility of cAMP would seem to prevent the cell from distinguishing subcellular pools, particularly within an organelle that is contiguous with the plasma membrane (Marley et al., 2013). One possible explanation for how cells can differentially ciliary versus non-ciliary cAMP would be if a physical barrier at the base, such as the ciliary transition zone, also prevented the free diffusion of cAMP. However, cAMP produced by ciliary and non-ciliary GPCRs does not stay restricted within the cilium (Marley et al., 2013).

How cAMP is regulated within the cilium during HH signaling is still unclear. The leading hypothesis is that the exit of GPR161 upon HH stimulation may cause a decrease in cAMP levels, due to the lack of G α s activity within the cilium (Mukhopadhyay et al., 2013). Furthermore, SMO is a GPCR-like protein that, at least biochemically, can couple to G α i (Ogden et al., 2008; Qi et al., 2019; Riobo et al., 2006).

As $G\alpha_i$ proteins inhibit adenylyl cyclases and reduce cAMP levels, trafficking of SMO into the cilium upon HH activation may dampen ciliary cAMP levels. In *Drosophila*, $G\alpha_i$ expression causes ectopic HH signaling (Ogden et al., 2008). However, in vertebrates, it is not clear that SMO couples to $G\alpha_i$ *in vivo*. Using chemical and genetic methods to deplete $G\alpha_i$ had no effect on HH-dependent skeletal development or limb patterning in mice (Regard et al., 2013). Furthermore, electroporation of a dominant negative version of $G\alpha_i$ did not disrupt HH-dependent neural tube progenitor domains in chick embryos (Low et al., 2008). However, injection of a chemical that inhibits most $G\alpha_i$ activity in zebrafish resulted in inhibition of select HH-dependent cell fates. Thus, there is no conclusive evidence that SMO functionally couples to $G\alpha_i$ during endogenous HH signaling, though it may regulate other GPCRs within the cilium. The best candidate of this hypothesis would be GPR161, as SMO entry upon HH activation triggers GPR161 exit from cilia (Pal et al., 2016).

Whether cAMP levels or PKA activity changes within the cilium in response to HH activation has not been shown. Though production of cAMP inhibits HH activity, HH activation does not seem to change whole cell cAMP levels (Moore et al., 2016). This may be due to the exceedingly small volume of the cilium compared to the rest of the cell. Under this paradigm, local increases in ciliary cAMP are rapidly diluted into the large cytoplasmic volume. This would parallel studies on ciliary calcium. Resting calcium in cilia is locally elevated compared to resting calcium within the cytoplasm (580nM versus 107nM, respectively) (Delling et al., 2013). However, local fluctuations of calcium within the cilium do not affect distal calcium in the cytoplasm. This is presumably due to the 1:30,000 fold difference in volume between the cilium and cytoplasm (ciliary volume to cytoplasmic volume ratio estimates range between 1:5,000 and 1:30,000) (Delling et al., 2013; Nachury, 2014).

Direct visualization of cAMP in the cilium has proved to be technically challenging, and measurements of resting cAMP levels in cilia vary (Jiang et al., 2019; Marley et al., 2013; Moore

et al., 2016; Mukherjee et al., 2016). Whether cAMP in the cilium is elevated relative to cytoplasmic cAMP is also unclear (Jiang et al., 2019; Marley et al., 2013; Moore et al., 2016). Additionally, whether HH signaling affects ciliary cAMP levels is also controversial and seems to depend on the cAMP biosensor utilized (Jiang et al., 2019; Moore et al., 2016). One possibility is that instead of locally concentrating cAMP, the cilium may function to functionally isolate ciliary GPCRs away from extraciliary GPCRs (Marley et al., 2013). In the absence of signaling events, the cilium may somehow inhibit cAMP production from ciliary GPCRs (Jiang et al., 2019). Future studies are necessary to conclusively determine whether cAMP is locally elevated within the cilium and whether ciliary signaling changes local cAMP concentration.

Regardless whether cAMP is physically compartmentalized within the cilium, whether these are different functional outputs between ciliary and extraciliary cAMP and GPCR signaling is an open question. Current approaches to generate cAMP rely on pharmacological or genetic methods that activate cAMP globally. The lack of tools to specifically perturb ciliary versus extraciliary cAMP and GPCR signaling has hindered progress in this area. Future studies and further development of ciliary-targeted cAMP biosensors and tools to manipulate cAMP are needed to determine the nature of cAMP dynamics within the cilium and how signaling events impinge upon ciliary cAMP (Hansen et al., 2020).

Hedgehog-dependent cell fates during development

The output of ciliary signaling events, namely HH signaling, is crucial in coordinating diverse developmental and homeostatic processes (Briscoe and Thérond, 2013; Ingham, 2018). Defects in HH signaling can cause phenotypes such as polydactyly, skeletal malformations, and midface narrowing (Varjosalo and Taipale, 2008). Within specific tissues, graded HH signaling is responsible for the specification of various cell types. For instance, cells within the developing neural tube and within somites are dependent on HH signaling for proper cell fate specification (Briscoe et al., 2000; Chiang et al., 1996; Ericson et al., 1996; Fan and Tessier-Lavigne, 1994).

In the developing ventral neural tube, Sonic Hedgehog (SHH) ligand secreted from the notochord and floor plate patterns ventral cell fates within the developing neural tube (Marti et al., 1995; Roelink et al., 1995). Lateral floor plate cells expressing *nkx2.2b* are specified by the highest levels of HH signaling, neighboring motor neuron progenitor cells expressing *olig2* are specified by intermediate levels of HH signaling, and cells of the dorsal neural tube express *pax3* (Guner and Karlstrom, 2007; Odenthal et al., 2000). These cells are exquisitely sensitive to both the concentration and duration of SHH exposure (Dessaud et al., 2007). Assaying the relative populations of these cell types can provide a measure of the relative strength of HH signaling within this tissue (Bangs and Anderson, 2017).

Zebrafish slow muscle

In both mice and in zebrafish, SHH plays crucial roles in the patterning of somites (Fan and Tessier-Lavigne, 1994). Somites are segmental mesodermal aggregates that give rise to multiple cell types, including muscle and components of the axial skeleton (Blagden et al., 1997; Devoto et al., 1996; Morin-Kensicki and Eisen, 1997; Roy et al., 2001). In zebrafish, the first somite forms shortly after the end of gastrulation from the paraxial mesoderm (Devoto et al., 1996). Adaxial cells, which are the precursor cells to slow muscle, are specified around 10.5 hours post fertilization (hpf) (Rossi and Messina, 2014).

In the developing zebrafish, formation of different slow muscle cell types is dependent on HH signaling emanating from the notochord (Barresi et al., 2000; Blagden et al., 1997; Currie and Ingham, 1996; Du et al., 1997). The notochord and floorplate patterns adjacent adaxial cells that give rise to cells within the slow muscle. The adaxial cells that reside closest to the notochord are thought to receive the most SHH ligand and give rise to muscle pioneers (MPs) which express the transcription factors Engrailed (En) and Prox1. Superficial slow fibers (SSFs) are specified by lower levels of Shh ligand and express the transcription factor Prox1 alone (Barresi et al., 2000; Hirsinger et al., 2004; Wolff et al., 2003). Both MPs and SSFs migrate radially toward the surface

of the myotome, and by 24hpf, form clear, chevron-shaped blocks of muscle (Devoto et al., 1996; Henry and Amacher, 2004).

Several lines of evidence have established that HH signaling is required for the specification of these muscle precursors. Mutations in genes that encode positive regulators of the HH pathway, such as Smo and Shh ligand cause a dramatic reduction in slow muscle fibers (Barresi et al., 2000; Blagden et al., 1997). Mutations in negative regulators of the HH pathway, such as mutations in Ptc or expression of a dominant negative form of PKA (dnPKA) induces excess slow muscle fibers at the expense of fast muscle (Blagden et al., 1997; Du et al., 1997). In zebrafish, primary cilia play roles in transducing HH signals during slow muscle specification as well (Huang and Schier, 2009). Loss of cilia dampens HH pathway activity in the developing slow muscle. However in these embryos, the HH pathway activity domain is spatially expanded, unlike cilia mouse mutants (Huang and Schier, 2009). This may be due to difference in Gli transcription factor requirements and dependencies between mice and zebrafish (Karlstrom et al., 2003).

Within the slow muscle, strong HH loss-of-function mutants, such as mutants for Smo, display a complete loss of both MPs and SSFs (Barresi et al., 2000). Weaker HH loss-of-function mutants or treatment with moderate doses of the Smo inhibitor cyclopamine results in a preferential loss of MPs but not slow-level SSFs (Ingham and Kim, 2005; Tschakner et al., 2021). As MPs and SSFs are differentially sensitive to HH perturbations, the relative numbers of these two cell types in the 24hpf embryo can be used as a readout of the strength of HH signaling.

Optogenetics to manipulate development

Developmental biology has undergone a revolution over the last 50 years. Genetic screens in *Drosophila* and the roundworm *C. elegans* uncovered central developmental signaling pathways that are fundamental to cellular communication and tissue morphogenesis. Key processes such as cell division, fate determination, and differentiation are regulated by a

shockingly few number of key factors. Forward genetic screens, such as the Heidelberg Screen, identified key components of core developmental pathways such as Hedgehog, Wnt, and BMP (Wieschaus and Nusslein-Volhard, 2016). Following studies worked to identify a molecular parts list of these signaling pathways and uncover a molecular framework governing these signaling events.

These loss-of-function approaches can uncover phenotypes that arise in the complete absence of a particular gene. However, the development of multicellular organisms is controlled by dynamic signaling events that are under tight spatial and temporal control. Most tools available to perturb development rely on genetic or pharmacological tools to globally inhibit signaling. For instance, pharmacological activation of adenylyl cyclase with the drug forskolin inhibits slow muscle formation in zebrafish (Barresi et al., 2000). Genetic depletion of $G\alpha_s$ causes overactivation of HH signaling in mouse skeleton (Regard et al., 2013). Though these data suggest cAMP is a negative regulator of HH signaling, any spatial information of the site or timing of action of cAMP is lost. As signaling within a cell and embryo is highly dynamic and spatially regulated, tools that enable researchers to have tight spatial and temporal control of signaling are sorely needed.

Recent advances in engineering proteins that are responsive to either light or otherwise pharmacologically inert chemicals can be used to achieve temporal and spatial control of signaling (Roth, 2016; Tischer and Weiner, 2014; Toettcher et al., 2011). These optogenetic or chemogenetic approaches, respectively, allow unprecedented control of cellular network function. Though initially developed by neuroscientists to control neuronal activity, light-activated proteins have been increasingly used to interrogate spatiotemporal control of signaling during development (Krueger et al., 2019; Rogers and Müller, 2020). The use of optogenetics in cell biology will be advanced by the recent development of inexpensive LED-based optogenetic microwell plates allows for programmable light stimulation during cell culture or *in vivo* experiments (Bugaj and Lim, 2019; Repina et al., 2019).

Model organisms that are optically clear during development, such as the developing fly or zebrafish embryo, are ideal for optogenetic perturbation. For instance, optogenetic Erk activation in developing *Drosophila* embryos identified temporal requirements in Erk signaling necessary to specify neurogenic ectoderm versus gut endoderm (Johnson and Toettcher, 2019). In another study, light-activated ion channels were used to identify the location of cardiac pacemaker cells within the developing zebrafish heart (Arrenberg et al., 2010).

Spatial and temporal control of cAMP

Excitingly, optogenetic and chemogenetic tools to manipulate GPCR and cAMP signaling have been developed. bPAC is a photoactivatable adenylyl cyclase that was originally isolated from bacteria (Stierl et al., 2010). This 350-amino acid protein consists of a blue light-sensing domain linked to a Type III adenylyl cyclase (Stierl et al., 2010). bPAC-expressing cells generate cAMP in proportion to the amount of blue light delivered. DREADDs (designer receptor exclusively activated by a designer drug) are GPCRs engineered to be selectively activated by the otherwise pharmacologically inert drug clozapine-N-oxide (CNO) (Armbruster et al., 2007; Roth, 2016). Activation of a $G\alpha_s$ -DREADD causes an increase in cAMP through coupling to the G-protein $G\alpha_s$ and downstream activation of adenylyl cyclase (Guettier et al., 2009). Taken together, bPAC and DREADD systems are orthogonal methods to control cAMP generation at the level of adenylyl cyclase, or GPCR activity, respectively.

With the use of optogenetics, subcellular control of protein activity can either be achieved through selective illumination or by targeting the protein to the subcellular site of interest. In the developing embryo, long-term selective illumination is technically challenging, as tissues undergo widespread morphological changes. Thus, targeting proteins to the site of interest allows for subcellular perturbation of signaling events with spatial and temporal control. bPAC has previously been utilized to generate cAMP at either the plasma membrane, cytoplasm, or endosomal compartments (Tsvetanova and von Zastrow, 2014). This study demonstrated that

endosomal cAMP generation was transcriptionally distinct from equivalent amounts of cAMP generation in the cytoplasm or plasma membrane (Tsvetanova and von Zastrow, 2014). bPAC has previously been used to control flagellar motility in sperm, and a recent proof-of-principle study used a nanobody tethering approach to localize bPAC to primary cilia (Hansen et al., 2020; Jansen et al., 2015). However, whether cells interpret GPCR signals from the cilium distinctly during ciliary signaling has not been tested. In this study, we target both bPAC and $G\alpha_s$ -DREADD to the cilium in both zebrafish embryos and in mouse fibroblasts to determine whether ciliary cAMP is functionally distinct from extraciliary cAMP during HH signaling.

Contribution to the field

During development, cells within the embryo are exposed to many different signals. These signals can range from mechanical cues, to transient molecular inputs, to stochastic noise. To form a proper embryo, cells need to be able to both receive signals from their outside environment and processes these cues to make proper cell fate decisions. One of the ways cells receive these cues is through an organelle called the primary cilium, which acts as a cellular antenna to compartmentalize signaling proteins. Various receptors, such as GPCRs localize to primary cilia and are important for transducing vertebrate HH signaling, a key developmental pathway. However, methods to interrogate the role for GPCR signaling and subsequent cAMP production at the cilium lack spatial and temporal resolution, particularly within the complexity of a developing organism.

We hypothesized that physically sequestering signaling pathways to either the cilium or the cell body allows parallel information processing without crosstalk. This work generated optogenetic and chemogenetic tools to test whether vertebrate cells differentially interpret ciliary versus extraciliary cAMP. We found that ciliary HH signaling is preferentially sensitive to ciliary, but not extraciliary cAMP production. This was true in both the formation of HH-dependent cell fates in the developing zebrafish neural tube and slow muscle, as well as in the transcription of

the key HH target gene *Gli1* in mouse fibroblasts. Furthermore, we adapted cilium-localized red-shifted cAMP biosensors to demonstrate that cAMP generated in the cilium is not spatially restricted by the presence of a diffusion barrier.

Finally, we collaborated with Ke Xu's lab at UC Berkeley to perform computational modeling of cAMP generation at discrete compartments within the cell. This modeling suggested that in the absence of a barrier to diffusion, the distinct geometries of the cilium allow for the preferential activation of a ciliary cAMP effector protein. The search for this effector protein led us to identify a ciliary pool of PKA that is localized to the cilium via the AKAP GPR161. We adapted and utilized a dominant negative approach to selectively inhibit PKA at the cilium, the basal body, and outside of the cilium. Deploying these tools in zebrafish showed that inhibition of PKA at the cilium, but not outside of the cilium or at the basal body, activates HH signaling. Furthermore, blocking PKA at the cilium was sufficient to block the effects of ciliary cAMP production via bPAC. Thus, a pool of ciliary PKA senses ciliary cAMP to preferentially inhibit HH signaling, and ciliary cAMP is functionally distinct from extraciliary cAMP in vertebrate cells.

Vertebrate cells differentially interpret ciliary and extraciliary cAMP

Melissa E. Truong¹, Sara Bilekova^{1,4}, Semil P. Choksi¹, Wan Li², Lukasz J. Bugaj³, Ke Xu^{2,5},
Jeremy F. Reiter^{1,5,6*}

¹Department of Biochemistry and Biophysics, Cardiovascular Research Institute, University of California, San Francisco, San Francisco, CA, 94158, USA

²Department of Chemistry, University of California, Berkeley, Berkeley, CA, 94720, USA

³Department of Bioengineering, University of Pennsylvania, Philadelphia, PA, 19104, USA

⁴Ludwig-Maximilians-Universität München, Munich, 80539, Germany

⁵Chan Zuckerberg Biohub, San Francisco, San Francisco, CA, 94158, USA

⁶Lead Contact

*Correspondence: jeremy.reiter@ucsf.edu

Author ORCIDs

Melissa E. Truong: <https://orcid.org/0000-0003-1526-1521>

Sara Bilekova: <https://orcid.org/0000-0001-6699-1386>

Lukasz J. Bugaj: <https://orcid.org/0000-0002-0749-2912>

Jeremy F. Reiter: <https://orcid.org/0000-0002-6512-320X>

INTRODUCTION

Development and homeostasis require cells to discriminate between signals, many of which are received by G protein-coupled receptors (GPCRs), the largest class of vertebrate receptors and the targets of many therapeutic drugs (Hauser et al., 2017; Pierce et al., 2002). Ligand binding rearranges GPCR transmembrane domains to activate heterotrimeric G proteins such as *G α s* and *G α i*. Activating *G α s* stimulates adenylyl cyclases to produce cAMP whereas activating *G α i* inhibits cAMP production (Pierce et al., 2002).

A subset of GPCRs localize not to the plasma membrane, but to the membrane of the primary cilium, an organelle specialized for signal transduction and present on most vertebrate cells (Anvarian et al., 2019; Gigante and Caspary, 2020). The distinct lipid and protein composition of the cilium is maintained through a diffusion barrier at the ciliary base called the transition zone (Gonçalves and Pelletier, 2017). More than 30 different GPCRs localize to cilia, including SSTR3, GPR161 and MC4R, as well as the GPCR-related protein Smoothed (SMO) (Mykytyn and Askwith, 2017).

SMO is the central component of the Hedgehog (HH) signal transduction pathway and, in vertebrates, functions at primary cilia to activate GLI transcriptional effectors (Bangs and Anderson, 2017; Corbit et al., 2005; Huangfu et al., 2003). In addition to positive effectors of HH signal transduction, negative pathway regulators localize to cilia, including GPR161 (Mukhopadhyay et al., 2013). Apart from GPR161, both cAMP and PKA negatively regulate HH signal transduction (Hammerschmidt et al., 1996; Jiang and Struhl, 1995; Kong et al., 2019; Li et al., 1995; Wang et al., 1999).

HH signaling orchestrates diverse developmental and homeostatic processes, including patterning of somites (Fan and Tessier-Lavigne, 1994). Somites are segmental mesodermal aggregates that give rise to multiple cell types, including muscle (Blagden et al., 1997; Devoto et al., 1996; Morin-Kensicki and Eisen, 1997; Roy et al., 2001). In zebrafish, the notochord produces Sonic hedgehog (Shh) which at high levels specifies muscle pioneers (MPs) which express the transcription factors *Engrailed* (*En*) and *Prox1* and at lower levels specifies superficial slow fibers (SSFs) which express the transcription factor *Prox1* alone (Barresi et al., 2000; Hirsinger et al., 2004; Wolff et al., 2003).

Despite the many signals communicated through cAMP, cells distinguish these signals in order to impart distinct effects (Calebiro and Koszegi, 2019; Zaccolo and Pozzan, 2002). For example, epinephrine and prostaglandin E1 induce similar increases in cAMP and PKA activity in cardiomyocytes, but only epinephrine induces Troponin I phosphorylation and increases contractility (Brunton et al., 1979; Keely, 1979).

How cells distinguish signals that induce a shared diffusible second messenger is poorly understood. One suggestion has been that different receptors form stable complexes with dedicated effectors (Tolkovsky and Levitzki, 1978a, 1978b). Another hypothesis is that different signals are transduced in distinct subcellular domains (Buxton and Brunton, 1983). Subcellular domains with differential GPCR activity include lipid nanodomains and clathrin-associated hot

spots within the plasma membrane (Agarwal et al., 2014; Allen et al., 2007; Insel et al., 2005; Sungkaworn et al., 2017).

We hypothesized that physically sequestering signaling pathways to either the cilium or the cell body allows parallel information processing without crosstalk. To test whether cells distinguish ciliary and nonciliary cAMP, we generated optogenetic and chemogenetic tools to specifically manipulate ciliary and nonciliary cAMP levels.

RESULTS

To assess whether cAMP generated inside or outside cilia communicate different information, we developed an optogenetic system based on a bacterial photoactivatable adenylyl cyclase (bPAC) (**Figure 1A**) (Stierl et al., 2010). bPAC generates cAMP in proportion to the amount of blue light delivered. We generated transgenic zebrafish that express either MYC-tagged cytoplasmic bPAC (Cyto-bPAC) or MYC-tagged ARL13B-bPAC (Cilia-bPAC) to investigate the functions of cytosolic and ciliary cAMP during vertebrate development. Immunofluorescence imaging of Cyto-bPAC and Cilia-bPAC in zebrafish embryos revealed that as expected, Cyto-bPAC localized to the cytoplasm and Cilia-bPAC localized to the cilium (**Figure 1B and Figure 2A**).

To assess whether Cyto-bPAC and Cilia-bPAC embryos generate cAMP specifically upon stimulation with blue light, we measured cAMP levels and found that Cyto-bPAC and Cilia-bPAC embryos raised in the dark contained levels of cAMP equivalent to those of wild-type embryos (**Figure 1C**). Treatment with the adenylyl cyclase agonist forskolin increased cAMP levels, as expected (**Figure 1C**). Similar to forskolin, blue light regimens induced equivalent amounts of cAMP in Cyto-bPAC and Cilia-bPAC transgenic embryos (**Figure 1C**). Transgenic embryos treated with these light regimens were morphologically indistinguishable from light-stimulated wild-type embryos or transgenic embryos raised in the dark, indicating that neither blue light nor the resultant cAMP grossly alters development (**Figure 2B**).

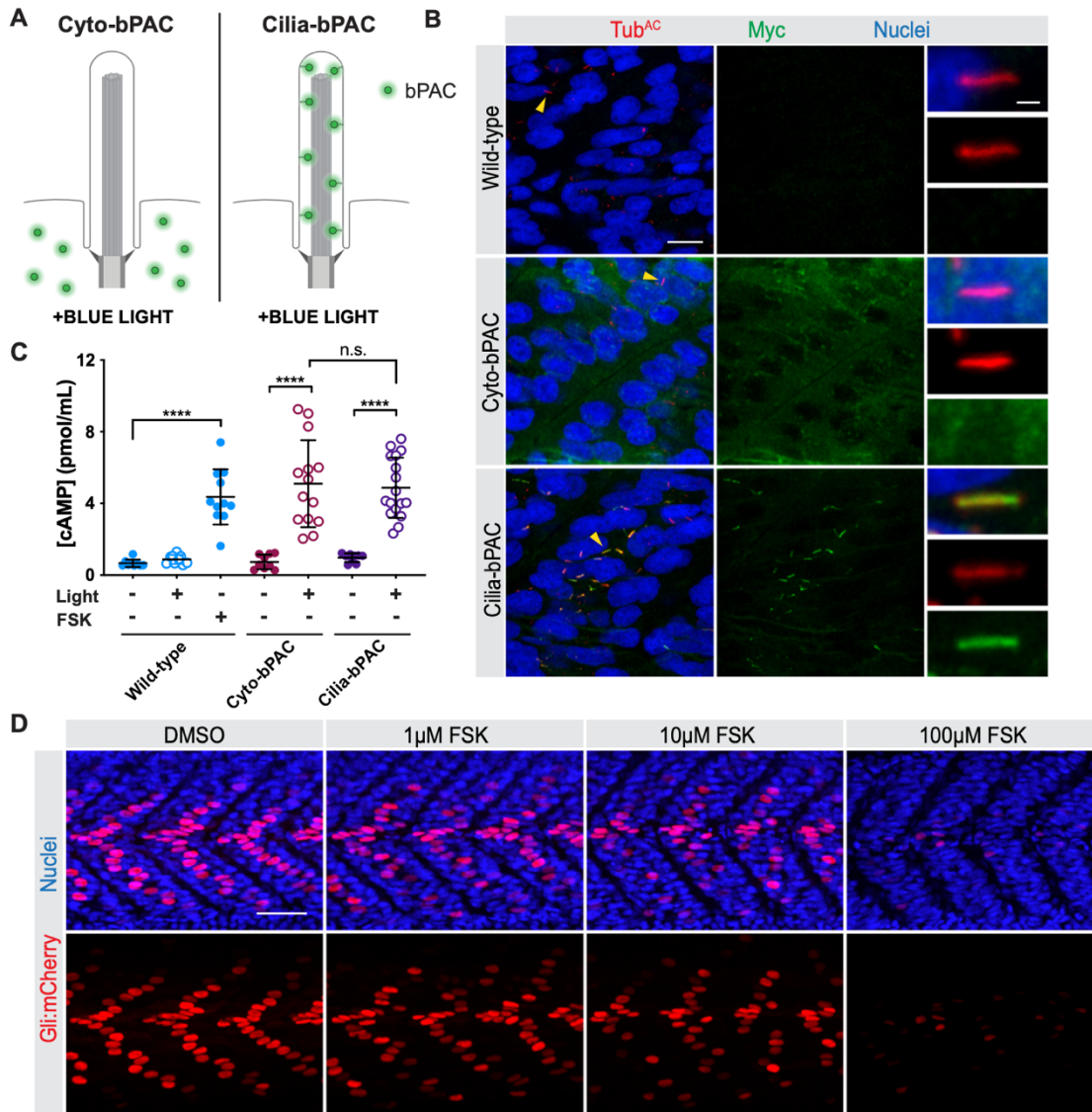


Figure 1. An optogenetic system for inducing cAMP *in vivo* at specific subcellular locations
(A) Schematic of system to optogenetically control cAMP generation by targeting bPAC, a blue-light activated adenylyl cyclase, to subcellular locations. Cyto-bPAC (green) localizes to the cytoplasm. Cilia-bPAC (green), a fusion of bPAC and the ciliary protein ARL13B, localizes to cilia.
(B) Immunofluorescence imaging of wild-type and transgenic zebrafish expressing either Myc-tagged Cyto-bPAC or Cilia-bPAC. Images depict 24hpf somites stained for bPAC (Myc, green), cilia (acetylated tubulin, Tub^{AC}, red) and nuclei (Hoechst, blue). Arrowheads indicate cilia depicted in the insets. Insets display overlay of bPAC, cilia and nuclei (top), cilia alone (middle), and bPAC alone (bottom). Scale bars, 10µm and 1µm (inset).
(C) Quantification of cAMP in wild-type and transgenic bPAC embryos with and without light stimulation. The adenylyl cyclase agonist forskolin (FSK, 10µM) increased cAMP in wild-type embryos. The phosphodiesterase inhibitor 3-isobutyl-1-methylxanthine (IBMX, 100µM) was used to inhibit cAMP degradation for all conditions. n=9-17 embryos per condition. Significance was determined via two-way ANOVA followed by Tukey's multiple comparison test throughout. A p

value less than 0.05 was considered statistically significant and is denoted as follows: * <0.05 , ** <0.01 , *** <0.001 , and **** <0.0001 . Data are represented as means \pm SD.

(D) Immunofluorescence imaging of somites expressing *Gli:mCherry*, a reporter of Hedgehog signal transduction. Embryos treated with increasing doses of FSK from 6 to 24 hpf were stained for *Gli:mCherry* (mCherry, red) and nuclei (Hoechst, blue). Scale bar, 40 μ m.

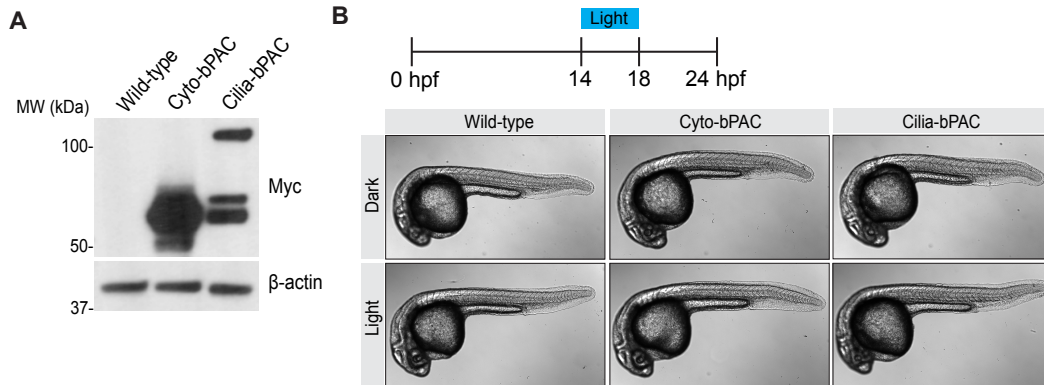


Figure 2. Light activation of Cilia-bPAC and Cyto-bPAC does not morphologically perturb development

(A) Immunoblot for Myc-tagged Cyto-bPAC and Cilia-bPAC in 24 hpf zebrafish embryo lysates. β -actin serves as a loading control.

(B) Whole-mount brightfield images of transgenic Cyto-bPAC and Cilia-bPAC zebrafish embryos either raised in the dark or stimulated with blue light from 14-18 hours post fertilization.

Ciliary cAMP specifically modulates HH signal transduction

As cAMP negatively regulates HH signal transduction (Barresi et al., 2000; Wang et al., 1999), we investigated whether ciliary or cytoplasmic cAMP affect HH signal transduction. To begin to investigate HH signaling, we assessed *Gli:mCherry*, a previously described reporter that induces mCherry expression upon activation of HH signaling (Mich et al., 2014). As expected, treating zebrafish embryos with forskolin reduced *Gli:mCherry* expression in the developing somite (**Figure 1D**). Cilia-bPAC expression in the absence of light had no effect on *Gli:mCherry* expression (**Figure 3A,B**), indicating that the ARL13B ciliary targeting sequence does not affect HH signaling. Notably, treating Cyto-bPAC transgenic zebrafish embryos with light had no effect on *Gli:mCherry* expression (**Figure 3A,B**). In striking contrast, activating Cilia-bPAC attenuated

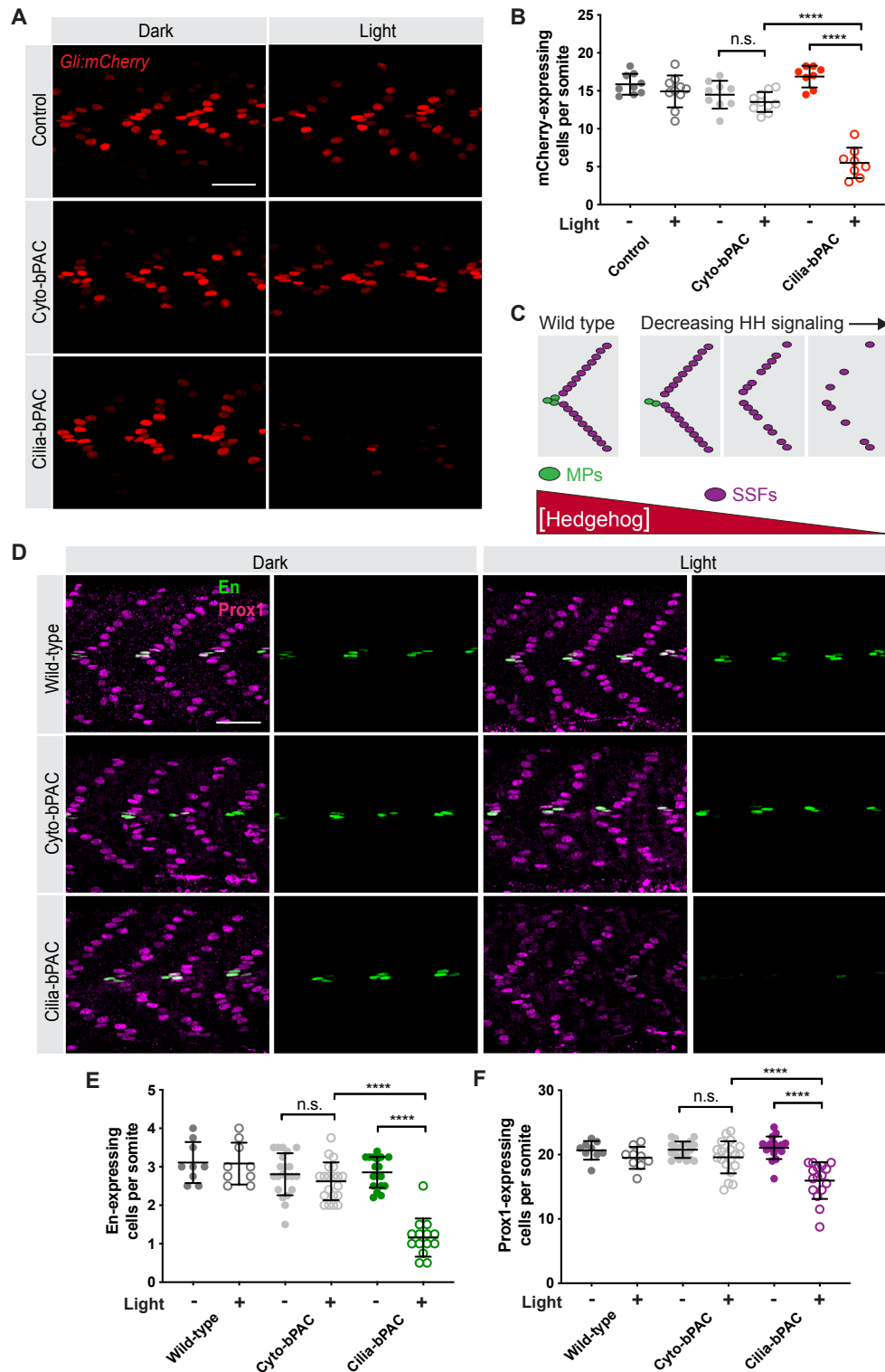


Figure 3. Cilium-generated cAMP specifically inhibits HH signal transduction

(A) Immunofluorescence imaging of somites 12-14 in 24hpf *Gli:mCherry* transgenic embryonic somites without bPAC (Control), expressing Cyto-bPAC or expressing Cilia-bPAC raised in the dark or stimulated with light. Scale bar, 40 μ m.

(B) Quantification of *Gli:mCherry*-expressing cells per somite. n=8-10 embryos collected over two independent clutches. Cells in somites 12 through 15 were counted and an average value of cells per somite was determined for each embryo. The average values per embryo were used as individual data points in all graphs and statistical analyses.

(C) Schematic of how HH signaling affects somitic cell fate. Muscle pioneer cells (MPs, green) express high levels of En and are specified by high levels of HH signaling. Superficial slow fibers (SSFs) express Prox1 and are specified by lower levels of HH signaling. Modest attenuation of HH signaling attenuates MP development, and more severe attenuation of HH signaling attenuates SFF development.

(D) Immunofluorescence imaging of En (green) and Prox1 (magenta) in wild-type and Cyto-bPAC- or Cilia-bPAC-expressing embryos with or without light stimulation. Scale bar, 40µm.

(E) Quantification of the average number of En-expressing cells per somite.

(F) Quantification of the average number of Prox1-expressing cells per somite.

n=9-20 embryos for each condition. Each data point represents the average number of En or Prox1 expressing cells per somite 12 through 15 per 24hpf embryo. Significance was determined via two-way ANOVA followed by Tukey's multiple comparison test. A p value less than 0.05 was considered statistically significant and is denoted as follows: *<0.05, **<0.01, ***<0.001, and ****<0.0001. Data are represented as means ± SD.

Gli:mCherry expression (**Figure 3A,B**).

As another control for the dependence on ciliary localization, we created a version of Cilia-bPAC containing a missense mutation in human ARL13B that prevents ciliary localization, V359A (Gigante et al., 2020; Higginbotham et al., 2012). We initially injected mRNA encoding GFP-tagged ARL13B-bPAC and ARL13B^{V359A}-bPAC. However, expression of this construct in embryos was low and did not potently generate cAMP (data not shown). We next injected mRNA encoding either MYC-tagged ARL13B^{V359A}-bPAC (Nonciliary-bPAC) or Cilia-bPAC. In contrast, MYC-tagged Nonciliary-bPAC was restricted outside of cilia in zebrafish embryos and generates cAMP upon blue light stimulation (**Figure 4A,B**). MYC-tagged Nonciliary-bPAC and MYC-tagged Cilia-bPAC protein was not detectable by 24hpf (data not shown), but was present from 14-18hpf, which was when bPAC was stimulated (**Figure 4A**). Similar to Cyto-bPAC, stimulating Nonciliary-bPAC-expressing embryos with blue light had no effect on *Gli:mCherry* expression (**Figure 4C,D**). In contrast, blue light stimulation of embryos injected with mRNA encoding Cilia-bPAC decreased *Gli:mCherry* expression (**Figure 4C,D**). Therefore, in developing somites, cAMP generated in cilia, but not outside cilia, affects HH signaling.

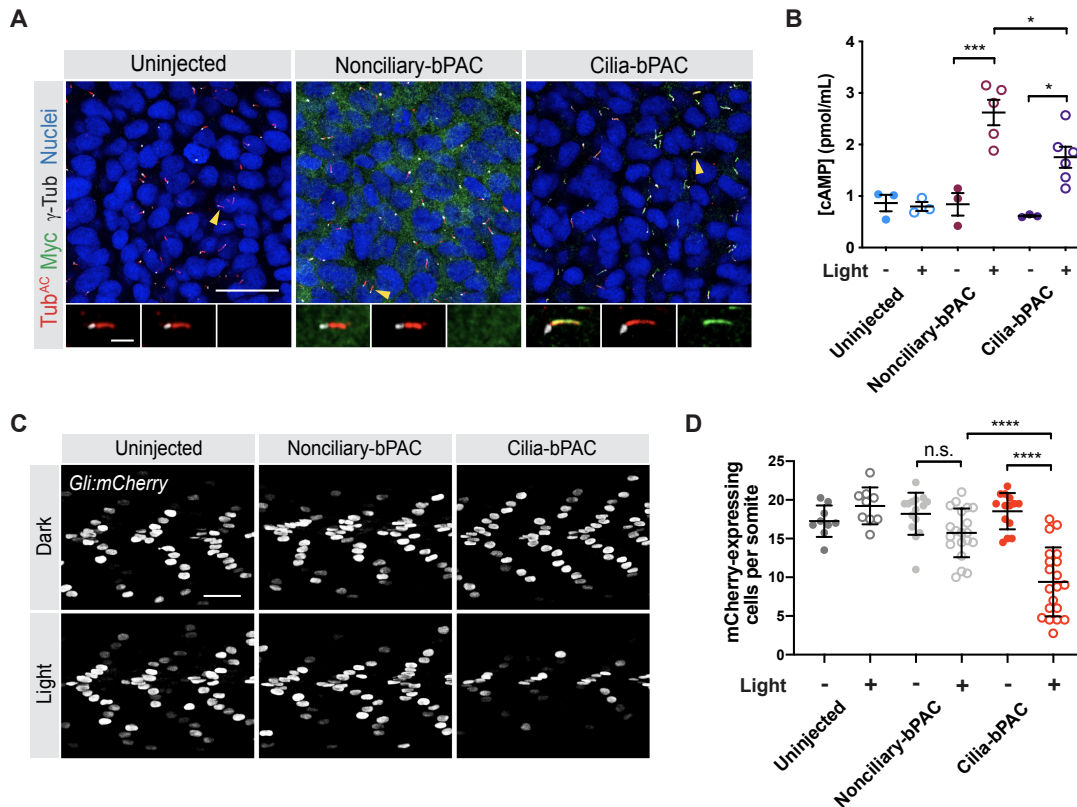


Figure 4. Cilium-generated cAMP specifically inhibits HH signal transduction

(A) Immunofluorescence images of zebrafish somites either uninjected or injected with mRNA encoding Myc-tagged Nonciliary-bPAC (ARL13B^{V359A}-bPAC-MYC) or Cilia-bPAC (ARL13B-bPAC-MYC). Images depict 18hpf somites stained for bPAC (Myc, green), cilia (Tub^{AC}, red), basal bodies (γTUB, grayscale) and nuclei (Hoechst, blue). Arrowheads indicate cilia depicted in insets. Insets display overlay of bPAC, cilia and basal bodies (left), overlay of cilia and basal bodies (middle), and bPAC alone (right). Scale bars, 20μm for main images and 2μm for insets.

(B) Quantification of cAMP in uninjected and embryos expressing either Nonciliary-bPAC or Cilia-bPAC. Embryos were stimulated in the presence of 100μM IBMX with 0.35mW/cm² 470nm pulsed blue light from 14-18hpf.

(C) Immunofluorescence images of *Gli:mCherry* transgenic embryos either uninjected, or injected with mRNA encoding Nonciliary-bPAC or Cilia-bPAC. Embryos were stained for mCherry (greyscale). Embryos were either raised in the dark or stimulated with 0.35mW/cm² 470nm pulsed blue light from 14-18hpf and then allowed to develop until 24hpf. Scale bar, 40μm.

(D) Quantification of *Gli:mCherry*-expressing cells per somite of uninjected embryos and those injected with mRNA encoding the indicated forms of bPAC. Each point represents the average number of mCherry-expressing cells over somites 12-15 of one embryo. Embryos were generated in three independent sets of injections. For both (B) and (D), significance was determined via two-way ANOVA with Tukey's multiple comparison test. A p value less than 0.05 was considered statistically significant and is denoted as follows: *<0.05, ***<0.001, and ****<0.0001. Data are represented as means ± SD.

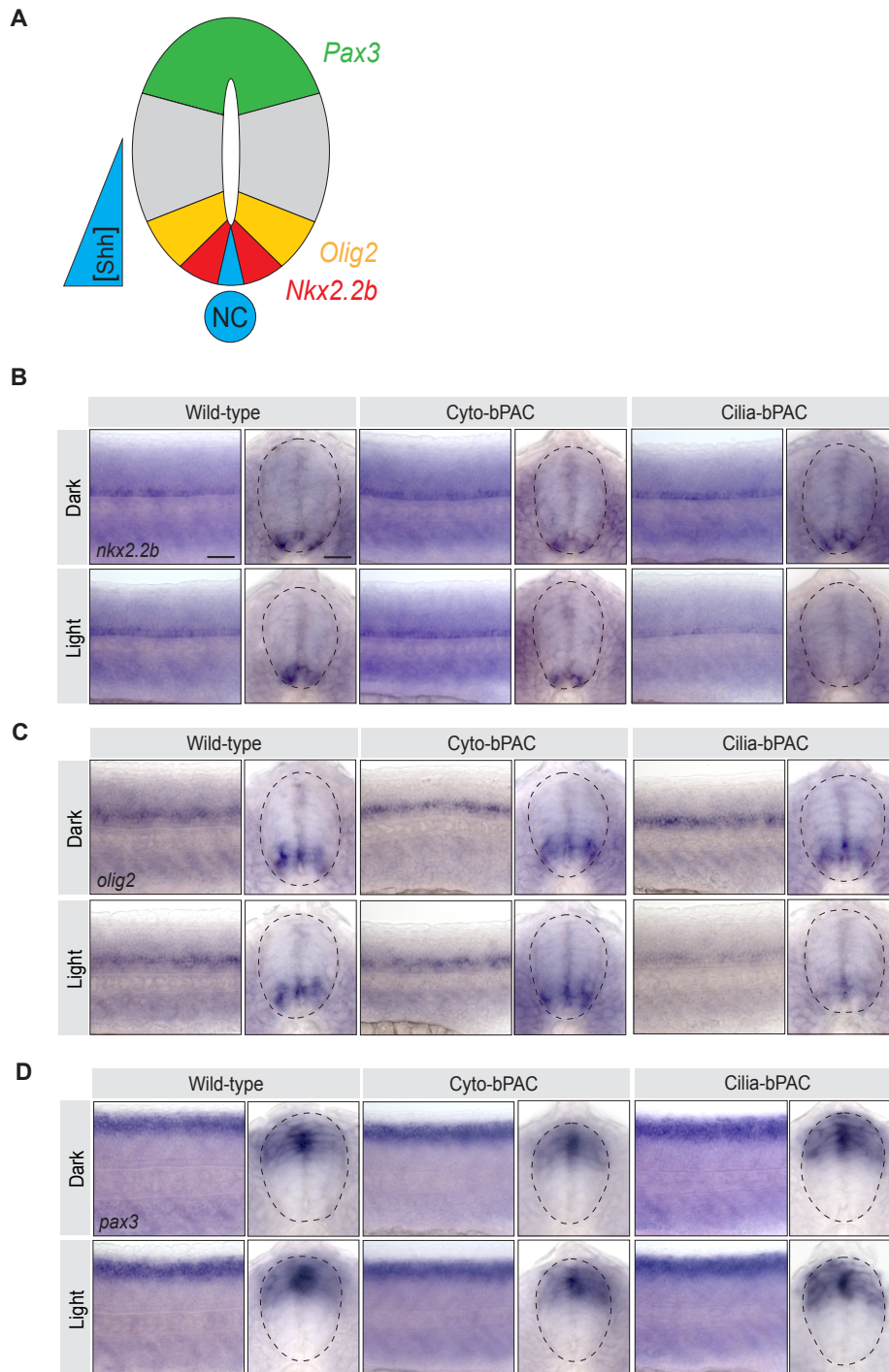


Figure 5. Cilium-generated cAMP specifically inhibits HH-dependent neural tube cell fates
(A) Schematic of HH-dependent neural tube patterning. A gradient of Shh secreted from the notochord (NT) and medial floorplate (blue) patterns lateral floor plate cells expressing *Nkx2.2b* (red) and motor neuron precursors expressing *Olig2* (yellow). Dorsal neural tube cells express *Pax3* (green).

(B-D) Whole-mount *in situ* hybridization to detect neural tube markers in Wild-type, Cyto-bPAC, and Cilia-bPAC-expressing transgenic zebrafish either raised in the dark or stimulated with blue

light. Left panels depict views of lateral whole mount 24hpf embryos. Right panels depict transverse cross-sections. Dotted lines outline the neural tubes. Expression of *Nkx2.2b* (**B**) and *Olig2* (**C**) are reduced specifically in Cilia-bPAC embryos stimulated with light. Expression of *Pax3* (**D**) is unchanged. Scale bar, 40 μ m.

In the developing zebrafish somite, HH signaling specifies slow muscle fiber types (Barresi et al., 2001; Blagden et al., 1997; Wolff et al., 2003). High levels of HH signaling specify high En- and Prox1-expressing MPs whereas lower levels specify Prox1-expressing SSFs. Attenuation of HH signaling therefore preferentially depletes MPs (**Figure 3C**). To test whether cytoplasmic or ciliary cAMP affect HH-dependent patterning, we quantified En- and Prox1-expressing somitic cells. Cyto-bPAC and Cilia-bPAC embryos raised in the dark produce numbers of En- and Prox1-expressing cells equivalent to those of wild-type embryos, confirming that the ARL13B ciliary targeting sequence does not affect HH signaling (**Figure 3D-F**). Stimulating wild-type or Cyto-bPAC embryos with light did not alter the number of En- or Prox1-expressing somitic cells (**Figure 3D-F**). In contrast, stimulating Cilia-bPAC embryos with light reduced the numbers of both En- and Prox1-expressing cells (**Figures 3D-F**). Thus, HH-dependent cell fates in the developing somite are preferentially inhibited by ciliary, but not cytoplasmic, cAMP production.

To test whether ciliary or cytoplasmic cAMP affect HH signaling in tissues beyond the somites, we examined how cAMP affects HH-dependent cell fates in the developing neural tube. In vertebrates, Shh produced in the notochord and medial floor plate patterns the ventral neural tube (**Figure 5A**) (Briscoe et al., 2000; Chiang et al., 1996; Ericson et al., 1996). Lateral floor plate cells expressing *nkx2.2b* are specified by high HH signaling, neighboring motor neuron progenitor cells expressing *olig2* are specified by lower HH signaling, and cells of the dorsal neural tube express *pax3* (Guner and Karlstrom, 2007; Odenthal et al., 2000). As in somite development, neither embryos expressing Cyto-bPAC and stimulated with light nor embryos expressing Cilia-bPAC and raised in the dark exhibited perturbation of HH-mediated patterning (**Figure 5B-D**). In contrast, Cilia-bPAC embryos treated with light exhibited decreased expression of both *nkx2.2b* and *olig2* (**Figure 5B,C**). Expression of *pax3* in Cilia-bPAC embryos treated with light was

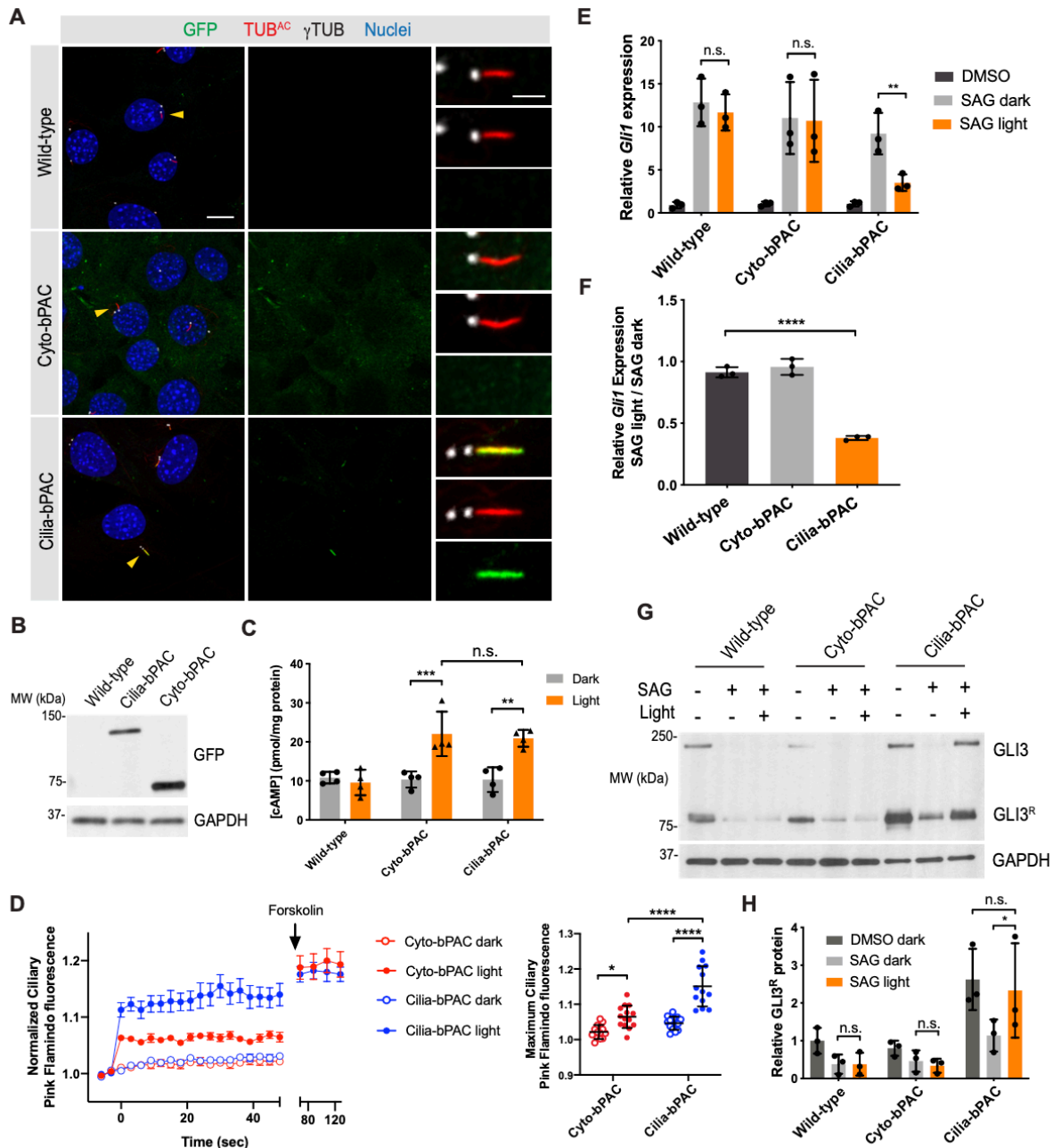


Figure 6. Cilium-generated cAMP inhibits HH signal transduction in mammalian cells

(A) Immunofluorescence imaging of wild-type and transgenic NIH/3T3 cells stably expressing GFP-tagged Cyto-bPAC or Cilia-bPAC under the control of a minimal δ -crystallin promoter stained for GFP-tagged bPAC (green), cilia (TUB^{AC}, red), basal bodies (γ TUB, grayscale) and nuclei (blue). Arrowheads indicate cilia depicted in insets. Insets display overlay (top), cilia and basal bodies alone (middle), and GFP-tagged bPAC alone (bottom). Scale bars, 10 μ m and 2 μ m (inset).

(B) Immunoblot of wild-type and transgenic NIH/3T3 cells stably expressing GFP-tagged Cyto-bPAC and Cilia-bPAC under the control of the EF1 α promoter. Whole-cell protein lysates were immunoblotted with antibodies to GFP and GAPDH loading control.

(C) Quantification of cAMP in wild-type or transgenic cells expressing Cyto-bPAC or Cilia-bPAC under the control of a minimal δ -crystallin promoter by ELISA. Cells were stimulated with pulsed $0.14\text{mW}/\text{cm}^2$ 470nm blue light or kept in the dark in the presence of $100\mu\text{M}$ IBMX for 30 minutes. cAMP concentration was determined by ELISA and normalized to total protein content. $n=4$ biological replicates. Significance was determined via two-way ANOVA followed by Tukey's multiple comparison test.

(D) Quantitation of Ciliary Pink Flamindo fluorescence in Cyto-bPAC-expressing (red) or Cilia-bPAC-expressing (blue) cells either with (open points) or without blue light (filled points). Cells were stimulated with 100ms pulses of $52.7\text{mW}/\text{cm}^2$ blue light every three seconds for 1 minute. At the end of that minute, $100\mu\text{M}$ Forskolin was added. We calculated the ratio of Pink Flamindo to mIFP fluorescence normalized to the ratio at $t=0$. Each trace represents $n>12$ cells from three independent experiments. The maximum Ciliary Pink Flamindo fluorescence upon blue light stimulation is also shown. Significance was assessed using two-way ANOVA followed by Tukey's multiple comparison test.

(E) qRT-PCR measurement of *Gli1* expression by wild-type, Cyto-bPAC-expressing or Cilia-bPAC-expressing cells stimulated for 4 hours with vehicle (DMSO), 200nM SAG, or 200nM SAG with pulsed $0.14\text{mW}/\text{cm}^2$ 470nm blue light. $n=3$ biological replicates. Significance was assessed using one-way ANOVA followed by Tukey's multiple comparison test.

(F) Ratios of *Gli1* expression in wild-type and Cyto-bPAC-expressing or Cilia-bPAC-expressing cells treated with 200nM SAG and blue light to *Gli1* expression treated with 200nM SAG alone. Significance was assessed using one-way ANOVA followed by Tukey's multiple comparison test.

(G) Immunoblots of GLI3 and GAPDH of whole-cell lysates from wild-type, Cyto-bPAC-expressing or Cilia-bPAC-expressing cells stimulated as in **(E)**.

(H) Quantification of GLI3 repressor (GLI3^R) normalized to GAPDH (loading control). $n=3$ biological replicates. For all panels, p values are indicated as follows: * <0.05 , ** <0.01 , *** <0.001 and **** <0.0001 . Data are represented as means \pm SD.

indistinguishable from wild-type embryos (**Figure 5D**). This is similar to zebrafish embryos mutant for *smoothened*, where *pax3* expression is unchanged (Guner and Karlstrom, 2007). Thus, in neural tube patterning, as in somite patterning, cilium-generated cAMP but not cytoplasm-generated cAMP inhibits HH signaling. We conclude that zebrafish cells interpret cAMP generated in the cilium differently from cAMP generated in the cytoplasm.

To assess whether mammalian cells also differentially interpret cilium- and cytoplasm-generated cAMP, we generated NIH/3T3 cell lines stably expressing either GFP-tagged Cyto-bPAC or Cilia-bPAC. These lines were initially generated using an EF1 α promoter to drive high expression of bPAC. Though Cyto- and Cilia-bPAC constructs were expressed at high levels and robustly generated cAMP, all Cilia-bPAC clones tested were unresponsive to HH signaling induction via the SMO agonist SAG (data not shown). However, all Cyto-bPAC clones responded

to SAG robustly (data not shown). This may be due to dark activity of high levels of bPAC-stimulated cAMP production in the cilium. As an alternative approach, we generated NIH/3T3 cell lines stably expressing either GFP-tagged Cyto-bPAC or Cilia-bPAC under the control of a minimal chicken lens δ -crystallin attenuated promoter (Ye et al., 2018). Immunofluorescence imaging revealed that, as in zebrafish, Cyto-bPAC localized to the cytoplasm and Cilia-bPAC localized to the cilium (**Figure 6A**). We were unable to detect attenuated promoter Cyto-bPAC or Cilia-bPAC expression by immunoblot, even upon immunoprecipitation of GFP (data not shown). This may be due to low levels of expression. More protein input may be necessary to detect this construct. However, immunoblot of Cyto-bPA and Cilia-bPAC under the control of the EF1 α promoter revealed that both constructs are expressed at comparable levels (**Figure 6B**). Blue light stimulation of attenuated promoter Cyto-bPAC and Cilia-bPAC cell lines generated similar levels of cAMP, as measured by ELISA (**Figure 6C**).

As cAMP is highly diffusible and no membrane barrier exists between the cilium and the cytoplasm, we predicted that cAMP generated in the cilium can enter the cytoplasm and vice versa. To test this hypothesis, we visualized cAMP dynamics in the cilium and cytoplasm upon Cyto-bPAC and Cilia-bPAC activation. To record cAMP levels independent of blue light stimulation of bPAC, we utilized a red fluorescent cAMP indicator, Pink Flamindo (Pink Fluorescent cAMP indicator) (Harada et al., 2017). cAMP increases Pink Flamindo fluorescence and, as expected, stimulating Cyto-bPAC and Cilia-bPAC with blue light induced similar increases in Pink Flamindo fluorescence (**Figure 7A**).

To generate a ratiometric cAMP biosensor targeted to cilia, we first tried fusing Pink Flamindo to ARL13B. However, though the sensor localized to the cilium, it was insensitive to perturbations in cAMP (data not shown). As an alternative approach, we fused Pink Flamindo to RAB23 Q68L, which constitutively localizes to cilia, and a far-red fluorescent protein mIFP to generate Ciliary Pink Flamindo (Lim and Tang, 2015; Yu et al., 2015). As expected, forskolin

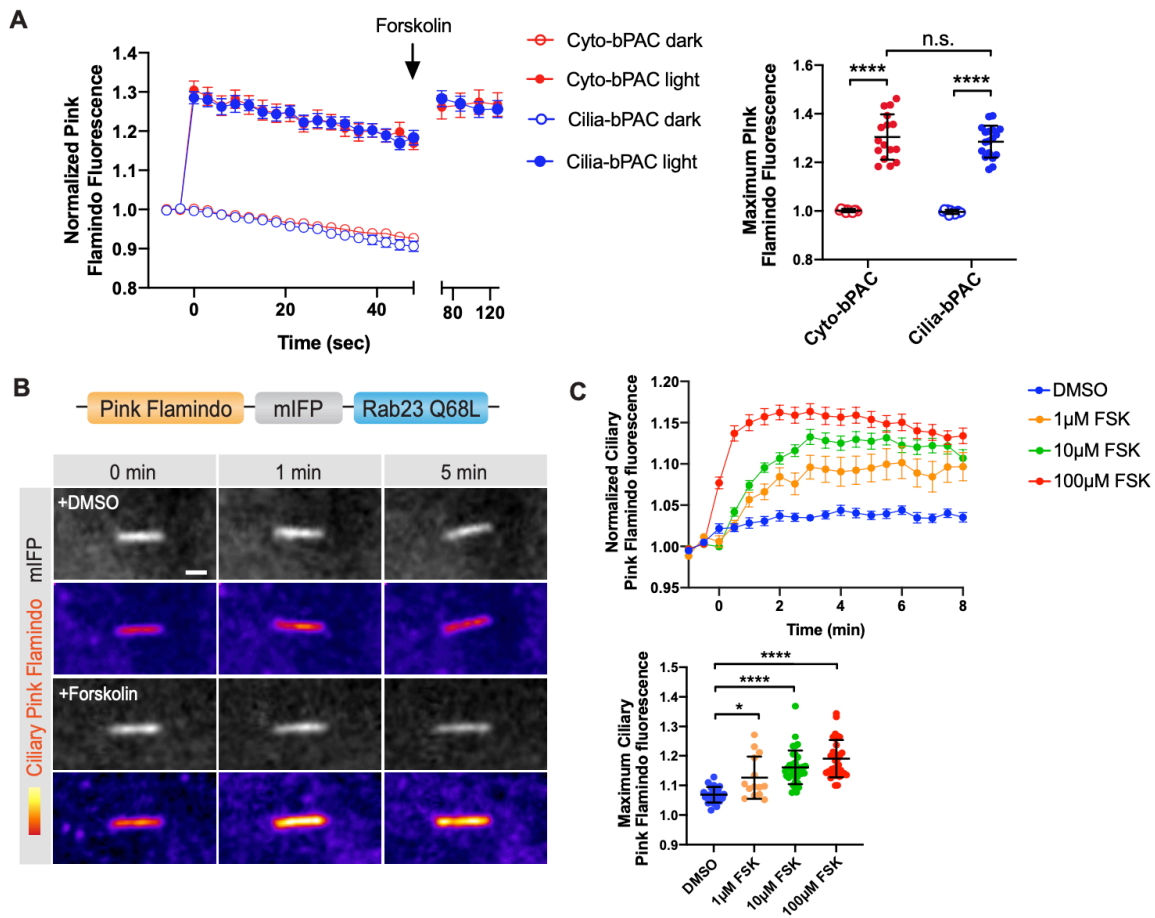


Figure 7. Ciliary targeted Pink Flamindo reports ciliary cAMP

(A) Untargeted Pink Flamindo expressed in either ciliated Cyto-bPAC (red) or ciliated Cilia-bPAC (blue) cells was stimulated with (open circles) or without (solid circles) 2.68mW blue light. 100μM Forskolin was added at the indicated time (arrow) after blue light stimulation. Left panel depicts quantification of Pink Flamindo fluorescence over time. Right panel depicts the maximum Pink Flamindo fluorescence after blue light stimulation. $n > 15$ cells quantified over two independent experiments. Significance was determined via two-way ANOVA followed by Tukey's multiple comparison test.

(B) A red-shifted cAMP sensor, Pink Flamindo, was fused to the far-red fluorescent protein mIFP and Rab23 Q68L, which constitutively localizes to the cilium, to generate Ciliary Pink Flamindo. Bottom panel depicts representative images of Pink Flamindo (Fire) and mIFP (greyscale) fluorescence in NIH/3T3 cells stably expressing Ciliary Pink Flamindo upon addition of either vehicle (DMSO) or 100μM Forskolin. Forskolin increases Pink Flamindo fluorescence. Scale bar, 2μm.

(C) Quantification of Ciliary Pink Flamindo fluorescence over time upon increasing concentrations of Forskolin. The ratio of Pink Flamindo fluorescence to mIFP fluorescence at cilia was measured, then normalized to baseline fluorescence (F/F_0). Traces represent the average of $n > 15$ cells over 3 independent experiments. The maximum Ciliary Pink Flamindo fluorescence (F_{max}/F_0) is also displayed for each cell. Significance was determined via one-way ANOVA followed by Tukey's multiple comparison test. p values less than 0.05 were considered statistically significant and is denoted as follows: * < 0.05 and **** < 0.0001 . Data are represented as means \pm SD.

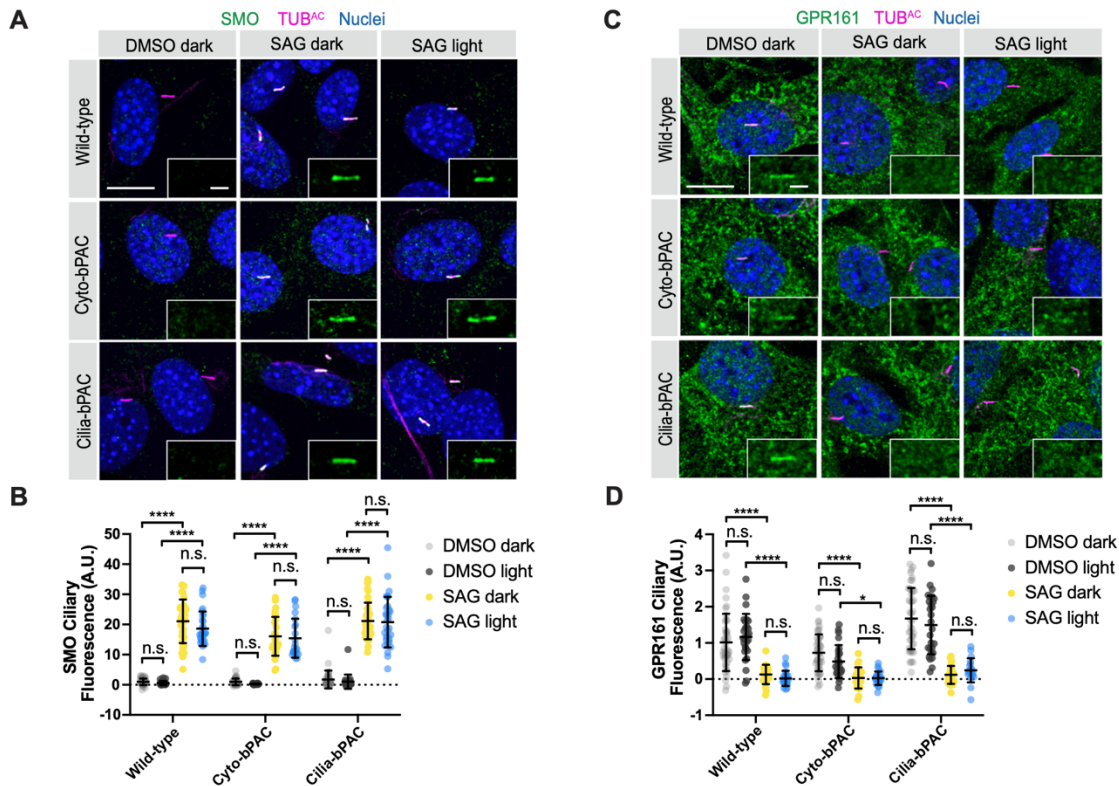


Figure 8. cAMP does not affect SMO or GPR161 trafficking to or from cilia

(A) Immunofluorescence images of wild-type, Cyto-bPAC and Cilia-bPAC NIH/3T3 cells treated with either vehicle (DMSO) or 200nM SAG in the presence or absence of 4 hours of 0.14mW/cm² pulsed blue light. Cells were stained for SMO (green), cilia (TUB^{AC}, magenta), and nuclei (Hoechst, blue). Insets display SMO localization to the cilium (defined by TUB^{AC} staining). Scale bar, 10μm. Inset scale bar, 2μm.

(B) Quantification of ciliary SMO immunofluorescence. Fluorescence was normalized to the mean of that of wild-type cells treated with vehicle in the dark.

(C) Immunofluorescence images of wild-type, Cyto-bPAC and Cilia-bPAC NIH/3T3 cells stimulated as above and stained for GPR161 (green), cilia (TUB^{AC}, magenta), and nuclei (Hoechst, blue). Insets display GPR161 localization to the cilium (defined by TUB^{AC} staining). Scale bar, 10μm. Inset scale bar, 2μm.

(D) Quantification of ciliary GPR161 fluorescence. For (B) and (D), significance was determined using one-way ANOVA followed by Tukey's multiple comparison test. A p value less than 0.05 was considered statistically significant and is denoted as follows: ****<0.0001. Data are represented as means ± SD.

increased the ratio of Pink Flamindo to mIFP fluorescence at the cilium (**Figure 7B,C**). To measure cAMP diffusion between the cytoplasm and cilium, we deployed Ciliary Pink Flamindo in Cyto-bPAC and Cilia-bPAC cells. Consistent with the absence of barriers to cAMP diffusion

between the cytoplasm and the cilium, stimulating Cyto-bPAC increased Ciliary Pink Flamindo fluorescence (**Figure 6D**). Interestingly, Cyto-bPAC activation did not increase Ciliary Pink Flamindo fluorescence to the same levels as did Cilia-bPAC activation (**Figure 6D**). Thus, cAMP produced in the cytoplasm diffuses into the cilium but does not reach levels equivalent to those caused by local production.

As cilium-generated cAMP specifically inhibits HH-dependent patterning in zebrafish embryos, we investigated whether cilium-generated or cytoplasm-generated cAMP inhibits HH signal transduction in mammalian cells. To this end, we treated wild type, Cyto-bPAC- or Cilia-bPAC-expressing cells with the Smoothed agonist SAG. Each cell line equivalently induced *Gli1* in response to SAG, indicating that neither unstimulated bPAC nor its ciliary targeting sequence perturbs HH signaling (**Figure 6E,F**). Stimulating Cyto-bPAC-expressing cells with blue light had no effect on SAG-mediated induction of *Gli1* (**Figure 6E,F**). In contrast, stimulating Cilia-bPAC-expressing cells with blue light inhibited SAG-mediated induction of *Gli1* (**Figure 6E,F**). Thus, as in zebrafish, cilium-produced cAMP preferentially inhibits HH signal transduction in mammalian cells.

To investigate how cilium-produced cAMP preferentially inhibits HH signal transduction, we examined whether cAMP affects the trafficking of SMO and GPR161 at cilia. In the absence of HH stimulation, the GPCR GPR161 accumulates in cilia (Mukhopadhyay et al., 2013). Addition of HH ligand causes coordinated trafficking of SMO into cilia and GPR161 out of cilia (Corbit et al., 2005; Pal et al., 2016). To determine whether ciliary cAMP impacts trafficking of SMO or GPR161 to or from cilia, we quantified SMO and GPR161 fluorescence at the cilium in wild-type, Cyto-bPAC and Cilia-bPAC-expressing cells, both with and without SAG. SMO robustly localized to cilia in the presence of SAG (**Figure 8A,B**). Stimulation of wild-type, Cyto-bPAC or Cilia-bPAC cells with blue light did not attenuate SAG-induced ciliary localization of SMO (**Figure 8A,B**). GPR161 localized to cilia in vehicle (DMSO)-treated cells and not upon SAG treatment (**Figure 8C,D**). Stimulation of wild-type, Cyto-bPAC and Cilia-bPAC cells with blue light in the presence

of SAG did not attenuate GPR161 exit from cilia (**Figure 8C,D**). Therefore, ciliary cAMP does not affect the regulated ciliary trafficking of SMO or GPR161.

In the absence of HH, GLI3 is proteolytically processed to form GLI3R, a truncated form that functions as a transcriptional repressor of HH transcriptional targets (Dai et al., 1999; Wen et al., 2010). Activation of HH signaling inhibits GLI3R formation (Humke et al., 2010; Jiang and Struhl, 1998; Wang et al., 2000). To determine whether cilium- or cytoplasm-generated cAMP affects GLI3 processing, we activated HH signaling in wild-type, Cyto-bPAC-expressing or Cilia-bPAC-expressing cells using SAG either with or without blue light stimulation and immunoblotted for GLI3. In the absence of blue light, SAG reduced GLI3R in all three cell lines (**Figure 6G,H**). Blue light had no effect on this reduction of GLI3R in wild-type or Cyto-bPAC-expressing cells (**Figure 6G,H**). In contrast, blue light blocked the SAG-induced reduction of GLI3R in Cilia-bPAC-expressing cells (**Figure 6G,H**). Thus, ciliary cAMP generation specifically inhibits HH signal transduction downstream of SMO and GPR161 trafficking and upstream of GLI3 processing.

Ciliary GPCRs regulate HH pathway output

If cilium-generated cAMP specifically inhibits the HH pathway, we hypothesized that ciliary GPCRs should regulate the HH pathway, but plasma membrane GPCRs should not. To test this hypothesis, we developed cilium- and plasma membrane-localized versions of a $G\alpha_s$ -coupled designer receptor exclusively activated by a designer drug (DREADD). DREADDs are GPCRs engineered to be selectively activated by the otherwise pharmacologically inert drug clozapine-N-oxide (CNO) (Armbruster et al., 2007; Roth, 2016). Upon binding of CNO, $G\alpha_s$ -coupled DREADD activates the production of cAMP (Guettier et al., 2009). To localize $G\alpha_s$ -coupled DREADD to cilia, we fused it to the ciliary protein ARL13B and GFP (hereafter referred to as Cilia-DREADD, **Figure 9A**). We generated NIH/3T3 fibroblast cell lines stably expressing GFP-tagged Cilia-DREADD or DREADD without ARL13B (hereafter referred to as Plasma membrane- or PM-

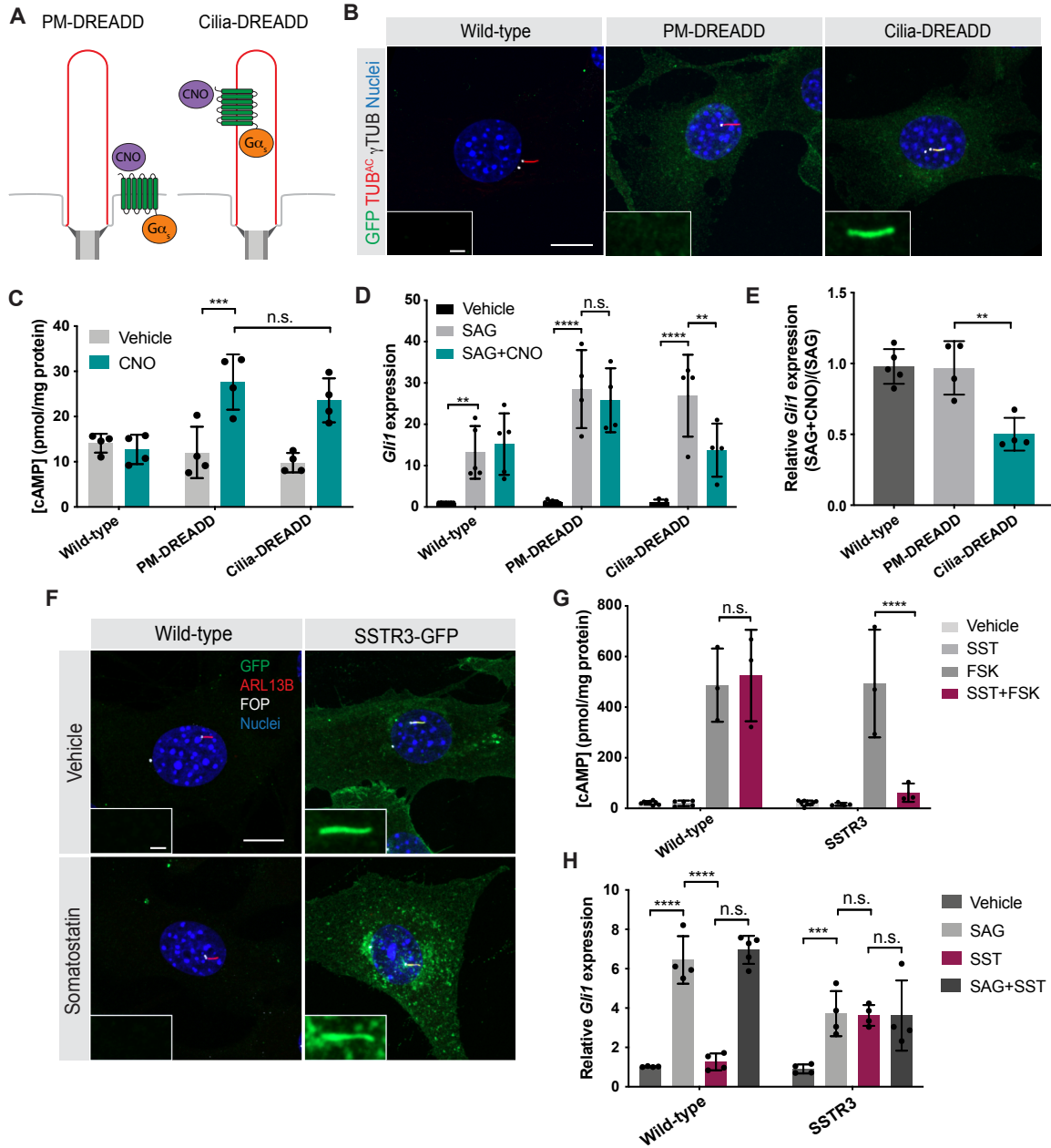


Figure 9. Ciliary GPCR activity specifically modulates HH signal transduction

(A) Schematic of tools to control a Gas-coupled designer GPCR at distinct subcellular locations. PM-DREADD localizes to the plasma membrane. Cilia-DREADD, a fusion with the ciliary protein ARL13B, localizes to cilia. These Gas-coupled DREADDs induce cAMP generation upon stimulation with their ligand, the otherwise pharmacologically inert drug CNO.

(B) Immunofluorescence imaging of wild-type and transgenic NIH/3T3 cells stably expressing GFP-tagged PM-DREADD or Cilia-DREADD. Images depict cells stained for the GFP-tagged DREADDs (GFP, green), cilia (TUB^{AC}, red), basal bodies (γ TUB, grayscale) and nuclei (Hoechst, blue). Insets indicate amount of GFP-tagged DREADD localization to the cilium (defined by TUB^{AC} and γ TUB). Scale bars, 10 μ m and 1 μ m (inset).

(C) Quantification of cAMP in wild-type and PM-DREADD- or Cilia-DREADD-expressing NIH/3T3 transgenic cell lines. Cells were stimulated with either vehicle (DMSO) or 100nM CNO in the presence of 10 μ M IBMX for 3 hours. cAMP concentration was determined by ELISA and normalized to total protein content. n=4 biological replicates. Significance was determined via two-way ANOVA followed by Tukey's multiple comparison test. Data are represented as means \pm SD.

(D) Expression of *Gli1* by wild-type and PM-DREADD- or Cilia-DREADD-expressing cells stimulated with vehicle (DMSO), 200nM SAG, or 200nM SAG and 5nM CNO for 5 hours before measurement by qRT-PCR. n=4-5 biological replicates. Significance was determined via one-way ANOVA followed by Tukey's multiple comparison test.

(E) Ratios of *Gli1* expression in WT and PM-DREADD- or Cilia-DREADD-expressing cells treated with 200nM SAG and 5nM CNO to *Gli1* expression treated with 200nM SAG alone. Significance was determined via one-way ANOVA followed by Tukey's multiple comparison test. n=4-5 biological replicates.

(F) Immunofluorescence imaging of wild-type and transgenic NIH/3T3 cells stably expressing SSTR3-GFP, a ciliary G α i-coupled GPCR, fused to GFP. Images depict cells stained for SSTR3-GFP (GFP, green), cilia (ARL13B, red), basal bodies (FOP, grayscale) and nuclei (Hoechst, blue). Cells were treated either vehicle (DMSO) or 10 μ M somatostatin (SST) for 5 hours. Insets depict SSTR3-GFP localization to the cilium (defined by ARL13B and FOP). Scale bars, 10 μ m and 1 μ m (inset).

(G) Quantification of SSTR3-mediated inhibition of cAMP production. Wild-type and SSTR3-GFP-expressing NIH/3T3 cells were stimulated with either vehicle (DMSO), 10 μ M FSK, or 10 μ M FSK and 10 μ M SST in the presence of 10 μ M IBMX for 30 minutes. cAMP concentration was measured by ELISA and normalized to total protein content. n=3-6 biological replicates. Significance was determined via one-way ANOVA followed by Tukey's multiple comparison test. Data are represented as means \pm SD.

(H) Expression of *Gli1* by wild-type and SSTR3-GFP-expressing NIH/3T3 cells treated with vehicle (DMSO), 3nM SAG, 10 μ M SST, or both 3nM SAG and 10 μ M SST for 5 hours and measured by qRT-PCR. n=4 biological replicates. Significance was determined via one-way ANOVA followed by Tukey's multiple comparison test. Data are represented as means \pm SD. For all panels, a p value less than 0.05 was considered statistically significant and is denoted as follows: *<0.05, **<0.01, ***<0.001, and ****<0.0001.

DREADD). Immunofluorescence imaging confirmed that, as expected, PM-DREADD localized to the plasma membrane and Cilia-DREADD localized to the cilium (**Figure 9B, Figure 10A**). Immunoblotting whole-cell lysates from PM-DREADD- and Cilia-DREADD-expressing cells for the GFP tag indicated that the DREADDs are expressed at similar levels (**Figure 10B**).

To test whether Cilia-DREADD can activate G proteins, we expressed mini-G, a fluorescently-tagged engineered G protein that is recruited to active GPCRs (Carpenter and Tate, 2016; Wan et al., 2018). In Cilia-DREADD-expressing cells, CNO induced translocation of mApple-tagged mini-G_s to the cilium (**Figure 10C,D**). Thus, Cilia-DREADD adopts an active

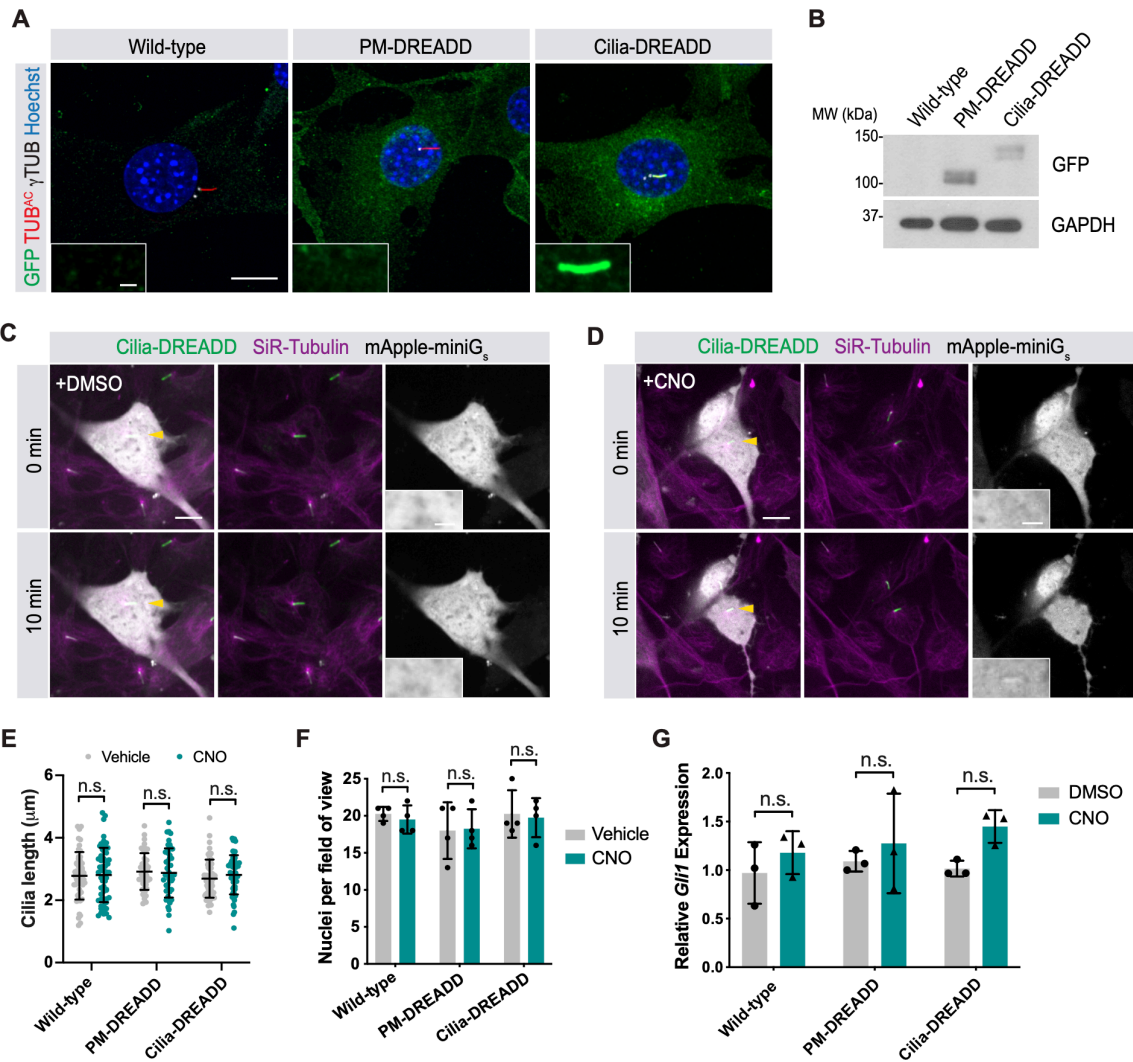


Figure 10. Ciliary targeted DREADD activates $G\alpha_s$ in cilia

(A) Oversaturated immunofluorescence images of transgenic NIH/3T3 cells stably expressing GFP-tagged PM-DREADD or Cilia-DREADD. Images depict cells stained for the GFP-tagged DREADDs (GFP, green), cilia (TUB^{AC}, red), basal bodies (γ TUB, grayscale) and nuclei (Hoechst, blue). Insets indicate amount of GFP-tagged DREADD localization to the cilium (defined by TUB^{AC} and γ TUB). Scale bars, 10 μ m and 1 μ m (inset). With increased exposure, PM-DREADD is not observed in the ciliary membrane.

(B) Immunoblot for GFP-tagged PM-DREADD and Cilia-DREADD. Immunoblot for GAPDH was used to control for protein loading.

(C) Mini-G sensors visualized G-protein activity in Cilia-DREADD-expressing cells. Cilia in live cells were identified through enrichment of a tubulin dye (SiR-Tubulin, magenta) and localization of GFP-tagged Cilia-DREADD (green). The mApple-tagged mini-G sensor (grayscale) was not enriched in cilia both before and 10 minutes after treatment with vehicle (DMSO). Yellow arrowheads indicate cilia depicted in insets. Scale bars, 10 μ m and 2 μ m (inset).

(D) In Cilia-DREADD cells incubated with 10 μ M CNO for 10 minutes, the mApple-tagged mini-G sensor (grayscale) accumulated in cilia. Scale bars, 10 μ m and 2 μ m (inset).

(E-F) Quantification of cilia length **(E)** and nuclei per field of view **(F)** in wild-type, PM-DREADD- or Cilia-DREADD-expressing cells upon treatment with either vehicle (DMSO) or 5nM CNO for 5 hours. $n > 50$ cilia were quantified over four random fields. For **(E)** and **(F)**, significance was determined via two-tailed unpaired t-test.

(G) Measurement of *Gli1* expression in wild-type, PM-DREADD- or Cilia-DREADD-expressing cells treated with either vehicle or 5nM CNO by qRT-PCR. $n = 3-4$ biological replicates. Significance was determined via one-way ANOVA followed by Tukey's multiple comparison test. A p value less than 0.05 was considered statistically significant. Data are represented as means \pm SD.

conformation in the cilium specifically upon ligand binding. We did not observe mini- G_s localization to the plasma membrane in PM-DREADD cells (data not shown). This may be due to weak coupling or differences in stoichiometry of expression between DREADD and mini G_s (data not shown). However, importantly, PM-DREADD- and Cilia-DREADD-expressing cells with CNO generated equivalent amounts of cAMP **(Figure 9C)**. Activating either DREADD with CNO did not affect cell survival or ciliary length **(Figure 10E,F)**.

Because we had found that ciliary, but not cytoplasmic, cAMP regulated HH signaling, we hypothesized that ciliary, but not plasma membrane, GPCR signaling would regulate HH signaling. To begin to test whether ciliary and nonciliary GPCRs can modulate HH pathway activity, we treated wild-type, PM-DREADD- or Cilia-DREADD-expressing NIH/3T3 cells with SAG. Each cell line induced *Gli1* in response **(Figure 9D)**. Treatment with CNO alone did not affect basal *Gli1* expression **(Figure 10G)**. Activating PM-DREADD with CNO in the presence of SAG did not affect *Gli1* induction **(Figure 9D,E)**. In contrast, activating Cilia-DREADD with CNO inhibited the ability of SAG to induce *Gli1* **(Figure 9D,E)**. Thus, as with cAMP, ciliary GPCR activity specifically affects HH signal transduction.

Whereas $G_{\alpha s}$ -coupled GPCRs, such as Cilia- and PM-DREADDs, stimulate cAMP production, $G_{\alpha i}$ -coupled GPCRs inhibit cAMP production. As Cilia-DREADD, a ciliary $G_{\alpha s}$ -coupled GPCR, inhibits the HH pathway, we hypothesized that a ciliary $G_{\alpha i}$ -coupled GPCR would activate the HH pathway. To test this hypothesis, we investigated the activity of SSTR3, a $G_{\alpha i}$ -coupled GPCR that localizes to primary cilia (Berbari et al., 2008; Green et al., 2015; Händel et

al., 1999). We stably expressed GFP-tagged SSTR3 in NIH/3T3 cells (**Figure 9F**). As expected, activating SSTR3 with somatostatin opposed forskolin-mediated induction of cAMP, confirming that SSTR3 is $G_{\alpha i}$ -coupled (**Figure 9G**).

We stimulated wild-type or SSTR3-expressing cells with somatostatin and assayed HH pathway activity. Wild-type cells showed increased expression of the HH target gene *Gli1* in response to SAG, but not somatostatin. However, stimulating SSTR3-expressing cells with somatostatin induced *Gli1* expression to similar levels as treatment with 3nM SAG ($EC_{50}=3nM$) (**Figure 9H**). However, it does not do so to the same extent as saturating levels of SAG. Furthermore, concurrent treatment with both somatostatin and SAG do not have synergistic effects on *Gli1* expression (**Figure 9H**). It is unclear whether this is due to SSTR3 exiting cilia upon somatostatin treatment, or whether $G_{\alpha i}$ activation is insufficient to fully activate the HH transcriptional response (Green et al., 2015). Thus, whereas ciliary cAMP inhibits the HH transcriptional response, activating a ciliary $G_{\alpha i}$ -coupled GPCR activates the HH transcriptional response.

Together, these experiments with engineered and natural GPCRs further support the conclusion, demonstrated above using subcellular control of cAMP generation, that ciliary and nonciliary cAMP convey separate information to the cell. Additionally, the ability of a ciliary $G_{\alpha i}$ -coupled GPCR to activate the HH transcriptional response and a ciliary $G_{\alpha s}$ -coupled GPCR to do the opposite indicates that HH signal transduction is responsive to both increases and decreases in ciliary cAMP.

Ciliary PKA regulates HH signal transduction

The diffusibility of cAMP between the cytoplasm and the cilium would seem to preclude the cell from distinguishing subcellular pools, critical for the ability of separate pools to impart distinct information (Marley et al., 2013). To investigate how the cell may distinguish ciliary and

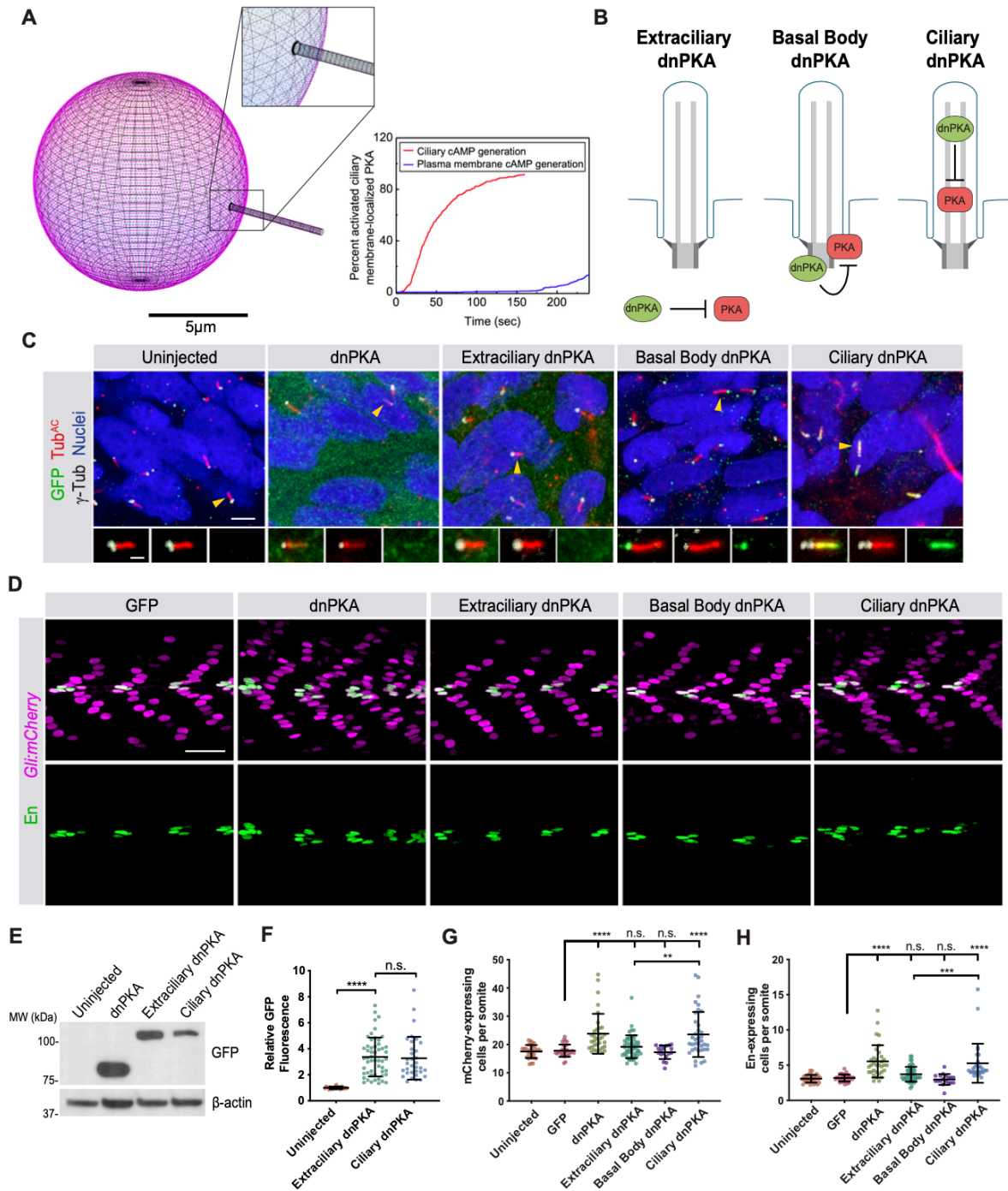


Figure 11. PKA acts at cilia to regulate HH signal transduction *in vivo*

(A) Modeling differential ciliary membrane localized PKA activation upon cAMP generated at either the ciliary membrane or at the plasma membrane. Left panel, simulated distribution of PKA localization to the plasma membrane and cilium (inset). Scale bar, 5 μ m. Right panel depicts the

percent of activated ciliary membrane localized PKA upon either ciliary membrane or plasma membrane cAMP generation.

(B) Schematic of tools to inhibit PKA at distinct subcellular locations. Dominant negative PKA (dnPKA), a form of PKA-R that constitutively binds and inhibits PKA-C, was fused to RAB23 S23N to prevent it from localizing to cilia (Extraciliary dnPKA). dnPKA was fused to RAB23 Q68L to localize it to cilia (Ciliary dnPKA). dnPKA was fused to 2x-PACT to localize it to the basal body (Basal Body dnPKA).

(C) Immunofluorescence imaging of zebrafish somites either uninjected or expressing GFP-tagged untargeted dnPKA, Extraciliary dnPKA, Basal Body dnPKA, or Ciliary dnPKA. Images depict 24hpf somites stained for the GFP tag on dnPKA (green), cilia (Tub^{AC}, red), basal bodies (γ TUB, grayscale) and nuclei (Hoechst, blue). Arrowheads indicate cilia depicted in inset. Insets display overlay of dnPKA, cilia and basal bodies (left), overlay of cilia and basal bodies (middle), and dnPKA alone (right). Scale bars, 4 μ m and 1 μ m (inset).

(D) Immunofluorescence imaging of *Gli:mCherry*-transgenic somites expressing GFP alone or the indicated dnPKAs. Images depict 24hpf somites stained for En (green) and mCherry (magenta). Scale bar, 40 μ m.

(E) Immunoblot of lysates from 24hpf zebrafish embryo expressing indicated GFP-tagged forms of dnPKA. Blotting for β -actin controls for loading.

(F) Relative GFP fluorescence of control uninjected embryos, Extraciliary dnPKA-expressing embryos and Ciliary dnPKA-expressing embryos. Fluorescence was normalized to the mean of uninjected embryos. Data are represented as means \pm SD.

(G) Quantification of *Gli:mCherry*-expressing cells per somite of uninjected embryos, and those expressing GFP, untargeted dnPKA, Extraciliary dnPKA, Basal Body dnPKA, or Ciliary dnPKA. Each point represents the number of mCherry-expressing cells averaged over four somites per embryo. Cells in somites 12 through 15 were counted and an average value of cells per somite was determined for each embryo. The average values per embryo were used as individual data points in all graphs and statistical analyses.

(H) Quantification of En-expressing MPs per somite of uninjected embryos, and those expressing GFP, untargeted dnPKA, Extraciliary dnPKA, Basal Body dnPKA, or Ciliary dnPKA. For Basal Body dnPKA-expressing embryos, n=18 and for all other conditions, n>30 from three independent injections. Significance was determined via one-way ANOVA followed by Tukey's multiple comparison test. A p value less than 0.05 was considered statistically significant and is denoted as follows: *<0.05, **<0.01, ***<0.001, and ****<0.0001. Data are represented as means \pm SD.

extraciliary cAMP even without barriers to its intracellular movement, we constructed a computational model of a ciliated cell and modeled the kinetics of how ciliary and extraciliary cAMP activate a cAMP effector protein, such as PKA, at the cilium (**Figure 11A** and **Figure 12A**).

Our model illustrated that the approximately 13-fold greater surface to volume ratio of the cilium can account for more efficient activation of a ciliary cAMP effector protein by ciliary cAMP than by nonciliary cAMP (**Figure 11A** and **Figure 12A-C**). Interestingly, this difference in effector sensitivity did not require differences in ciliary and nonciliary diffusion or PKA concentrations but did depend on both ciliary length and diameter (**Figure 12D,E**). Thus, the different geometries of

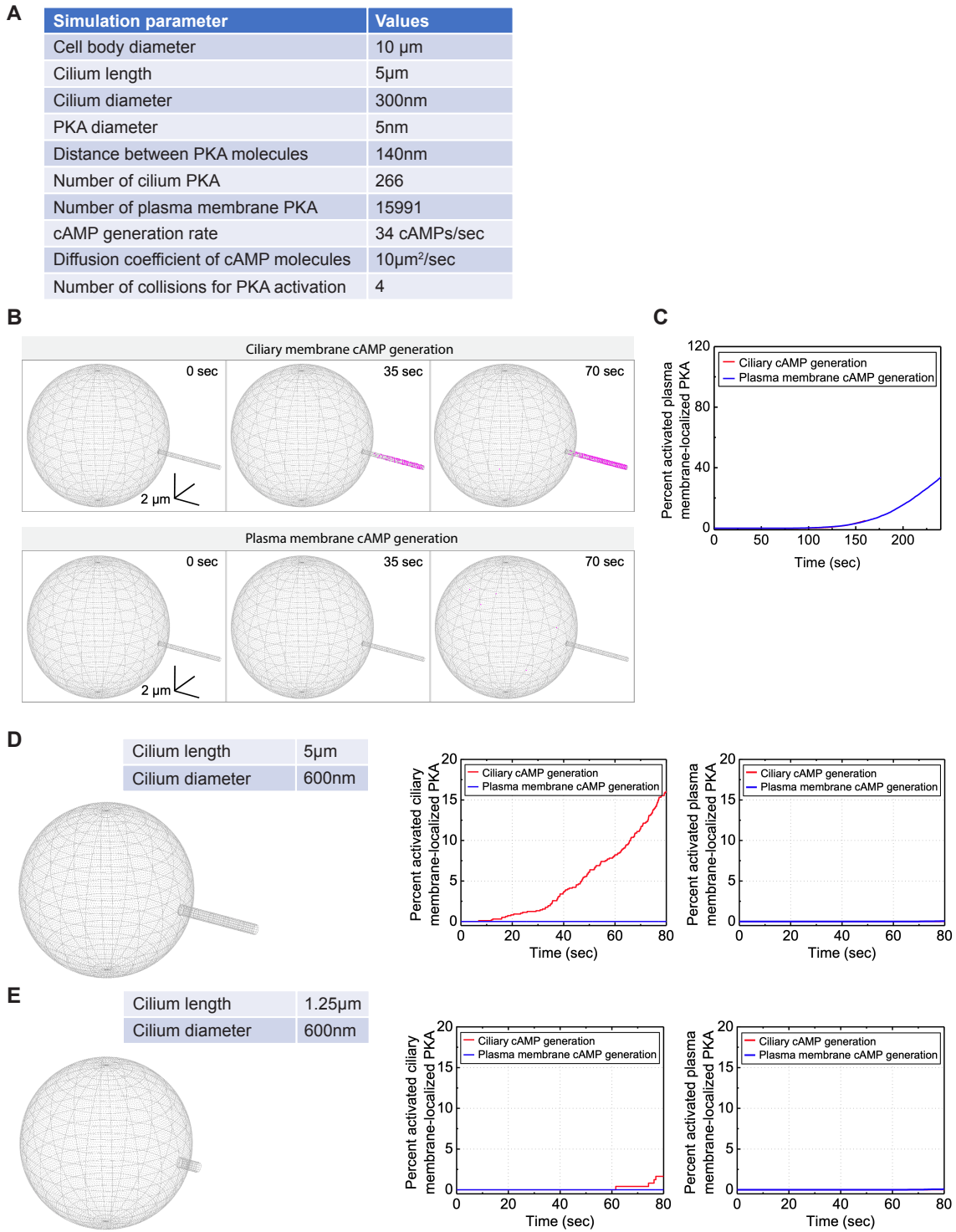


Figure 12. Modeling of PKA at the ciliary and plasma membrane upon ciliary and plasma membrane cAMP generation

(A) Simulation parameters used. The distance between PKA molecules in the ciliary and plasma membranes is equal.

(B) Graphical depiction of PKA activation upon either ciliary membrane or plasma membrane cAMP generation. Grey points indicate inactive PKA. Magenta points indicate PKA computed to have bound 4 cAMP molecules and thus be active. Scale bar, 5 μ m.

(C) Percent of activated plasma membrane PKA following either ciliary (red) or plasma membrane (blue) cAMP generation, as a function of time (compare to **Figure 11A**).

(D) The model was re-run with a doubling of ciliary diameter (with a concomitant fourfold increase in ciliary volume). Percent of activated ciliary membrane (middle) and plasma membrane (right) PKA following either ciliary (red) or plasma membrane (blue) cAMP generation, as functions of time. Increasing ciliary diameter is predicted to compromise the difference between ciliary PKA activation by ciliary and plasma membrane cAMP (compare to **Figure 11A**).

(E) To model the effects of changing ciliary diameter and volume separately, the model was re-run with the larger ciliary diameter, but keeping ciliary volume equal to the original model described in **Figure 12A** by reducing ciliary length. Percent of activated ciliary membrane (middle) and plasma membrane (right) PKA following either ciliary (red) or plasma membrane (blue) cAMP generation, as functions of time. Decreasing ciliary length is predicted to further compromise the difference between ciliary PKA activation by ciliary and plasma membrane cAMP.

the cilium and cell body may allow cells to differentially activate cAMP effector proteins at the cilium and cell body.

One prediction of this computational model is that producing supraphysiological levels of cAMP will overcome the geometric differences preventing cytoplasmic cAMP from triggering ciliary effectors (**Figure 13A-C**). To test this prediction, we shined more light on Cilia-bPAC- or Cyto-bPAC-expressing zebrafish embryos. Increasing the amount of blue light delivered to Cilia-bPAC-expressing zebrafish embryos 5.4-fold or 13.4-fold further reduced the number of En-expressing somite cells, and blocked En-expressing cell formation at the high level (**Figure 13D**). As predicted by the model, stimulating Cyto-bPAC-expressing zebrafish embryos with more light attenuated the number of En-expressing somite cells (**Figure 13D**). Interestingly, even at the highest amount of light, Cilia-bPAC more potently inhibited the induction of En-expressing cells (**Figure 13D**). Similarly, in Cilia-DREADD-expressing NIH/3T3 cells, treatment with 20-fold increased concentrations of CNO further inhibited *Gli1* induction in response to SAG (**Figure 13E**). As predicted by the model, treatment with high concentrations of CNO also attenuated relative *Gli1* induction in response to SAG in PM-DREADD cells (**Figure 13E**). These results suggest that differential interpretation of cAMP generated inside and outside of the cilium can be

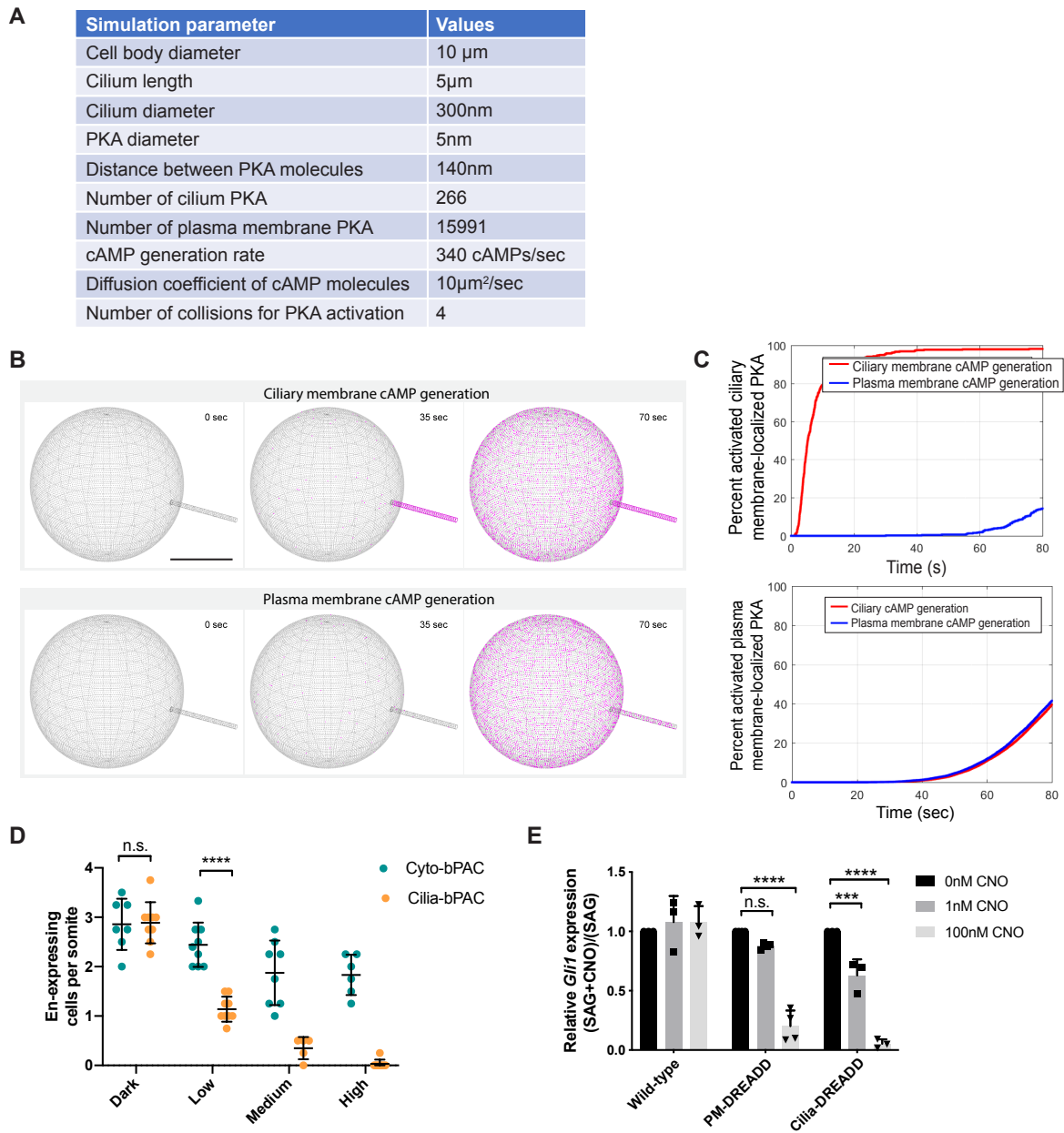


Figure 13. Modeling of PKA at the ciliary and plasma membrane upon supraphysiological levels of ciliary and plasma membrane cAMP generation

(A) Simulation parameters used to model PKA activation upon high levels of cAMP production.

(B) Graphical depiction of PKA activation upon high levels of either ciliary membrane or plasma membrane cAMP generation. Grey points indicate inactive PKA. Magenta points indicate PKA computed to have bound 4 cAMP molecules and thus be active. Scale bar, 5 μm .

(C) Percent of activated ciliary membrane- (top panel) or plasma membrane- (bottom panel) localized PKA upon 340 cAMPs/second generation at either ciliary or plasma membranes.

(D) Quantification of En-expressing somitic cells in Cyto-bPAC and Cilia-bPAC transgenic zebrafish embryos stimulated with low (0.065 mW/cm^2 , as utilized in **Figure 2**), medium (0.35 mW/cm^2), or high (0.87 mW/cm^2) intensity blue light from 14-18hpf. Each data point

represents the average number of En-expressing cells per somite 12 through 15 per 24hpf embryo. Statistical significance was assessed using a two-way ANOVA followed by Tukey's multiple comparison test. A p value less than 0.05 was considered statistically significant and is denoted as follows: * <0.05 , ** <0.01 , *** <0.001 , and **** <0.0001 . Data are represented as means \pm SD.

(D) Ratios of *Gli1* expression in WT and PM-DREADD- or Cilia-DREADD-expressing cells treated with 200nM SAG and indicated concentrations of CNO to *Gli1* expression treated with 200nM SAG alone. Significance was determined via one-way ANOVA followed by Tukey's multiple comparison test. A p value less than 0.05 was considered statistically significant and is denoted as follows: *** <0.001 , and **** <0.0001 . Data are represented as means \pm SD.

overwhelmed by high, possibly supraphysiological concentrations of cAMP.

As the model suggested that even in the absence of a barrier to cAMP diffusion, differences in geometry can account for differential activation of a ciliary cAMP effector by cilium- and nonciliary-generated cAMP, we investigated whether the cAMP effector PKA was present in the cilium. In its inactive state, PKA is comprised of regulatory (e.g., PKA-R1 α) and catalytic subunits (e.g., PKA-C α) bound to an A kinase anchoring protein (AKAP) (Taylor et al., 2012; Wong and Scott, 2004). To test whether PKA can localize to cilia, we co-expressed PKA-R1 α , PKA-C α and the previously described ciliary AKAP GPR161 in NIH/3T3 cells (Bachmann et al., 2016). Co-expressed PKA-R1 α and PKA-C α co-localized with GPR161 in cilia (**Figure 14A-C**), suggesting that a ciliary pool PKA may allow the cell to discriminate between ciliary and cytoplasmic cAMP.

Previous work suggested that PKA acts at the basal body to regulate HH output, as PKA antibody staining shows an enrichment at the ciliary base (Barzi et al., 2009; Tuson et al., 2011). To test where within the cell PKA regulates HH signal transduction, we targeted dominant negative PKA (dnPKA), a constitutively repressive version of PKA-R1 that is insensitive to cAMP (Clegg et al., 1987; Ungar and Moon, 1996), to three subcellular locations: the basal body, the cilium and outside of the cilium (**Figure 11B**). More specifically, we targeted dnPKA to the basal body by fusing it to tandem PACT domains (Gillingham and Munro, 2000). To target dnPKA

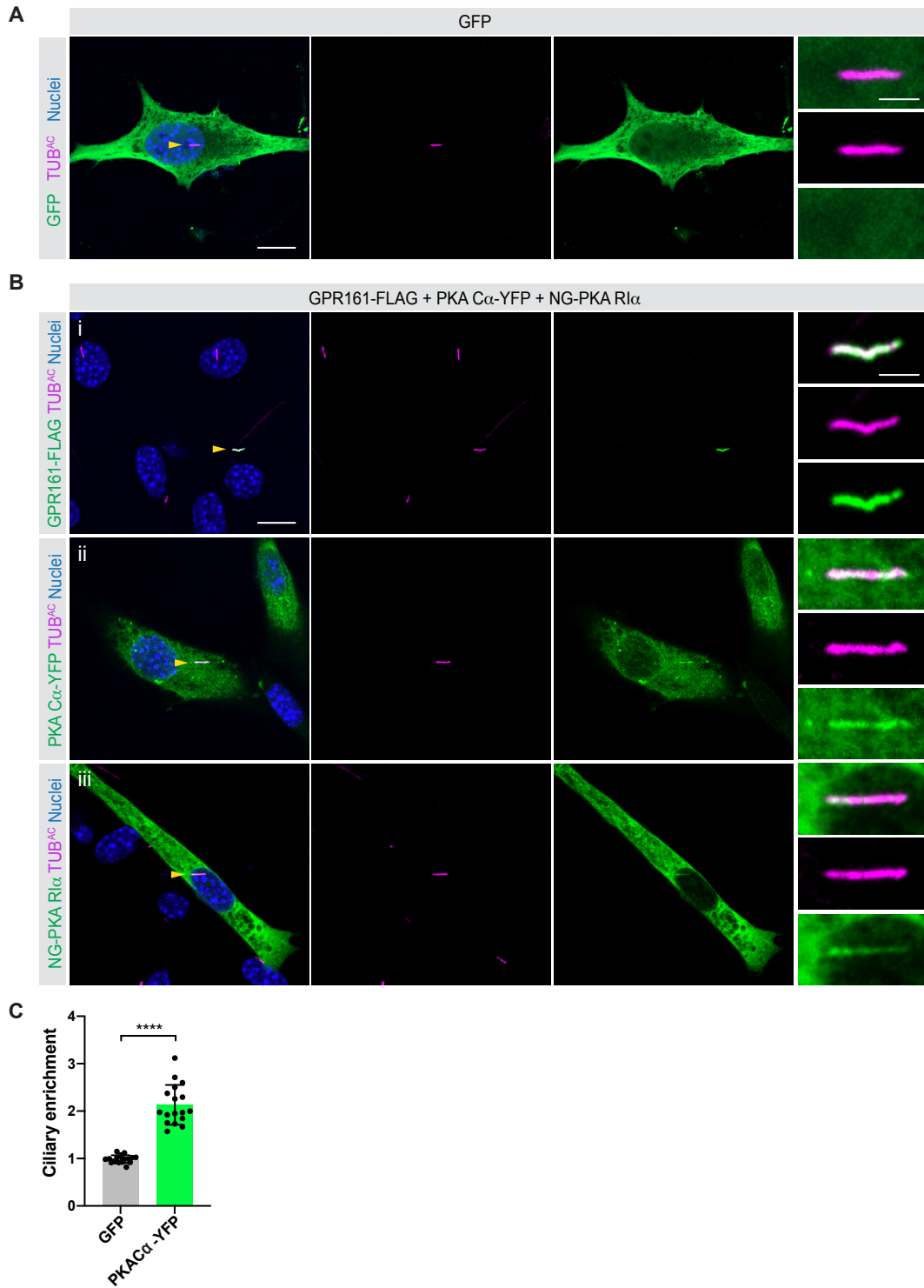


Figure 14. PKA localizes to cilia

(A) Immunofluorescence imaging of NIH/3T3 cells transfected with GFP alone and stained for GFP and cilia (TUB^{AC}). Nuclei are stained with Hoechst. Arrowheads indicate cilia depicted in inset. Scale bars, 10 μ m and 2 μ m (inset).

(B) NIH/3T3 cells were co-transfected with GPR161-FLAG, PKA-C α -YFP, and NeonGreen-PKA-Rl α and stained for cilia (TUB^{AC}) and indicated constructs: **(i)** GPR161-FLAG (FLAG), **(ii)** PKA C α -YFP (YFP), **(iii)** NG-PKA Rl α (NeonGreen). Nuclei are stained with Hoechst. Yellow arrowheads indicate cilia depicted in inset. Scale bars, 10 μ m and 2 μ m (inset).

(C) Quantification of relative ciliary enrichment of PKA-C α -YFP compared to GFP alone. n=18 cells from 3 independent experiments. Significance was determined via two-tailed unpaired t-test. p values less than 0.05 were considered statistically significant and are denoted as follows: ****<0.0001. Data are represented as means \pm SD.

to the cilium, we fused it to RAB23 Q68L, which constitutively localizes to cilia (Lim and Tang, 2015). To exclude dnPKA from the cilium, we fused it to RAB23 S23N, which localizes to the cell body (Leaf and von Zastrow, 2015). Expression of either RAB23 S23N or RAB23 Q68L by themselves in zebrafish did not affect somite patterning (**Figure 15A-C**). To assess the subcellular localization of the targeted forms of dnPKA, we expressed GFP-tagged versions in zebrafish embryos and assessed subcellular localization. As anticipated, dnPKA-GFP-2x-PACT localized to the ciliary base, dnPKA-GFP-RAB23 Q68L localized to cilia, and dnPKA-GFP-RAB23 S23N was extraciliary (**Figure 11C**). Therefore, we subsequently refer to these three forms of dnPKA as Basal body dnPKA, Ciliary dnPKA and Extraciliary dnPKA, respectively.

We hypothesized that, if ciliary PKA responds to ciliary cAMP to inhibit HH signaling, then blocking PKA within the cilium, but not at the basal body or outside the cilium, would activate the HH pathway. To begin to test this hypothesis, we assessed how inhibiting different subcellular pools of PKA affected the *Gli:mCherry* reporter of HH signaling in zebrafish embryos. Consistent with earlier reports, expression of GFP alone did not affect HH pathway activity and expression of untargeted dnPKA-GFP increased HH pathway activity (**Figure 11D,G**) (Barresi et al., 2000; Du et al., 1997). Neither Basal body dnPKA nor Extraciliary dnPKA affected *Gli:mCherry* reporter activity (**Figure 11D,G**). In contrast, expression of equivalent amounts of Ciliary dnPKA, as assayed by immunoblot and immunofluorescence quantification, expanded *Gli:mCherry* reporter activity (**Figure 11D-G**).

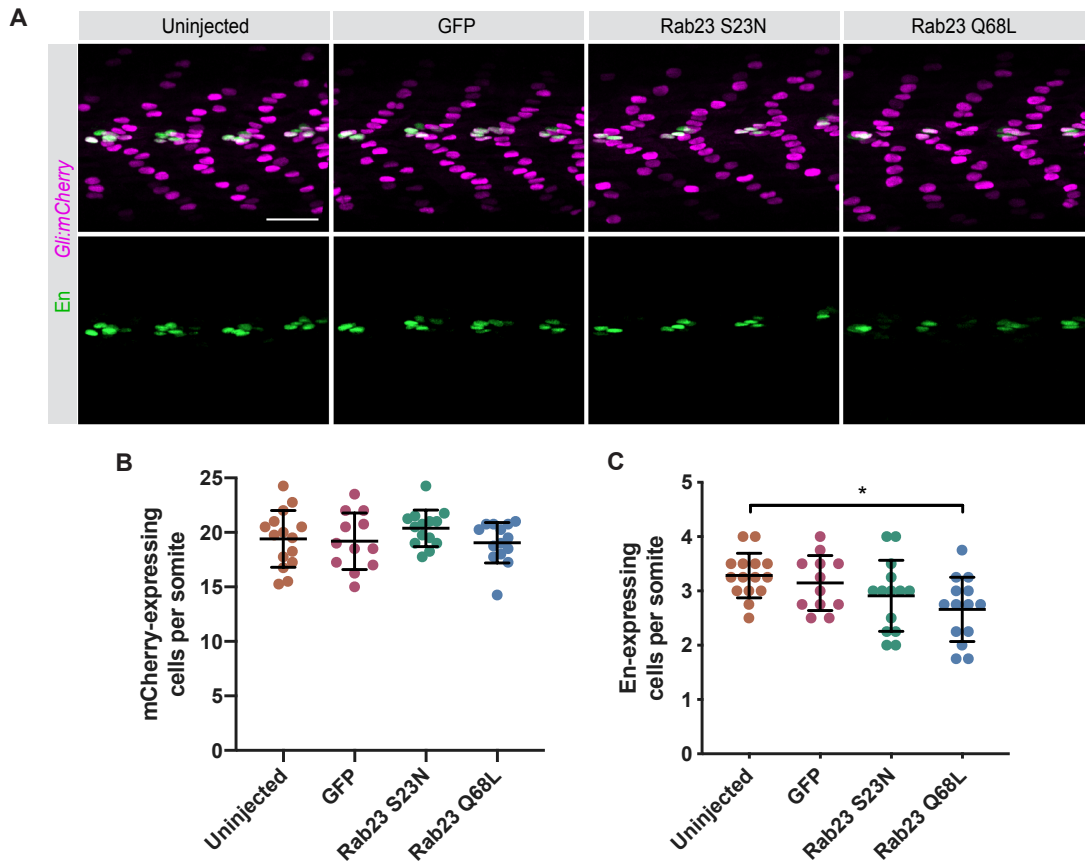


Figure 15. RAB23 misexpression does not expand zebrafish somite HH signaling or HH-dependent fates

(A) Immunofluorescence imaging of somites 12-15 in *Gli:mCherry* transgenic embryos expressing GFP alone, RAB23 S23N, or RAB23 Q68L. Images depict 24hpf somites stained for MPs (En, green) or mCherry (magenta).

(B) Quantification of *Gli:mCherry*-expressing cells per somite of uninjected embryos, and those expressing GFP, RAB23 S23N, or RAB23 Q68L. mCherry-expressing cells in somites 12 through 15 were counted and the average per somite determined for each embryo.

(C) Quantification of En-expressing MPs per somite of uninjected embryos, and those expressing GFP, RAB23 S23N, or RAB23 Q68L. $n > 12$ embryos quantified from two injections. Significance was determined by one-way ANOVA followed by Tukey's multiple comparison test. p values less than 0.05 were considered statistically significant and are denoted as follows: $* < 0.05$. Data are represented as means \pm SD.

To assess whether ciliary PKA regulates, in addition to HH signal transduction, HH-mediated patterning, we examined whether inhibiting PKA in different subcellular locations affects somite patterning. Consistent with previous reports, expression of untargeted dnPKA-GFP

increased the number of En-expressing cells per somite (**Figure 11D,H**) (Hammerschmidt et al., 1996). Extraciliary and Basal body dnPKA did not affect numbers of En-expressing cells. In contrast, Ciliary dnPKA increased En-expressing cells (**Figures 11D,H**). As inhibiting PKA in the cilium, but not elsewhere, activates GLI-dependent transcription and increases a HH-dependent fate, we conclude that a ciliary pool of PKA specifically regulates the HH pathway.

Ciliary PKA interprets ciliary cAMP

As we had found that ciliary PKA controls HH signal transduction, we hypothesized that ciliary PKA specifically interprets ciliary cAMP. However, *Drosophila* PKA acts in the HH pathway independent of cAMP (Jiang and Struhl, 1995). We predicted that if vertebrate ciliary PKA acts differently from *Drosophila* PKA and interprets ciliary cAMP levels, inhibiting ciliary PKA, but not extraciliary PKA, would restore HH-dependent cell fates suppressed by ciliary cAMP.

To begin to test the hypothesis that vertebrate PKA interprets ciliary cAMP, we made use of Cilia-bPAC transgenic embryos. Consistent with prior results, light-stimulated Cilia-bPAC transgenic embryos formed fewer HH-dependent high En-expressing cells than Cilia-bPAC transgenic embryos not stimulated with light (**Figure 16A,B**). Injection of untargeted *dnPKA-GFP* mRNA into Cilia-bPAC embryos stimulated with light restored the number of high En-expressing cells. Thus, cAMP affects HH-dependent patterning through activating PKA.

To address whether ciliary and extraciliary PKA respond differently to cilium- and cytoplasm-produced cAMP, we injected Cilia-bPAC transgenic embryos with mRNA encoding Basal Body, Extraciliary or Ciliary dnPKA and stimulated them with light. Expression of Basal Body or Extraciliary dnPKA did not restore En-expressing cells. In contrast, expression of Ciliary dnPKA specifically restored formation of En-expressing cells in Cilia-bPAC transgenic embryos treated with light (**Figures 16A,B**). These data demonstrate that ciliary PKA interprets ciliary cAMP to regulate vertebrate HH signal transduction *in vivo*.

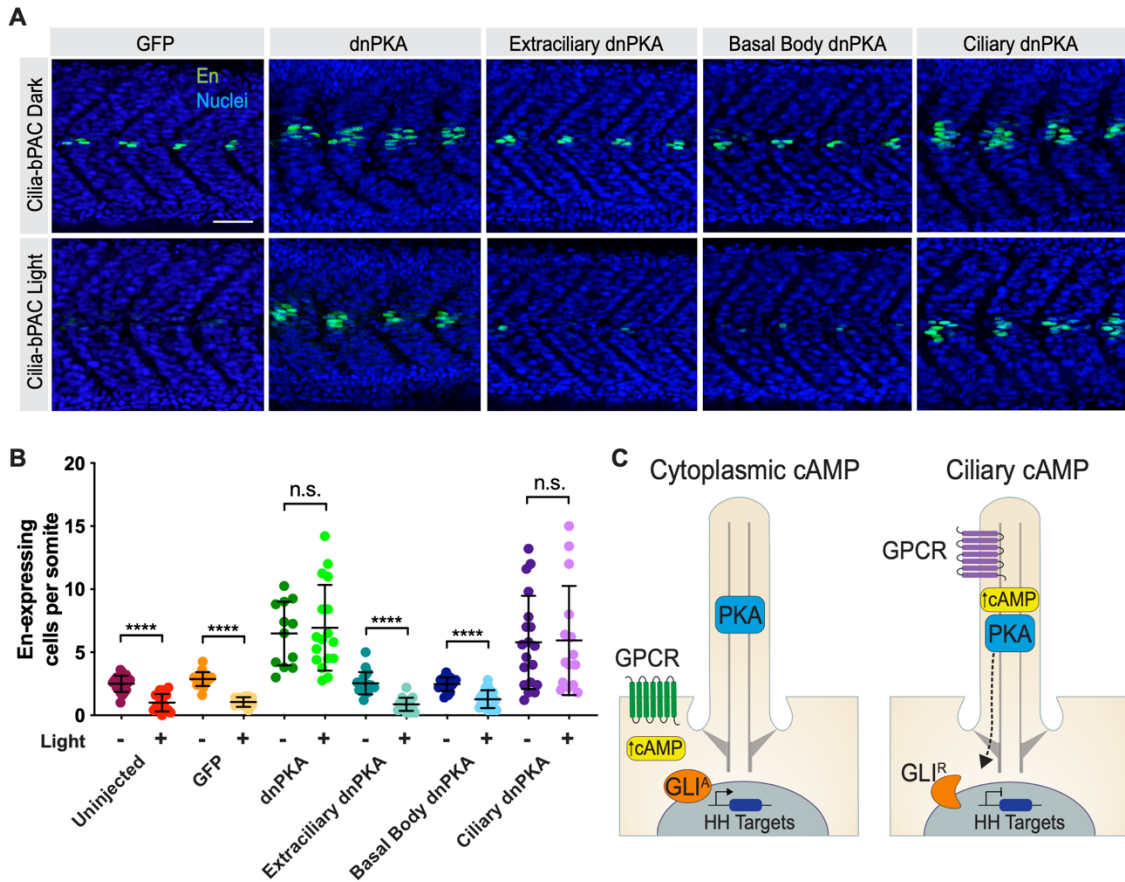


Figure 16. Ciliary PKA interprets ciliary cAMP to inhibit HH signal transduction

(A) Immunofluorescence imaging of Cilia-bPAC transgenic embryos expressing GFP, untargeted dnPKA, Extraciliary dnPKA, Basal Body dnPKA, or Ciliary dnPKA and either raised in the dark or stimulated with light. Images depict 24hpf somites stained for MPs (En, green) and nuclei (Hoechst, blue). Scale bar, 40µm.

(B) Quantification of En-expressing cells per somite. Dark bars indicate embryos raised in the dark. Light bars indicate embryos stimulated with light. n=12-20 embryos per condition, from three independent injections. Statistical significance was assessed using a two-tailed unpaired t-test to compare dark- and light-treated embryos for each construct. A p value less than 0.05 was considered statistically significant and is denoted as follows: *<0.05, **<0.01, ***<0.001, and ****<0.0001. Data are represented as means ± SD.

(C) Schematic model of how ciliary cAMP and PKA regulate HH signal transduction. Ciliary cAMP regulated by ciliary GPCRs locally activates a pool of ciliary PKA, which phosphorylates GLI to generate its transcriptional repressor form (GLI^R). Equivalent amounts of cAMP produced by GPCRs in the plasma membrane do not activate ciliary PKA. Thus, upon HH stimulation and in the absence of ciliary PKA activity, GLI assumes its transcriptional activator form (GLI^A) and induces HH target genes in the nucleus.

DISCUSSION

The primary cilium transduces some forms of intercellular signaling, including signaling via the HH pathway and select ciliary GPCRs (Gigante and Caspary, 2020). Ciliary signals are transduced through diffusible second messengers, such as cAMP and calcium, that are shared with nonciliary signaling, raising the question of whether cells distinguish ciliary and extraciliary signaling. To investigate whether cells distinguish ciliary and extraciliary cAMP, we engineered novel optogenetic and chemogenetic tools that enable precise spatiotemporal control of cAMP production or GPCR activation specifically inside or outside of cilia.

Using the optogenetic tools in mammalian cells or zebrafish development revealed that activating cAMP production in cilia, but not outside cilia, preferentially inhibited HH signal transduction and HH-dependent cell fate specification *in vivo*. Similarly, in mammalian cells, generating cAMP in cilia, but not outside cilia, inhibited HH signal transduction. Thus, cilia-generated cAMP is functionally distinct from cAMP produced in the cytoplasm, and the information content of cAMP depends on its site of origin.

The conventional view of GPCR signaling is that coupling to heterotrimeric G proteins occurs at the plasma membrane (Neves et al., 2002). The primary ciliary membrane is contiguous to, but compositionally distinct from, the plasma membrane. To directly test how ciliary and plasma membrane GPCRs may function differently, we engineered a $G\alpha_s$ -coupled DREADD localized to either the ciliary or plasma membranes. Interestingly, we found that only ciliary DREADD activation inhibited HH target gene induction. Thus, both subcellularly targeted bPAC and DREADDs reveal that the cell distinguishes between cilium-generated and nonciliary cAMP (**Figure 16C**).

We conclude that, by discriminating between ciliary and plasma membrane production of cAMP, cells independently interpret GPCR-mediated information in these two compartments even though both are transduced through a common, diffusible second messenger. In addition to SSTR3 and GPR161, approximately 30 GPCRs localize to primary cilia (Hilgendorf et al., 2016;

Mykytyn and Askwith, 2017). We previously demonstrated that one of these, MC4R, operates at the primary cilia of hypothalamic neurons to trigger satiety and control feeding behavior (Siljee et al., 2018). We propose that the dependence of MC4R and other cilium-localized GPCRs on the cilium reflects the fact that their physiological effects are mediated, like HH patterning, specifically by ciliary cAMP.

One possible explanation for how cells differentially interpret equivalent amounts of cAMP produced in the cilium or cytoplasm would be if the ciliary transition zone, in addition to controlling protein trafficking between the cilium and cell body, also prevented the free diffusion of cAMP. However, the use of the Ciliary Pink Flamingo cAMP biosensor revealed that no barrier to cAMP diffusion exists. Instead, our computational model suggested that ciliary PKA can be specifically activated by ciliary cAMP to generate specific outputs, such as modulating HH signal transduction. Generating an equal amount of cAMP in the cilium or cytoplasm is expected to result in a higher local concentration in the cilium due to the approximately 5,000-fold difference in volume. Thus, even in the absence of a barrier to the free diffusion of cAMP separating the two compartments or differences in PKA concentration, ciliary PKA is differentially sensitive to ciliary cAMP.

In addition, as adenylyl cyclases are integral membrane proteins and the ratio of membrane area to cytosol volume is higher for a cylindrical cilium than for a spherical cell, the different geometries of the two compartments are also expected to contribute to differential sensitivity of ciliary PKA to ciliary cAMP. Our modeling further suggests that the length and diameter of the cilium tunes the cell's differential sensitivity to ciliary and nonciliary cAMP. Similarly, modeling of neurons indicates that the length and diameter of dendrites and their spines affects cAMP-regulated calcium dynamics (Neves et al., 2008; Ohadi and Rangamani, 2019). While the model we computed does not incorporate the possibility that different adenylyl cyclases generate different basal levels of cAMP in the cell body and cilium, nor account for the possibility of differential sensitivity of PKA to cAMP (Jiang et al., 2019; Koschinski and Zaccolo; Moore et al., 2016), it does indicate that differences in geometry can explain how different subcellular

locales can impart different information to the cell, even if the locales are contiguous and the information is diffusible.

PKA is a prominent effector of cAMP and an evolutionarily conserved regulator of the HH pathway (Hammerschmidt et al., 1996; Jiang and Struhl, 1995; Li et al., 1995). PKA prominently localizes to the basal body, where it has been proposed to inhibit the HH pathway (Tuson et al., 2011). Previous proteomics studies have identified PKA subunits in cilia (Bachmann et al., 2016; Mick et al., 2015). To test whether PKA acts at the basal body or cilium to interpret ciliary cAMP, we targeted dnPKA to the basal body, the cilium, or outside of cilia in zebrafish embryos. Whereas inhibiting PKA outside the cilium or at the basal body had no effect on HH signal transduction, blocking PKA within the cilium specifically activated HH signal transduction and expanded HH-dependent cell fates. Moreover, blocking PKA in the cilium restored MPs suppressed by Cilia-bPAC stimulation indicating that a functionally distinct pool of PKA within the cilium interprets ciliary cAMP. Importantly, blocking PKA in the cilium was sufficient to perturb HH signaling downstream of endogenous cAMP concentrations in the developing embryo.

We conclude that a ciliary pool of PKA is regulated specifically by ciliary cAMP to control HH signal transduction, and this local interpretation allows ciliary and extraciliary cAMP to impart different information to the cell. Ultimately, it is likely that ciliary PKA activity is communicated to the cell via regulation of GLI transcription factors that move from the cilium to the nucleus (**Figure 6C**) (Aza-Blanc et al., 1997; Méthot and Basler, 1999; Niewiadoski et al., 2013; Price and Kalderon, 1999; Wang et al., 1999). Consistent with this possibility, we found that generating cAMP in the cilium specifically affected GLI3 proteolytic processing. The finding that ciliary cAMP promotes GLI3 processing does not exclude the possibility that ciliary cAMP also inhibits GLI2 activation, especially as the fates inhibited by ciliary cAMP in the somite and neural tube partially depend on GLI2 activation (Karlstrom et al., 2003; Tyurina et al., 2005). It will be interesting to assess whether other second messengers use specific local effectors to distinguish the information content of different subcellular pools. Calcium may be another example, as it, like

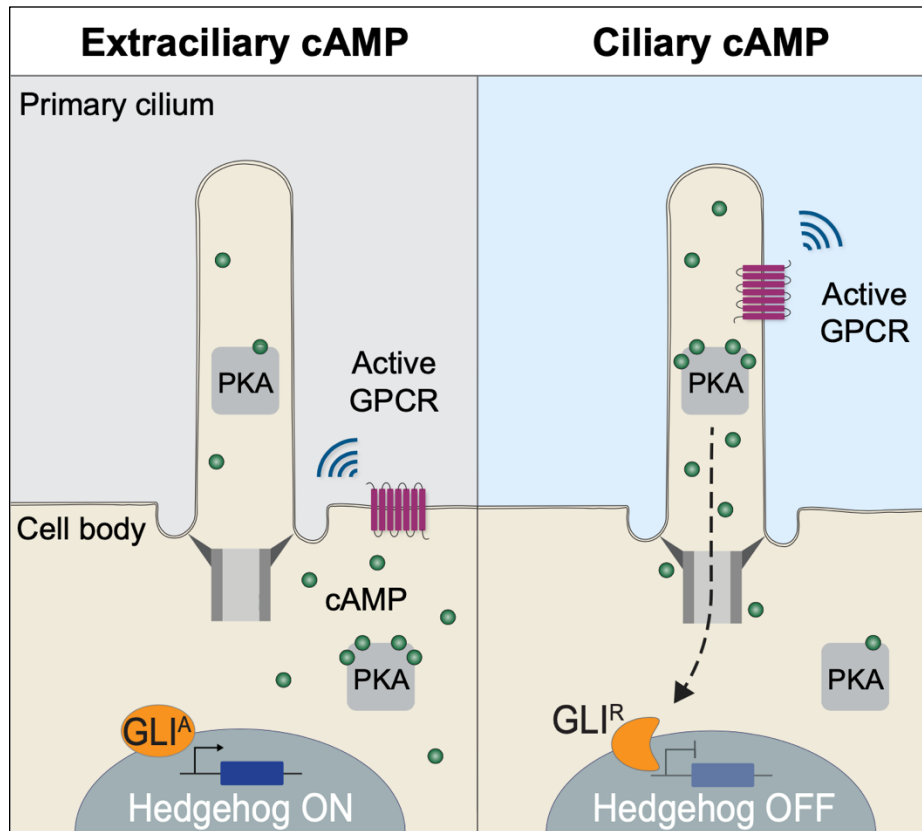


Figure 17. Summary figure

Using optogenetic and chemogenetic methods, we found that ciliary cAMP is differentially interpreted than cAMP generated in the cytoplasm. Ciliary cAMP and GPCR activity preferentially inhibited HH-dependent patterning and transcriptional targets both in zebrafish and mammalian cells through preferential activation of a ciliary pool of PKA.

cAMP, diffuses and its concentration within the cilium and cell body can be independently regulated to have distinct biological effects (Delling et al., 2013; McGrath et al., 2003; Nonaka et al., 1998; Pazour et al., 2002; Pennekamp et al., 2002; Yoshida et al., 2012).

This work reveals that ciliary cAMP, but not cytoplasmic cAMP, preferentially inhibits HH signaling *in vivo*. Ciliary cAMP activates PKA in the cilium to modulate HH signaling (**Figure 17**). More generally, our results reveal that cells differentially interpret cAMP generated in different subcellular domains, allowing for a shared second messenger to denote different meanings to the cell.

Limitations of the Study

The mathematical model of activation of PKA by ciliary and nonciliary cAMP assumed that the diffusion constant of cAMP in zebrafish cilia is similar to that measured in mammalian cytoplasm and that ciliary ATP is not limiting. Moreover, our model did not incorporate phosphodiesterase function, as the k_{cat} , V_{max} and subcellular locale of many phosphodiesterases are poorly defined. To investigate the ciliary and nonciliary functions of cAMP and PKA, we used multiple orthogonal tools that we localized to cilia, cytosol or plasma membrane using a variety of mechanisms. A small proportion of each may not localize to the principal subcellular location, and this subpopulation may contribute to the observed outputs. The recapitulation of key results using bPAC, a GPCR (SSTR3) and chemogenetic tools (DREADDs) suggests that levels of ciliary cAMP generated in this work are physiological. Confirming that the experimentally produced ciliary cAMP levels are physiological will require measuring ciliary cAMP concentrations in cilia under different signaling conditions.

MATERIALS AND METHODS

Table 1. Key Resource Table

Table 1 describes key resources and primers used in this study.

REAGENT or RESOURCE	SOURCE	IDENTIFIER
Antibodies		
Rabbit anti-TUB ^{AC}	Cell Signaling	Cell Signaling Technology Cat# 5335; RRID:AB_10544694
Rabbit anti-mCHERRY	Abcam	Abcam Cat# ab167453; RRID:AB_2571870
Mouse anti-ENG	Developmental Studies Hybridoma Bank	DSHB Cat# 4D9 anti-engrailed/inveccted; RRID:AB_528224
Rabbit anti-PROX1	EMD Millipore	Millipore Cat# AB5475; RRID:AB_177485
Goat anti-GFP	Rockland	Rockland Cat# 600-101-215; RRID:AB_218182
Mouse anti- γ TUB	Sigma Aldrich	Sigma-Aldrich Cat# T6557; RRID:AB_477584
Mouse anti-ARL13B	UC Davis/NIH Neuromab Facility	UC Davis/NIH NeuroMab Facility Cat# 73-287; RRID:AB_11000053
Mouse anti-SMO	Santa Cruz	Santa Cruz Biotechnology Cat# sc-166685; RRID:AB_2239686
Mouse anti-TUB ^{AC}	Sigma Aldrich	Sigma-Aldrich Cat# T6793; RRID:AB_477585
Rabbit anti-GPR161	Proteintech	Proteintech Cat# 13398-1-AP; RRID:AB_2113965
Goat anti-MYC	Novus	Novus Cat# NB600-335; RRID:AB_10002720
Rabbit anti-FOP	Proteintech	Proteintech Cat# 11343-1-AP; RRID:AB_2103362
Mouse anti-FLAG, clone M2	Sigma Aldrich	Sigma-Aldrich Cat# P2983; RRID:AB_439685
Mouse anti-mNeonGreen	ChromoTek	ChromoTek Cat# 32f6-100; RRID:AB_2827566
Donkey secondary antibodies for immunofluorescence	ThermoFisher Scientific	N/A
Hoechst 33342	ThermoFisher Scientific	CAT# H2570
Goat anti-GLI3	R&D Systems	R&D Systems, Cat # AF3690
Mouse anti- β -actin	Proteintech	Proteintech, Cat# 66009-1-Ig; RRID:AB_2687938
Mouse anti-GAPDH	Proteintech	Proteintech, Cat# 60004-1-Ig; RRID:AB_2107436
Goat secondary HRP conjugated antibodies	Jackson ImmunoResearch Laboratories, Inc	N/A
Chemicals, Peptides, and Recombinant Proteins		
Forskolin	Cayman Chemical	CAS# 66575-29-9, CAT# 11018
3-isobutyl-1-methylxanthine (IBMX)	Millipore Sigma	CAS# 28822-58-4, CAT# 15879
SAG	Millipore Sigma	CAS# 364590-63-6, CAT# 566660
Clozapine N-oxide	Abcam	CAS# 34233-69-7, CAT# ab141704
Somatostatin	Millipore Sigma	CAS# 38916-34-6, CAT# S1763
SiR-Tubulin	Spirochrome	CAT# CHF420.00

REAGENT or RESOURCE	SOURCE	IDENTIFIER
Hygromycin	Thermo Fisher Scientific	CAT# 10687010
Puromycin	EMD Millipore	CAT# 5.08838.0001
DMSO	ATCC	CAT# ATCC 4-X
Critical Commercial Assays		
mMessage Machine Sp6 Transcription Kit	ThermoFisher	CAT# AM1340
RNeasy Plus Mini Kit	Qiagen	CAT# 74136
iSCRIPT cDNA synthesis Kit	Bio-Rad	CAT# 74136
cAMP ELISA	Enzo	CAT# ADI-901-066
Experimental Models: Cell Lines		
G _s -DREADD-EGFP	This paper	N/A
G _s -DREADD-ARL13B-EGFP	This paper	N/A
SSTR3-EGFP	Gift from Mark von Zastrow	N/A
EF1a-Cyto-bPAC-GFP	This paper	N/A
EF1a-Arl13b-bPAC-GFP	This paper	N/A
CRYS-Cyto-bPAC-GFP	This paper	N/A
CRYS-Arl13b-bPAC-GFP	This paper	N/A
CRYS-Cyto-bPAC-GFP + Pink Flamindo-mIFP-Rab23 Q68L	This paper	N/A
CRYS-Arl13b-bPAC-GFP + Pink Flamindo-mIFP-Rab23 Q68L	This paper	N/A
Flp-In NIH/3T3 Cell Line	ThermoFisher	CAT# R76107
Experimental Models: Organisms/Strains		
Zebrafish: <i>Tg(8xGli:mCherry-NLS-Odc1)</i>	Mich et al., 2014	N/A
Zebrafish: <i>Tg(Arl13b-bPAC-Myc)</i>	This paper	N/A
Zebrafish: <i>Tg(Cyto-bPAC-Myc)</i>	This paper	
Zebrafish <i>Danio rerio Ekkwill wildtype</i>	EkkWill Waterlife Resources	<i>EkkWill</i>
Oligonucleotides		
Cyto-bPAC R genotyping primer (TCGTAGTACTTCTGGGCCTCAT)	Integrated DNA Technologies	N/A
Cyto-bPAC F genotyping primer (GTCAACCGGTACTTCAGCATCT)	Integrated DNA Technologies	N/A
Cilia-bPAC F genotyping primer (AGATGACTGTGCTCCTGAGA)	Integrated DNA Technologies	N/A
Cilia-bPAC R genotyping primer (ACCAGGATTTTCTTGACAGCT)	Integrated DNA Technologies	N/A
Gli1 qPCR F primer (TTATGGAGCAGCCAGAGAGA)	Integrated DNA Technologies	N/A
Gli1 qPCR R primer (GAGCCCGCTTCTTTGTTAAT)	Integrated DNA Technologies	N/A
HPRT qPCR F primer (CATAACCTGGTTCATCATCGC)	Integrated DNA Technologies	N/A

REAGENT or RESOURCE	SOURCE	IDENTIFIER
HPRT qPCR R primer (TCCTCCTCAGACCGCTTTT)	Integrated DNA Technologies	N/A
RPLP0 qPCR F primer (TATAACCCTGAAGTGCTCGACA)	Integrated DNA Technologies	N/A
RPLP0 qPCR R primer (GCGCTTGTACCCATTGATGAT)	Integrated DNA Technologies	N/A
Recombinant DNA		
pPGKFLPobpA	Gift from Philippe Soriano, Addgene	CAT# 13793
pgLAP5-EF1 α -bPAC-GFP	This paper	N/A
pgLAP5-EF1 α -Arl13b-bPAC-GFP	This paper	N/A
pgLAP5-CRYS-bPAC-GFP	This paper	N/A
pgLAP5-CRYS-Arl13b-bPAC-GFP	This paper	N/A
pgLAP5	Gift from Peter Jackson, Addgene	CAT#19706
pgLAP5-G _s -DREADD-EGFP	Gift from Mark von Zastrow	N/A
pgLAP5-G _s -DREADD-ARL13B-EGFP	Gift from Mark von Zastrow	N/A
mApple-C1-Mini G _s	Gift from Roshanak Irannejad	N/A
pIRES-Neo3-SS-Flag-hGPR161	Gift from Mark von Zastrow	N/A
pcDNA3.1-PKAC	Gift from Roshanak Irannejad (Irannejad et al., 2017)	N/A
pEF5B-mNeonGreen-PKARI	Gift from Maxence Nachury (Mick et al., 2015)	N/A
pCS2+-dnPKA-GFP: linearize NotI, polymerase SP6	Gift from Randall Moon, Addgene	CAT# 16716
pCS2+-dnPKA-GFP-Rab23 Q68L: linearize NotI, polymerase SP6	This paper	N/A
pCS2+-dnPKA-GFP-Rab23 S23N: linearize NotI, polymerase SP6	This paper	N/A
pCS2+-dnPKA-GFP-2x PACT: linearize NotI, polymerase SP6	This paper	N/A
pEGFP-C1-RAB23 Q68L	Gift from Carol Wicking (Evans et al., 2003)	N/A

REAGENT or RESOURCE	SOURCE	IDENTIFIER
pCS2+-EGFP-Rab23 Q68L	This paper	N/A
pCS2+-EGFP-Rab23 S23N	This paper	N/A
6x Halo-EGFP-2x PACT	Gift from Michael Lampson (Akera et al., 2017), Addgene	CAT# 107265
pcDNA3.1-bPAC	Gift from Mark von Zastrow (Tsvetanova et al., 2014)	N/A
pcDNA3.1-Pink Flamindo	Gift from Tetsuya Kitaguchi (Harada et a., 2017), Addgene	CAT# 102356
mIFP	Gift from Xiaokun Shu (Yu et al., 2015), Addgene	CAT# 54620
pLVX-Pink Flamindo-mIFP-Rab23 Q68L	This paper	N/A
pCS2+-Arl13b-bPAC-6x Myc: linearize NotI, polymerase SP6	This paper	N/A
pCS2+-Arl13b V359A-bPAC-6x Myc: linearize NotI, polymerase SP6	This paper	N/A
<i>nkx2.2b</i> <i>in situ</i> probe: linearize BamHI, polymerase T7	Gift from Peng Huang	N/A
<i>olig2</i> <i>in situ</i> probe: linearize <i>BglII</i> , polymerase T3	Gift from Peng Huang	N/A
<i>pax3</i> <i>in situ</i> probe: linearize <i>NotI</i> , polymerase T7	Gift from Peng Huang	N/A
pTol2-Ubi-bPAC-Myc-6x Myc	This paper	N/A
pTol2-Ubi-ARL13B-bPAC-6x Myc	This paper	N/A
Software and Algorithms		
Adobe Illustrator version 24.1.0	Adobe Systems	https://www.adobe.com/products/illustrator.html
KiCad software suite	KiCad	https://www.kicad-pcb.org/
MATLAB R2020a	MathWorks	https://www.mathworks.com/products/matlab.html
Arduino IDE version 1.8.0	Arduino	https://www.arduino.cc/en/main/software
Fiji	Open Source	https://fiji.sc/
GraphPad Prism version 8	GraphPad Software	https://www.graphpad.com/scientific-software/prism/

EXPERIMENTAL MODEL AND SUBJECT DETAILS

Zebrafish husbandry

Adult *Danio rerio* zebrafish were maintained under standard laboratory conditions. Embryos were maintained at 28°C and staged as described previously (Kimmel et al., 1995). Cyto-bPAC and Cilia-bPAC transgenic zebrafish were raised in the dark until 5 days post fertilization, and then maintained on a 14h light/10h dark cycle. Zebrafish of Ekkwill (EKW) background were used as wild type. Cyto-bPAC and Cilia-bPAC transgenic lines were maintained on an EKW background. *Gli:mCherry* (Tg(8xGliBS:mCherry-NLS-Odc1)) transgenic zebrafish were a gift from James Chen (Mich et al., 2014). Embryos were maintained in egg water containing 60µg/mL sea salt (Instant Ocean) in distilled water. For forskolin treatment, embryos were incubated in forskolin dissolved in DMSO from 6 hours post fertilization (hpf) until 24hpf. Embryos selected for experiments were 24hpf, a stage at which sex cannot be readily determined. All zebrafish protocols were approved by the Institutional Animal Care and Use Committee (IACUC) of the University of California, San Francisco.

Mammalian Cell culture

NIH/3T3 Flp-In cells (ThermoFisher Scientific) were cultured in Dulbecco's modified Eagle's medium with high glucose (Gibco Cat# 11965118) supplemented with 10% newborn bovine calf serum (Gibco Cat #16010159) and GlutaMAX supplement (Gibco Cat #35050061). Cells were grown in the absence of antibiotics. To induce ciliation, cells were grown to confluence and starved overnight in Opti-MEM reduced serum medium (UCSF Cell Culture Facility).

EXPERIMENTAL PROTOCOLS

Vector construction and mRNA synthesis

We amplified bPAC and full length human ARL13B (PfuUltra II, Stratagene) and cloned the amplicons into pDONR221 using BP Clonase II (ThermoFisher) to create pENTR-Cyto-bPAC-

6x Myc and pENTR-Cilia-bPAC-6x Myc. To generate transposons, we combined pENTR-Cyto-bPAC or pENTR-Cilia-bPAC with p5E-Ub, Tol2 and p3E-MT-pA using LR Clonase II Plus (ThermoFisher Scientific) (Kwan et al., 2007). Clones were verified by sequencing (Integrated DNA Technologies).

For generating NIH/3T3 Flp-In cell lines expressing bPAC, Cyto-bPAC-GFP and Cilia-bPAC-GFP were cloned into a version of pGLAP5 with a minimal chicken lens δ -crystallin promoter (Ye et al., 2018) using the In-Fusion HD cloning kit (Takara). To generate a red-shifted ratiometric ciliary cAMP sensor, Pink Flamindo was fused to monomeric infrared fluorescent protein (mIFP) and RAB23 Q68L using In-Fusion. mIFP and RAB23 Q68L were gifts from Xiaokun Shu and Carol Wicking, respectively (Evans et al., 2003; Yu et al., 2015). Both Ciliary Pink Flamindo and Pink Flamindo alone were cloned into lentiviral vector pLVX to generate pLVX-Pink Flamindo-mIFP-RAB23 Q68L and pLVX-Pink Flamindo, respectively. Lentivirus was generated using the Lenti-X packaging single shot kit according to the manufacturer's protocol (Takara).

For generating mRNA encoding ARL13B-bPAC-6xMyc, ARL13B-bPAC-6xMyc was cloned into the pCS2+8 expression vector using In-Fusion HD. The nonciliary control, ARL13B^{V359A}-bPAC-6x Myc, was subsequently generated by site-directed mutagenesis using In-Fusion. To generate ciliary, nonciliary, and basal body dnPKA constructs, Rab23 or tandem PACT domains were appended to the 3' end of pCS2+-dnPKA-GFP (Ungar and Moon, 1996) using In-Fusion. dnPKA is a PKA R1 α (Prkar1a) containing mutations at cAMP binding sites (Addgene #16716) (Clegg et al., 1987). 2x PACT was amplified from 6x Halo-EGFP-2x PACT (Addgene #107265). RAB23 Q68L and RAB23 S23N constructs were gifts from Carol Wicking. For zebrafish injections, we synthesized capped messenger RNA using the mMACHINE SP6 kit (Ambion) from pCS2+ constructs linearized with *NotI*.

Generation of stable cell lines

NIH/3T3 cell lines stably expressing Cyto-bPAC, Cilia-bPAC, PM-DREADD, Cilia-DREADD and SSTR3 were generated using the Flp-In system following manufacturer's instructions. In brief, Flp-In NIH/3T3 cells were transfected with Lipofectamine LTX with Plus reagent (Invitrogen Cat #A1262) with the appropriate plasmids and selected with 70 μ g/mL hygromycin (Gibco Cat #10687010), with the exception of clones expressing bPAC under the control of an attenuated promoter when 40 μ g/mL was used. Single colonies were expanded, and protein expression was confirmed by immunoblotting and fluorescence microscopy for GFP (1:1000, Rockland, RRID:AB_218182). Transient transfections were performed using Transit-X2 transfection reagents (Mirus Bio) according to manufacturer's instructions for NIH/3T3 cells.

To generate bPAC cell lines stably expressing Pink Flamindo-based cAMP biosensors, cells were transduced with lentivirus containing either Pink Flamindo or Ciliary Pink Flamindo in the presence of 4 μ g/mL polybrene and selected with 1 μ g/mL puromycin.

Generation of transgenic zebrafish and mRNA injection

Transgenic zebrafish were generated through Tol2-based transgenesis, as previously described (Kawakami et al., 2004). The resulting adults were mated with wild-type EKW fish and founders transmitting Cyto-bPAC or Cilia-bPAC were identified by genotyping progeny. Genotyping was performed using DNA extracted from either dechorionated embryos or adult fins. In brief, samples were incubated in DNA extraction buffer (10mM Tris pH8.0, 2mM EDTA, 0.2% Triton X-100) supplemented with 200 μ g/mL Proteinase K (Millipore Sigma) for 2 hours at 55°C. Proteinase K was inactivated by incubation at 100°C for 5 minutes. Genotyping was performed with specified primers (see Oligonucleotides) using DreamTaq Green DNA Polymerase (ThermoFisher Scientific). We outcrossed founders to EKW wild-type zebrafish at least three times before experimentation. For each experiment, eggs were collected from a natural mating of one Cyto-bPAC or Cilia-bPAC transgenic animal and one EKW wild-type animal. This yielded

approximately 50% transgenic embryos in each clutch. For *dnPKA* mRNA injections, we injected 45pg of capped mRNA at the one-cell stage. For *bPAC* mRNA injections, we injected 4.5pg of capped mRNA at the one-cell stage, examined localization of Nonciliary-bPAC and Cilia-bPAC at 18hpf, and stimulated with pulsed (500ms on, 500ms off) $0.35\text{mW}/\text{cm}^2$ 470nm blue light from 14-18hpf. For injection of *Rab23 S23N* and *Rab23 Q68L* alone, we injected 18pg of capped mRNA at the one-cell stage. We incubated injected embryos in egg water and unfertilized embryos were removed 6-8 hours post injection.

Optogenetic stimulation

We performed optogenetic experiments in 35mm dishes using custom LED devices. Briefly, the device consisted of 1) a printed circuit board with LEDs and control circuitry positioned to illuminate six individual 35 mm dishes; 2) a 3D printed adapter to ensure diffuse illumination and no cross-stimulation between samples; 3) an Arduino microcontroller to control the LED illumination during the experiment. The printed circuit board was designed using KiCad Electronic Design Automation software (KiCad) and manufactured by PCB Unlimited. The circuit board accommodated 10 blue/red bi-color LEDs (Würth, Cat #150141RB73100) under each of six 35mm wells. Groups of five LEDs were controlled by one pin of a constant-current LED driver chip (Texas Instruments, Cat# TLC5947) supporting independent 12-bit control (4096 steps) by pulse-width modulation, as used in similar devices (Bugaj and Lim, 2019; Repina et al., 2019). The LED drivers were controlled by an Arduino Uno microcontroller, which was programmed with a custom script written in the Arduino Integrated Development Environment. 3D printed adapters that mated the LED array with the 35 mm plates were designed using Inventor CAD software (Autodesk) and printed on a uPrint 3D printer (Stratasys).

We collected zebrafish embryos from timed natural matings and raised them in the dark. We identified transgenic lines that generate equivalent amounts of cAMP upon light stimulation. For light titration experiments, we stimulated embryos with four hours of pulsed (500ms on, 500ms off) low ($0.065\text{mW}/\text{cm}^2$), medium ($0.35\text{mW}/\text{cm}^2$) or high ($0.87\text{mW}/\text{cm}^2$) amounts of 470nm blue

light. For all other activations of transgenic bPAC-expressing zebrafish, we used the low ($0.065\text{mW}/\text{cm}^2$) amount of 470nm blue light. We measured lighting power density with a digital power meter console (Thorlabs Cat #PM100D). For each zebrafish experiment, eggs were collected from a natural mating of one Cyto-bPAC or Cilia-bPAC transgenic zebrafish and one EKW wild-type zebrafish, yielding approximately 50% transgenic embryos in each clutch. For immunofluorescence analyses, we stimulated embryos from 14-18hpf, fixed at 24hpf, and assessed patterning of somites 12-15. A four hour blue light stimulation from 14-18hpf was chosen because this regime reproducibly disrupted somites 12-15, with all other somites phenotypically indistinguishable from wild-type, and to minimize blue light stimulation during development.

For embryos injected with mRNA encoding either Cilia-bPAC (ARL13B-bPAC) and Nonciliary-bPAC (ARL13B^{V359A}-bPAC), we stimulated at 14-18hpf with pulsed (500ms on, 500ms off) $0.35\text{mW}/\text{cm}^2$ 470nm blue light, fixed at 24hpf, and assessed patterning of somites 12-15. For cAMP measurements in transgenic animals, we stimulated embryos from 24-28hpf with $0.065\text{mW}/\text{cm}^2$ light in the presence of $100\mu\text{M}$ IBMX. For cAMP measurements in injected embryos, we stimulated embryos from 14-18hpf with $0.35\text{mW}/\text{cm}^2$ 470nm pulsed blue light in the presence of $100\mu\text{M}$ IBMX.

To optogenetically stimulate bPAC-expressing NIH/3T3 cell lines, we plated cells in 35mm dishes, grew them to confluency, and serum starved overnight in Opti-MEM to promote ciliation. Prior to qRT-PCR, immunofluorescence or immunoblot analysis, we stimulated the cells for four hours of pulsed (500ms on, 500ms off) $0.14\text{mW}/\text{cm}^2$ 470nm blue light while incubating with the indicated drugs diluted in Opti-MEM. This light intensity was chosen because extended blue light stimulation was toxic to cells (data not shown). This was presumably either due to phototoxicity or due to heat accumulation in the OptoPlate in the absence of a cooling system. Furthermore, high intensities of blue light inhibited *Gli1* transcription in both Cyto-bPAC and Cilia-bPAC cells,

similar to that observed upon high stimulation of bPAC embryos and DREADD cells (**Figure 13**). Prior to ELISA-based measurement of cAMP levels, we stimulated the cells with 0.87mW/cm² 470nm blue light for 30 minutes in the presence of 100μM IBMX.

Immunofluorescence staining

We fixed zebrafish embryos in 4% methanol-free PFA (Electron Microscopy Sciences Cat# 100504-782) diluted in PBS for 2 hours at room temperature on a nutator and then stored them in 100% methanol at -20° C until further analysis. We rehydrated embryos in a graded series of methanol and PBST (PBS+0.1% Tween) solutions (75%, 50%, 25% and 0% methanol). For Engrailed staining, we incubated embryos in -20°C acetone for 7 minutes. We blocked embryos in 10% donkey serum, 1% DMSO, 1% BSA and 0.5% Triton X-100 in PBS for 1 hour. After blocking, we incubated embryos overnight at 4°C with primary antibodies diluted in PBDT (1% DMSO, 1% BSA, 0.5% Triton X-100 in PBS). Primary antibodies used were: goat anti-Myc (1:500, Novus, RRID:AB_10002720), rabbit anti-Tub^{AC} (1:500, Cell Signaling, RRID:AB_10544694), rabbit anti-mCherry (1:500, Abcam, RRID:AB_2571870), mouse anti-Eng (1:10, DSHB, RRID:AB_528224), rabbit anti-Prox1 (1:100, EMD Millipore, RRID:AB_177485), goat anti-GFP (1:1000, Rockland, RRID:AB_218182), mouse anti-γ-Tub (1:500, Sigma Aldrich, RRID:AB_477584). Subsequently, we incubated embryos in donkey Alexa Fluor-conjugated secondary antibodies (1:500, Life Technologies) and Hoechst (ThermoFisher Scientific) diluted in PBDT for 2 hours at room temperature, nutating. We mounted embryos in ProLong Diamond antifade mountant (ThermoFisher Scientific Cat# P36970).

We seeded cells on 12mm coverslips (Azer Scientific, CAT# ES0117520) at a density of 5x10⁴ cells per well in a 24-well plate and starved in Opti-MEM reduced serum media (UCSF Tissue Culture). We transfected PKA using TransIT-X2 (Mirus Bio) 24h after seeding. 48h after seeding, we starved cells overnight in Opti-MEM. We fixed cells for 10 minutes in 4% PFA diluted in PBS. We also fixed PKA-transfected cells in -20°C methanol for 3 minutes after PFA fixation.

We blocked cells in 0.1% Triton X-100, 2.5% BSA and PBS for 1h at room temperature. We diluted primary antibodies in blocking buffer and incubated them overnight at 4°C. Primary antibodies used were goat anti-GFP (1:1000, Rockland, RRID:AB_218182), rabbit anti-TUB^{AC} (1:500, Cell Signaling, RRID:AB_10544694), mouse anti- γ -TUB (1:500, Sigma Aldrich, RRID:AB_477584), mouse anti-ARL13B (1:1000, NeuroMab, RRID:AB_11000053), rabbit anti-FOP (1:500, ProteinTech, RRID:AB_2103362), mouse anti-FLAG (1:500, Sigma Aldrich, RRID:AB_439685), mouse anti-mNeonGreen (1:1000, ChromoTek, RRID:AB_2827566), mouse anti-SMO (1:100, Santa Cruz Biotechnology, RRID:AB_2239686), mouse anti-TUB^{AC} (1:500, Sigma-Aldrich, RRID:AB_477585), rabbit anti-GPR161 (1:100, Proteintech, RRID:AB_2113965). Subsequently, we incubated cells in donkey Alexa Fluor-conjugated secondary antibodies (1:500, Life Technologies) and Hoechst (ThermoFisher Scientific) diluted in blocking buffer at room temperature for 2 hours. We mounted coverslips in ProLong Diamond antifade mountant (ThermoFisher Scientific Cat# P36970).

Image Acquisition

We imaged live zebrafish with a Zeiss Observer D1 microscope and an AxioCam MRc camera. We imaged live cells using a Yokogawa CSU-X1 spinning disk confocal equipped with a 60x 1.4 numerical aperture oil objective, a Nikon Perfect Focus system, and a Prime95B sCMOS camera (Photometrics). We seeded cells onto 35mm dishes with Poly-D-Lysine coated No. 1.5 coverslips (MatTek Cat# P35GC-1.5-10-C). After 24h of growth, we transfected cells using Transit-X2 transfection reagents (Mirus Bio). 48h after seeding, we starved cells in Opti-MEM reduced serum media overnight. On the day of imaging, we incubated cells in SiR-Tubulin without verapamil (Spirochrome) to label cilia. During imaging, we maintained cells at 37°C and 5% CO₂ using an OkoLab Cage Incubator and CO₂ mixer. We added drugs one minute after the start of image acquisition and imaged cells every 30 seconds for 15 minutes in FluoroBrite DMEM (ThermoFisher Cat# A1896701) supplemented with 25mM HEPES, pH7.4 (ThermoFisher Cat#

15630080). For Ciliary Pink Flamindo and Pink Flamindo imaging, we stimulated bPAC-expressing NIH/3T3 cells with 100ms 52.7mW/cm² light (Axiom Optics, Argo-POWER) using the 488nm laser (Vortran) during image acquisition. For each cell, images were continuously acquired for 1 minute with the 488nm laser to stimulate bPAC, the 640nm laser to identify cilia stained either with SiR-Tubulin (in the case of cytoplasmic Pink Flamindo) or mIFP (in the case of Ciliary Pink Flamindo), and the 561nm laser to image Pink Flamindo fluorescence. bPAC stimulation began after two acquisitions of ciliary and Pink Flamindo fluorescence detection in the absence of blue laser stimulation. Cells were stimulated with 100µM Forskolin after bPAC stimulation was completed.

We imaged fixed cells with a Zeiss LSM 800 laser scanning confocal microscope equipped with a 63x/1.4 oil immersion objective and captured using the Zen Imaging Software (Zeiss). We imaged fixed zebrafish with either a Leica TCS SPE or a Zeiss LSM 800 laser scanning confocal microscope. We imaged zebrafish somite cilia using a 63x/1.4 oil immersion objective and somites 12 through 15 using either a 20x air objective or 40x oil objective. While collecting images, we held constant the gain, offset and laser power for each antibody combination. We processed images identically and used FIJI software to generate maximal projections.

cAMP measurement

To measure cAMP concentrations in cultured cells, we used a Direct cAMP ELISA kit (Enzo, Cat# ADI-900-066) without the optional acetylation step. Prior to determining cAMP concentration in DREADD- or SSTR3-expressing cells, we seeded NIH/3T3 cells in 12-well plates at a density of 1×10^5 cells per well. For bPAC-based NIH/3T3 experiments, we seeded bPAC-expressing cells in 35mm dishes at a density of 2×10^5 cells per well. 24h after seeding, we starved cells overnight in Opti-MEM reduced serum medium to promote ciliation. On the day of treatment, we treated cells with drugs or light in the presence of 10µM IBMX for DREADD and SSTR3 experiments and 100µM IBMX for bPAC cells (Millipore Sigma) diluted in Opti-MEM reduced

serum medium. We stimulated SSTR3-expressing cells with Somatostatin for 30 minutes. We stimulated DREADD-expressing cells with CNO for 3 hours. Immediately after stimulation, cells were scraped into lysis buffer (0.1M HCl, Enzo). We calculated cAMP concentrations using a 4-parameter logistic (4PL) curve fitting program (Prism version 8, GraphPad Software). We normalized interpolated cAMP values using total protein concentrations determined by BCA assay (Thermo Scientific Pierce Cat# PI23228).

To measure cAMP in zebrafish embryos stably expressing bPAC, we stimulated embryos from 24-28hpf with pulsed blue light or 10 μ M forskolin in the presence of 100 μ M IBMX (Millipore Sigma) diluted in egg water. For embryos injected with mRNA encoding either Cilia-bPAC (ARL13B-bPAC) or Nonciliary-bPAC (ARL13B^{V359A}-bPAC), we shined pulsed (500ms on, 500ms off) 0.35mW/cm² 470nm blue light in the presence of 100 μ M IBMX from 14-18hpf. Injected embryos were lysed at 18hpf. After light stimulation, we dechorionated and lysed embryos in 0.1M HCl (Enzo). We lysed control embryos raised in the dark in batches of 10 embryos and calculated the average concentration per embryo. Transgenic embryos stably expressing bPAC were lysed individually. Injected embryos were lysed in pairs at 18hpf and the average concentration of cAMP per embryo reported. ELISA was performed as described above using 100 μ L undiluted embryo lysate without the optional acetylation protocol. cAMP concentration was determined utilizing a 4-parameter logistic (4PL) curve fitting program (Prism version 8, GraphPad software).

Immunoblotting

Cells were lysed using RIPA buffer (150mM NaCl, 50mM Tris, pH 7.6, 0.1% SDS, 0.1% NP-40 and 0.5% sodium deoxycholate) supplemented with protease inhibitors (Roche). Protein concentration was determined using a Pierce BCA Protein Assay Kit (Thermo Fisher Scientific). Zebrafish embryos were deyolked before lysis in RIPA buffer supplemented with protease inhibitors, as previously described (Link et al., 2006). All lysates were boiled for 5 minutes in 4x SDS-PAGE loading buffer, except prior to immunoblotting for DREADD expression, for which

lysates were incubated at room temperature for 45 minutes. Protein samples were separated on 4-15% gradient TGX precast gels (Bio-Rad) and transferred to PVDF membrane (Bio-Rad). 5% non-fat dried milk in TBS with 0.1% Tween was used to block membranes and to dilute antibodies. HRP signal was detected using Clarity Western ECL substrate (Bio-Rad). Primary antibodies used were goat anti-GFP (1:1,000, Rockland, RRID:AB_218182), mouse anti-GAPDH (1:100,000, Proteintech, RRID:AB_2107436), goat anti-GLI3 (1:200, R&D Systems, Cat #AF3690), goat anti-c-Myc (1:5,000, Novus, RRID:AB_10004121) and mouse anti- β -actin (1:100,000, Proteintech, RRID:AB_2687938). We used HRP-conjugated secondary antibodies at 1:5,000 dilution (Jackson ImmunoResearch Laboratories, Inc).

***In situ* hybridization**

In situ probes for *Nkx2.2b*, *Olig2* and *Pax3* were gifts from Peng Huang. *Nkx2.2b* was digested with *Bam*HI and *in vitro* transcribed using T7 RNA polymerase. *Olig2* was digested with *Bgl*II and *in vitro* transcribed using T3 RNA polymerase. *Pax3* was digested with *Not*I and *in vitro* transcribed using T7 RNA polymerase. Probes were purified using lithium chloride and ethanol precipitation. Whole mount *in situ* hybridization was performed on 24hpf embryos fixed overnight at 4°C in 4% paraformaldehyde and stored in methanol at -20°C. Hybridization with digoxigenin (DIG) (Roche)-labeled riboprobes was performed following standard procedures, as described previously (Reiter et al., 1999). In brief, embryos were rehydrated into PBST (0.1% Tween-20), digested with 10 μ g/mL proteinase K (Roche) for 10 minutes and re-fixed with 4% paraformaldehyde, followed by thorough washing. Embryos were prehybridized in hybridization solution (50% formamide, 5x SSC, 500 μ g/mL yeast tRNA, 50 μ g/mL heparin, 0.1% Tween-20, 9mM citric acid) for at least 1 hour at 68°C, followed by hybridization overnight at 68°C. Embryos were blocked for 2 hours (PBST, 2mg/mL BSA, 5% sheep serum), then incubated with anti-Digoxigenin-AP, Fab fragments (Roche) diluted in block overnight at 4°C. The next day, embryos were washed extensively in PBST/BSA, equilibrated in fresh NTMT buffer (0.1M Tris, pH 9.5,

0.1M NaCl, 0.05M MgCl₂, 0.1% Tween-20), then stained with NBT and BCIP (Roche) diluted in NTMT buffer. Embryos were mounted in 70% glycerol. Transverse sections and wholemount embryos were imaged using a Zeiss Observer D1 microscope equipped with an Axiocam MRc camera.

Quantitative RT-PCR

Cells were seeded in 12-well plates at a density of 1×10^5 cells per well. 24h after seeding, cells were starved in Opti-MEM reduced serum media overnight to promote ciliation. Cells were incubated with indicated drugs diluted in Opti-MEM for 5 hours. RNA was extracted using RNeasy Mini (Qiagen) according to the manufacturer's instructions. RNA was used to make cDNA using the iSCRIPT cDNA synthesis kit (Bio-Rad). qRT-PCR was performed in technical quadruplicates on a 384-well plate (USA Scientific, Cat# 1438-4700) using PowerUp SYBR Green master mix (Applied Biosystems) and run on a QuantStudio 5 real-time PCR system (Applied Biosystems). Relative expression was calculated using the $\Delta\Delta CT$ method normalized to *HPRT* and *RLPL0* expression. Data were normalized to wild-type cells treated with DMSO.

Mathematical modeling of cAMP subcellular dynamics and PKA activation

A frame-by-frame Monte Carlo simulation was performed for the diffusion of cAMP molecules in cells. The cell-cilium system was modeled as a ball-shaped cell body (radius $R = 5 \mu\text{m}$) connected with a cylindrical-shaped cilium (length $L = 5 \mu\text{m}$, diameter $\Phi = 300 \text{ nm}$) through a smooth junction at the ciliary base.

cAMP molecules were introduced at random locations in either the ciliary membrane or the plasma membrane at a constant rate of 34 molecules per second (**Figure 11A and Figure 12**) or 340 molecules per second (**Figure 13**) to simulate ciliary and plasma membrane cAMP generation, respectively. The cAMP molecules underwent random walks in the cell (Berg, 1993). For each step of random walk, the probability distribution function for a cAMP initially located at position (x_0, y_0, z_0) in a frame to be found at position (x, y, z) in the next frame after time Δt takes the form of 3D-Gaussian distribution:

$$p(x, y, z, \Delta t | x_0, y_0, z_0) = \frac{1}{(\sqrt{2\pi}\sigma)^3} \exp\left(-\frac{(x-x_0)^2 + (y-y_0)^2 + (z-z_0)^2}{2\sigma^2}\right) \quad (1)$$

Here, σ is the standard deviation of each step, and is related to the diffusion coefficient (D) and the time interval between two frames (Δt) by

$$D = \sigma^2 / 2\Delta t \quad (2)$$

In our simulation, we used $\sigma = 100$ nm. This value was specified to be smaller than the smallest dimension of the cell (diameter of cilium $\Phi = 300$ nm), yet not exceedingly small to allow for reasonable computation speed. An assumed diffusion coefficient $D = 10 \mu\text{m}^2/\text{s}$ therefore corresponded to $\Delta t = 0.5$ ms. We considered elastic collisions between the cAMP and the cell membrane so that the cAMPs appeared at their mirrored positions with respect to the cell membrane in cases where cAMP trajectories would have exited the cell after the application of equation (1). We recorded the PKA interaction locations (x_c, y_c, z_c) for the further analysis of the PKA activation.

The PKA molecules were modeled to be evenly distributed on the ciliary and the plasma membranes at the same surface density, $\rho = 1 \text{ PKA} / (140\text{nm})^2$. Each PKA holoenzyme was activated by binding of 4 cAMP molecules. To simulate binding, we modeled PKA molecules to have a radius of $r_{\text{PKA}} = 2.5$ nm, and one binding event was counted when a cAMP molecule collided with the adjacent membrane within r_{PKA} of the PKA center ($x_{\text{PKA}}, y_{\text{PKA}}, z_{\text{PKA}}$):

$$(x_c - x_{\text{PKA}})^2 + (y_c - y_{\text{PKA}})^2 + (z_c - z_{\text{PKA}})^2 < r_{\text{PKA}}^2 \quad (3)$$

A PKA molecule was considered activated after encountering 4 such binding events.

QUANTIFICATION AND STATISTICAL ANALYSIS

For all cell culture experiments shown, sample size (n) indicates the number of independent experiments. In all data panels, representative data from 3-5 independent experiments are shown. For zebrafish experiments, all sample sizes (n) are indicated for the

number of embryos used in each experiment. To calculate the number of En-expressing, mCherry-expressing or Prox1-expressing cells per somite, images were converted to binary images using the threshold function and a minimum/maximum size exclusion filter was applied in Fiji. Cells were counted using the 3D objects counter function in Fiji. Cells in somites 12 through 15 were counted and an average value of cells per somite was determined for each embryo. The average values per embryo were used as individual data points in all graphs and statistical analyses.

For fluorescence intensity measurements, a sum projection containing 10 slices was generated. Raw integrated density was measured in Fiji for a region of interest that was used for all measurements. For quantification of ciliary enrichment and quantification of SMO and GPR161 trafficking in cultured cells, a sum projection containing 10 optical sections was generated. A 5-pixel-wide segmented line was used to trace cilia, as defined by staining for Tub^{AC}. For ciliary enrichment, raw integrated density was measured in Fiji and calculated as the ratio of signal at the cilium to the average of two cell body measurements. For quantification of ciliary SMO and GPR161 fluorescence, the average of two background fluorescence measurements adjacent to the cilium was subtracted from ciliary fluorescence. A negative value indicates background fluorescence was greater than ciliary fluorescence. Fluorescence was normalized to the mean of wild-type cells treated with vehicle in the dark.

For quantification of ciliary cAMP levels, a 5-pixel-wide segmented line was used to trace cilia at each timepoint. The ratio of ciliary Pink Flamindo to mIFP raw integrated density was measured for each timepoint using Fiji software. Relative intensity change was calculated using the fluorescence intensity ratio F/F_0 . Quantification of cytoplasmic Pink Flamindo fluorescence was performed on unprocessed TIFF images using MATLAB (Jullié et al., 2020). Briefly, Pink Flamindo fluorescence intensity was measured after thresholding and background fluorescence subtraction. Data are represented as the ratio of Pink Flamindo F/F_0 , where F_0 is the Pink

Flamindo fluorescence before stimulation. Average measurements for >20 cells over three independent experiments are reported.

Quantification of GLI3^R was performed in Fiji. In brief, Mean Grey Value was measured for each band using a defined region of interest and an adjacent background value was subtracted. This resulting value for this GLI3^R band was normalized to the loading control (GAPDH). All values were normalized to Wild-type cells treated with vehicle and no light.

For statistical analyses of two samples, significance was determined via two-tailed unpaired t-test. For more than two samples, significance was determined via one-way ANOVA followed by Tukey's multiple comparison test for one variable or two-way ANOVA followed by Tukey's multiple comparison test for two variables. A p value less than 0.05 was considered statistically significant and is denoted as follows: *<0.05, **<0.01, ***<0.001, and ****<0.0001.

ACKNOWLEDGEMENTS

We thank members of the Reiter laboratory for discussion and advice, Roshanak Irannejad, Markus Delling, Didier Stainier and Mark von Zastrow for comments on the manuscript, DeLaine Larsen and Kari Herrington from the UCSF Center for Advanced Light Microscopy for microscope use and imaging assistance, and the UCSF Cardiovascular Building fish facility for zebrafish husbandry. We also thank Peng Huang, James Chen, Xiaokun Shu, Maxence Nachury, Roshanak Irannejad, Aaron Marley and Mark von Zastrow for providing reagents. The UCSF Center for Advanced Light Microscopy is funded by the UCSF Research Evaluation and Allocation Committee, the Gross Fund, and the Heart Anonymous Fund. L.J.B. was funded by an Arnold O. Beckman Postdoctoral Fellowship. M.E.T. was supported by UCSF Discovery Fellowship and NIH grant T32HD007470. This work was supported by grants from the NIH (R01DE029454 and R01AR054396) to J.F.R. K.X. and J.F.R. acknowledge support by the Packard Fellowships for Science and Engineering. K.X. and J.F.R. are Chan Zuckerberg Biohub Investigators.

AUTHOR CONTRIBUTIONS

M.E.T. and J.F.R. conceived, designed the study, and wrote the manuscript. M.E.T. performed and analyzed experiments. S.P.C. contributed to generation of bPAC transgenic zebrafish, microinjection of embryos, and image analysis. S.B. contributed to DREADD and SSTR3 cell culture experiments. W.L. and K.X. performed the computational modeling. L.J.B. designed and engineered the 6-well OptoPlate. J.F.R. supervised the study.

FUTURE DIRECTIONS AND CONSIDERATIONS

In this study, we demonstrate that ciliary cAMP is functionally distinct from extraciliary cAMP. Rather than simply sensing the total amount of cAMP within the cell, ciliary HH signaling is preferentially inhibited by ciliary, but not extraciliary cAMP. This held true in both HH-dependent cell fates in the ventral neural tube and slow muscle in zebrafish, as well as in mouse fibroblast cells. Furthermore, we identify a ciliary pool of PKA that is regulated by ciliary cAMP to control HH signaling. Discrimination between ciliary and extraciliary cAMP allows cells to multiplex GPCR signaling, allowing cells to have parallel conversations with the outside world.

However, there are both outstanding unanswered questions and new questions raised by this study: What shapes the cAMP gradient in cilia? What happens to ciliary PKA during HH signaling? How do different GPCRs within a cilium avoid crosstalk? How does HH signaling integrate ciliary cAMP over time? In the following paragraphs, I touch on a few of these questions and propose potential approaches.

First, do ciliary phosphodiesterases shape the cAMP gradient in cilia? Phosphodiesterases (PDEs) are the sole route of cAMP degradation within the cell (Baillie, 2009). Discretely positioned PDEs act as “sinks” to degrade cAMP within localized microdomains. These PDE “sinks” have been proposed to provide a local barrier against cAMP diffusion, though whether or not they are sufficient to restrict free diffusion of cAMP is contested (Agarwal et al., 2016; Conti et al., 2014). A recent study suggests that individual PDEs create nanometer-size domains of low cAMP. Receptor stimulation causes cAMP to flood these nanodomains in order to trigger activation of effector proteins (Bock et al., 2020).

Whether or not PDEs play a role in shaping the ciliary cAMP response is largely unknown. Identification of ciliary PDEs, potentially using a candidate approach from candidates identified in ciliary proteomics screens, will be crucial (Mick et al., 2015; Sigg et al., 2017). Selective inhibition through pharmacological antagonists can be utilized to measure ciliary cAMP upon acute inhibition, though this approach comes with the caveat that these inhibitors affect global PDE

activity. A targeted approach to selectively inhibit ciliary PDEs would be ideal. This could be achieved by targeting a light-inducible PDE to the cilium (Gasser et al., 2014; Hansen et al., 2020). If PDE activity operates at the cilium, activation of LAPD would locally degrade ciliary cAMP. This may phenocopy the increase in HH signaling we see upon $G\alpha_i$ -coupled SSTR3 activation (**Figure 9F-H**).

In this study, we show that ciliary cAMP activates a ciliary pool of PKA to modulate HH signaling. However, the nature of PKA within the cilium remains mysterious. What happens to ciliary PKA during HH signaling? Is there a resident pool of PKA within cilia or is its trafficking dynamic? What are the relative abundances of PKA subunits within cilia? Though PKA is highly enriched at the ciliary base, PKA subunits can localize to the cilium via the AKAP GPR161 (**Figure 14**) (Bachmann et al., 2016). However, the activation of SMO causes the β -arrestin-mediated removal of GPCR161 from the primary cilium (Pal et al., 2016). Furthermore, GPR161 is thought to be tonically active, constitutively coupling to $G\alpha_s$ to generate cAMP (Mukhopadhyay et al., 2013). If GPR161 exits cilia upon HH signaling, do PKA subunits exit with it? A recent time-resolved proteomic study suggested that PKA-R1 α exits cilia with similar kinetics as GPR161 (May et al., 2020). Proteomic analysis did not identify PKA-C exiting cilia as a top tier hit, but further validation is needed (May et al., 2020). As PKA-C does not robustly localize to cilia upon either endogenous staining or by overexpression of PKA-C alone (data not shown), co-expressing GPR161, PKA-R1 α and PKA-C may shed light on this question.

Exit of PKA-C with GPR161 may act to promote processing of GLI proteins into their activator forms. This may work through physical sequestration of PKA away from the GLI proteins, thus inhibiting phosphorylation and downstream processing into the repressor state. However, if GPR161 is tonically active, does exit of GPR and PKA cause activation of non-ciliary cAMP targets? Or perhaps the ciliary microenvironment plays a permissive role for GPR161 activation, potentially through interaction with ciliary lipids. For instance, serotonin receptors have high levels

of basal activity, but are subject to regulation by lipids (Xu et al., 2021). Might GPR161 behave similarly? More broadly, might the privileged lipid microdomain within the cilium regulate other ciliary GPCR activity, such as activity of the ciliary serotonin receptor 5HT6, distinctly from the plasma membrane?

If PKA-C does not exit the cilium with GPR161 and PKA-R1 α upon HH activation, what happens to it? In the absence of negative regulation by PKA-R1 α , does it float around and phosphorylate effectors, such as GLI proteins, in its path? This seems unlikely, as PKA activity is tightly regulated in cells. As phosphorylation of the GLI proteins promotes repressor formation, constitutive PKA-C activity would prevent GLI^A formation in response to HH stimulation. A quantitative mass spectrometry approach demonstrated that PKA regulatory subunits are in large molar excess to catalytic subunits in human embryonic kidney cells (~17 fold) (Walker-Gray et al., 2017). If similar stoichiometry is present in cilia, enough PKA-R may remain in cilia after GPR161 exit to inhibit PKA-C activity. Alternatively, SMO entering the cilium may directly sequester PKA-C subunits at the membrane (Arveseth et al., 2020). One hypothesis is that this association with the membrane could occur through myristoylation of PKA-C (Tillo et al., 2017). In this model, the GPR161/ PKA-R1 α complex could perform a “hand off” of PKA-C to SMO while exiting the cilium. However, further experimentation utilizing live imaging of PKA-C within the cilium is required to distinguish between these models.

The complement of GPCRs that localize to cilia is an area of active investigation. Future ciliary proteomic analysis can be utilized to determine tissue specific ciliary GPCR populations. In this study, we showed that exogenous GPCRs can modulate HH signaling. For instance, stimulation of Cilia-DREADD preferentially inhibits *Gli1* transcription in NIH/3T3 cells (**Figure 9**). The somatostatin receptor SSTR3 is a G α i-coupled GPCR that is expressed in neuronal cilia, but absent from cilia in NIH/3T3 cells (Green et al., 2015; Ye et al., 2018). However, expression and

stimulation of SSTR3 in NIH/3T3 cells activated HH signaling (**Figure 9**). Thus, HH output is not dependent on the activation of HH-specific GPCRs such as GPR161.

However, how do different GPCRs within a cilium avoid crosstalk? Are there cells that simultaneously signal through both HH and non-HH ciliary GPCRs? If so, how is signal specificity achieved? For instance, in preadipocytes, ciliary HH signaling inhibits adipogenesis, but the ciliary GPCR FFAR4 activates adipogenesis (Hilgendorf et al., 2019; Kopinke et al., 2017). As both pathways impinge upon cAMP, how do cells distinguish between different GPCRs? Differential dependencies on cAMP effector proteins may play a role in ensuring signal fidelity. For instance, HH signaling operates through PKA, while FFAR4 seems to operate through a protein called EPAC (exchange factor directly activated by cAMP). Selective activation of effector proteins may allow multiple ciliary signaling events to occur simultaneously. Whether activation of FFAR4 inhibits GLI activator formation may be interesting to test, as this would suggest crosstalk between ciliary GPCR pathways.

Alternatively, might differences in signaling dynamics between ciliary GPCRs encode different responses? For instance, within the developing *Drosophila* embryo, transient Erk signaling helps specify neural ectoderm, while sustained Erk activity induces posterior midgut differentiation. Similarly, sustained or pulsatile Notch activity either inhibits or promotes myogenesis in chick embryos, respectively, despite the use of the same Notch receptor (Nandagopal et al., 2018). In the case of ciliary GPCR signaling in pre-adipocytes, HH-related GPCRs versus FFAR4 may activate cAMP with temporal differences. The fine temporal control of cAMP generation using bPAC is the ideal model to test how ciliary GPCR signaling is integrated over time. This would be applicable both to questions of ciliary GPCR crosstalk, as well as questions to how HH signaling integrates ciliary cAMP over time to specify cell fates.

REFERENCES

- Adrian, M., Kusters, R., Wierenga, C.J., Storm, C., Hoogenraad, C.C., and Kapitein, L.C. (2014). Barriers in the brain: Resolving dendritic spine morphology and compartmentalization. *Front. Neuroanat.* 8, 142.
- Agarwal, S.R., Yang, P.-C., Rice, M., Singer, C.A., and Nikolaev, V.O. (2014). Role of Membrane Microdomains in Compartmentation of cAMP Signaling. *PLoS One* 9, 95835.
- Agarwal, S.R., Clancy, C.E., and Harvey, R.D. (2016). Mechanisms Restricting Diffusion of Intracellular cAMP. *Sci. Rep.* 6, 19577.
- Allen, J.A., Halverson-Tamboli, R.A., and Rasenick, M.M. (2007). Lipid raft microdomains and neurotransmitter signalling. *Nat. Rev. Neurosci.* 8, 128–140.
- Anvarian, Z., Mykytyn, K., Mukhopadhyay, S., Pedersen, L.B., and Christensen, S.T. (2019). Cellular signalling by primary cilia in development, organ function and disease. *Nat. Rev. Nephrol.* 15, 199–219.
- Arnbruster, B.N., Li, X., Pausch, M.H., Herlitze, S., and Roth, B.L. (2007). Evolving the lock to fit the key to create a family of G protein-coupled receptors potently activated by an inert ligand. *Proc. Natl. Acad. Sci. U. S. A.* 104, 5163–5168.
- Arrenberg, A.B., Stainier, D.Y.R., Baier, H., and Huisken, J. (2010). Optogenetic control of cardiac function. *Science (80-)*. 330, 971–974.
- Arveseth, C.D., Happ, J.T., Hedeem, D.S., Zhu, J.-F., Capener, J.L., Klatt Shaw, D., Deshpande, I., Liang, J., Xu, J., Stubben, S.L., et al. (2020). Smoothened Transduces Hedgehog Signals via Activity-Dependent Sequestration of PKA Catalytic Subunits.
- Avidor-Reiss, T., Maer, A.M., Koundakjian, E., Polyanovsky, A., Keil, T., Subramaniam, S., and Zuker, C.S. (2004). Decoding cilia function: Defining specialized genes required for compartmentalized cilia biogenesis. *Cell* 117, 527–539.
- Aza-Blanc, P., Ramírez-Weber, F.A., Laget, M.P., Schwartz, C., and Kornberg, T.B. (1997). Proteolysis that is inhibited by hedgehog targets cubitus interruptus protein to the

- nucleus and converts it to a repressor. *Cell* 89, 1043–1053.
- Bachmann, V.A., Mayrhofer, J.E., Ilouz, R., Tschakner, P., Raffener, P., Röck, R., Courcelles, M., Apelt, F., Lu, T.-W.W., Baillie, G.S., et al. (2016). Gpr161 anchoring of PKA consolidates GPCR and cAMP signaling. *Proc. Natl. Acad. Sci. U. S. A.* 113, 7786–7791.
- Baillie, G.S. (2009). Compartmentalized signalling: spatial regulation of cAMP by the action of compartmentalized phosphodiesterases. *FEBS J.* 276, 1790–1799.
- Bandarigoda Nipunika Somatilaka, A., Hwang, S.-H., Reddy Palicharla, V., Andrew White, K., Badgandi, H., Michael Shelton, J., and Mukhopadhyay Correspondence, S. (2020). Ankyr2 Prevents Smoothed-Independent Hyperactivation of the Hedgehog Pathway via Cilia-Regulated Adenylyl Cyclase Signaling. *Dev. Cell.*
- Bangs, F., and Anderson, K. V (2017). Primary cilia and Mammalian Hedgehog signaling. *Cold Spring Harb. Perspect. Biol.* 9.
- Barresi, M.J., Stickney, H.L.L., Devoto, S.H.H., F Barresi, M.J., Stickney, H.L.L., and Devoto, S.H.H. (2000). Slow muscle requires Slow-muscle-omitted. *Development* 127.
- Barresi, M.J.F., D'Angelo, J.A., Hernández, L.P., and Devoto, S.H. (2001). Distinct mechanisms regulate slow-muscle development. *Curr. Biol.* 11, 1432–1438.
- Barzi, M., Berenguer, J., Menendez, A., Alvarez-Rodriguez, R., and Pons, S. (2009). Sonic-hedgehog-mediated proliferation requires the localization of PKA to the cilium base. *J. Cell Sci.* 123.
- Batista, W.L., Ogata, F.T., Curcio, M.F., Miguel, R.B., Arai, R.J., Matsuo, A.L., Moraes, M.S., Stern, A., and Monteiro, H.P. (2013). S-Nitrosoglutathione and Endothelial Nitric Oxide Synthase-Derived Nitric Oxide Regulate Compartmentalized Ras S-Nitrosylation and Stimulate Cell Proliferation. *Antioxid. Redox Signal.* 18, 221–238.
- Beavo, J.A., and Brunton, L.L. (2002). Cyclic nucleotide research - Still expanding after half a century. *Nat. Rev. Mol. Cell Biol.* 3, 710–718.

- Berbari, N.F., Johnson, A.D., Lewis, J.S., Askwith, C.C., and Mykytyn, K. (2008). Identification of ciliary localization sequences within the third intracellular loop of G protein-coupled receptors. *Mol. Biol. Cell* *19*, 1540–1547.
- Berg, H.C. (1993). *Random Walks in Biology*, New and Expanded Edition.
- Bishop, G.A., Berbari, N.F., Lewis, J., and Mykytyn, K. (2007). Type III adenylyl cyclase localizes to primary cilia throughout the adult mouse brain. *J. Comp. Neurol.* *505*, 562–571.
- Blagden, C.S., Currie, P.D., Ingham, P.W., and Hughes, S.M. (1997). Notochord induction of zebrafish slow muscle mediated by sonic hedgehog. *Genes Dev.* *11*, 2163–2175.
- Bock, A., Annibale, P., Konrad, C., Hannawacker, A., Anton, S.E., Maiellaro, I., Zabel, U., Sivaramakrishnan, S., Falcke, M., and Lohse, M.J. (2020). Optical mapping of cAMP signaling at the nanometer scale. *Cell* *182*, 1–12.
- Briscoe, J., and Théron, P.P. (2013). The mechanisms of Hedgehog signalling and its roles in development and disease. *Nat. Rev. Mol. Cell Biol.* *14*, 418–431.
- Briscoe, J., Pierani, A., Jessell, T.M., and Ericson, J. (2000). A homeodomain protein code specifies progenitor cell identity and neuronal fate in the ventral neural tube. *Cell* *101*, 435–445.
- Brunton, L.L., Hayes, J.S., and Mayer, S.E. (1979). Hormonally specific phosphorylation of cardiac troponin I and activation of glycogen phosphorylase [24]. *Nature* *280*, 78–80.
- Bugaj, L.J., and Lim, W.A. (2019). High-throughput multicolor optogenetics in microwell plates. *Nat. Protoc.* *14*, 2205–2228.
- Buxton, I.L.O., and Brunton, L.L. (1983). Compartments of cyclic AMP and protein kinase in mammalian cardiomyocytes. *J. Biol. Chem.* *258*, 10233–10239.
- Calebiro, D., and Koszegi, Z. (2019). The subcellular dynamics of GPCR signaling. *Mol. Cell. Endocrinol.* *483*, 24–30.
- Calebiro, D., and Maiellaro, I. (2014). cAMP signaling microdomains and their observation by

- optical methods. *Front. Cell. Neurosci.* 8, 350.
- Carpenter, B., and Tate, C.G. (2016). Engineering a minimal G protein to facilitate crystallisation of G protein-coupled receptors in their active conformation. *Protein Eng. Des. Sel.* 29, 583–594.
- Chen, Y., Gallaher, N., Goodman, R.H., and Smolik, S.M. (1998). Protein kinase a directly regulates the activity and proteolysis of cubitus interruptus. *Proc. Natl. Acad. Sci. U. S. A.* 95, 2349–2354.
- Chiang, C., Litingtung, Y., Lee, E., Young, K.E., Corden, J.L., Westphal, H., and Beachy, P.A. (1996). Cyclopia and defective axial patterning in mice lacking Sonic hedgehog gene function. *Nature* 383, 407–413.
- Choi, Y.-H., Suzuki, A., Hajarnis, S., Ma, Z., Chapin, H.C., Caplan, M.J., Pontoglio, M., Somlo, S., and Igarashi, P. (2011). Polycystin-2 and phosphodiesterase 4C are components of a ciliary A-kinase anchoring protein complex that is disrupted in cystic kidney diseases. *Proc. Natl. Acad. Sci. U. S. A.* 108, 10679–10684.
- Clegg, C.H., Correll, L.A., Cadd, G.G., and McKnight, G.S. (1987). Inhibition of intracellular cAMP-dependent protein kinase using mutant genes of the regulatory type I subunit. *J. Biol. Chem.* 262, 13111–13119.
- Conti, M., Mika, D., and Richter, W. (2014). Cyclic AMP compartments and signaling specificity: Role of cyclic nucleotide phosphodiesterases. *J. Gen. Physiol.* 143, 29–38.
- Corbit, K.C., Aanstad, P., Singla, V., Norman, A.R., Stainier, D.Y.R., and Reiter, J.F. (2005). Vertebrate Smoothed functions at the primary cilium. *Nature* 437, 1018–1021.
- Currie, P.D., and Ingham, P.W. (1996). Induction of a specific muscle cell type by a hedgehog-like protein in zebrafish. *Nature* 382, 452–455.
- Dai, P., Akimaru, H., Tanaka, Y., Maekawa, T., Nakafuku, M., and Ishii, S. (1999). Sonic hedgehog-induced activation of the Gli1 promoter is mediated by GLI3. *J. Biol. Chem.* 274, 8143–8152.

- Delling, M., DeCaen, P.G., Doerner, J.F., Febvay, S., and Clapham, D.E. (2013). Primary cilia are specialized calcium signalling organelles. *Nature* 504, 311–314.
- Dessaud, E., Yang, L.L., Hill, K., Cox, B., Ulloa, F., Ribeiro, A., Mynett, A., Novitch, B.G., and Briscoe, J. (2007). Interpretation of the sonic hedgehog morphogen gradient by a temporal adaptation mechanism. *Nature* 450, 717–720.
- Devoto, S.H., Melancon, E., Eisen, J.S., and Westerfield, M. (1996). Identification of separate slow and fast muscle precursor cells in vivo, prior to somite formation. *Development* 122.
- Du, S.J., Devoto, S.H., Westerfield, M., and Moon, R.T. (1997). Positive and Negative Regulation of Muscle Cell Identity by Members of the hedgehog and TGF- β Gene Families. *J. Cell Biol.* 139.
- Edwards, H. V, Christian, F., and Baillie, G.S. (2011). cAMP: Novel concepts in compartmentalised signalling. *Semin. Cell Dev. Biol.* 23, 181–190.
- Ericson, J., Morton, S., Kawakami, A., Roelink, H., and Jessell, T.M. (1996). Two critical periods of Sonic Hedgehog signaling required for the specification of motor neuron identity. *Cell* 87, 661–673.
- Evans, T.M., Ferguson, C., Wainwright, B.J., Parton, R.G., and Wicking, C. (2003). Rab23, a Negative Regulator of Hedgehog Signaling, Localizes to the Plasma Membrane and the Endocytic Pathway. *Traffic* 4, 869–884.
- Fan, C.-M., and Tessier-Lavigne, M. (1994). Patterning of Mammalian Somites by Surface Ectoderm and Notochord: Evidence for Sclerotome Induction by a Hedgehog Homolog. *Cell* 79, 1175–1186.
- Garcia-Gonzalo, F.R., and Reiter, J.F. (2017). Open Sesame: How transition fibers and the transition zone control ciliary composition. *Cold Spring Harb. Perspect. Biol.* 9.
- Garcia, G., Raleigh, D.R., and Reiter, J.F. (2018). How the Ciliary Membrane Is Organized Inside-Out to Communicate Outside-In. *Curr. Biol.* 28, R421–R434.
- Gasser, C., Taiber, S., Yeh, C.M., Wittig, C.H., Hegemann, P., Ryu, S., Wunder, F., and

- Moöglich, A. (2014). Engineering of a red-light-activated human cAMP/cGMP-specific phosphodiesterase. *Proc. Natl. Acad. Sci. U. S. A.* *111*, 8803–8808.
- Ge, X., Milenkovic, L., Suyama, K., Hartl, T., Purzner, T., Winans, A., Meyer, T., Scott, M.P., Adams, J., McGlone, M., et al. (2015). Phosphodiesterase 4D acts downstream of Neuropilin to control Hedgehog signal transduction and the growth of medulloblastoma. *Elife* *4*, 2447–2454.
- Gigante, E.D., and Caspary, T. (2020). Signaling in the primary cilium through the lens of the Hedgehog pathway. *Wiley Interdiscip. Rev. Dev. Biol.* e377.
- Gigante, E.D., Taylor, M.R., Ivanova, A.A., Kahn, R.A., and Caspary, T. (2020). ARL13B regulates Sonic Hedgehog signaling from outside primary cilia. *Elife* *9*.
- Gillingham, A.K., and Munro, S. (2000). The PACT domain, a conserved centrosomal targeting motif in the coiled-coil proteins AKAP450 and pericentrin. *EMBO Rep.* *1*, 524–529.
- Goetz, S.C., and Anderson, K. V. (2010). The primary cilium: a signalling centre during vertebrate development. *Nat. Rev. Genet.* *11*, 331–344.
- Gonçalves, J., and Pelletier, L. (2017). The ciliary transition zone: Finding the pieces and assembling the gate. *Mol. Cells* *40*, 243–253.
- Green, J.A., Schmid, C.L., Bley, E., Monsma, P.C., Brown, A., Bohn, L.M., and Mykytyn, K. (2015). Recruitment of β -arrestin into Neuronal Cilia Modulates Somatostatin Receptor Subtype 3 Ciliary Localization. *Mol. Cell. Biol.* MCB.00765-15.
- Guettier, J.M., Gautam, D., Scarselli, M., De Azua, I.R., Li, J.H., Rosemond, E., Ma, X., Gonzalez, F.J., Armbruster, B.N., Lu, H., et al. (2009). A chemical-genetic approach to study G protein regulation of β cell function in vivo. *Proc. Natl. Acad. Sci. U. S. A.* *106*, 19197–19202.
- Guner, B., and Karlstrom, R.O. (2007). Cloning of zebrafish *nkx6.2* and a comprehensive analysis of the conserved transcriptional response to Hedgehog/Gli signaling in the zebrafish neural tube. *Gene Expr. Patterns* *7*, 596–605.

- Hammerschmidt, M., Bitgood, M.J., and McMahon, A.P. (1996). Protein kinase A is a common negative regulator of Hedgehog signaling in the vertebrate embryo. *Genes Dev.* 10, 647–658.
- Händel, M., Schulz, S., Stanarius, A., Schreff, M., Erdtmann-Vourliotis, M., Schmidt, H., Wolf, G., and Höllt, V. (1999). Selective targeting of somatostatin receptor 3 to neuronal cilia. *Neuroscience* 89, 909–926.
- Hansen, J.N., Kaiser, F., Klausen, C., Stüven, B., Chong, R., Bönigk, W., Mick, D.U., Möglich, A., Jurisch-Yaksi, N., Schmidt, F.I., et al. (2020). Nanobody-directed targeting of optogenetic tools to study signaling in the primary cilium. *Elife* 9.
- Harada, K., Ito, M., Wang, X., Tanaka, M., Wongso, D., Konno, A., Hirai, H., Hirase, H., Tsuboi, T., and Kitaguchi, T. (2017). Red fluorescent protein-based cAMP indicator applicable to optogenetics and in vivo imaging. *Sci. Rep.* 7, 7351.
- Hauser, A.S., Attwood, M.M., Rask-Andersen, M., Schiöth, H.B., and Gloriam, D.E. (2017). Trends in GPCR drug discovery: New agents, targets and indications. *Nat. Rev. Drug Discov.* 16, 829–842.
- He, X., Zhang, L., Chen, Y., Remke, M., Shih, D., Lu, F., Wang, H., Deng, Y., Yu, Y., Xia, Y., et al. (2014). The G protein alpha subunit Galphas is a tumor suppressor in Sonic hedgehog-driven medulloblastoma. *Nat. Med.* 20, 1035–1042.
- Henry, C.A., and Amacher, S.L. (2004). Zebrafish Slow Muscle Cell Migration Induces a Wave of Fast Muscle Morphogenesis. *Dev. Cell* 7, 917–923.
- Higginbotham, H., Eom, T.Y., Mariani, L.E., Bachleda, A., Hirt, J., Gukassyan, V., Cusack, C.L., Lai, C., Caspary, T., and Anton, E.S. (2012). Arl13b in Primary Cilia Regulates the Migration and Placement of Interneurons in the Developing Cerebral Cortex. *Dev. Cell* 23, 925–938.
- Hilgendorf, K.I., Johnson, C.T., and Jackson, P.K. (2016). The primary cilium as a cellular receiver: organizing ciliary GPCR signaling. *Curr. Opin. Cell Biol.* 39, 84–92.

- Hilgendorf, K.I., Johnson, C.T., Mezger, A., Rice, S.L., Norris, A.M., Demeter, J., Greenleaf, W.J., Reiter, J.F., Kopinke, D., and Jackson, P.K. (2019). Omega-3 Fatty Acids Activate Ciliary FFAR4 to Control Adipogenesis. *Cell* 179, 1289-1305.e21.
- Hirsinger, E., Stellabotte, F., Devoto, S.H., and Westerfield, M. (2004). Hedgehog signaling is required for commitment but not initial induction of slow muscle precursors. *Dev. Biol.* 275, 143–157.
- Huang, P., and Schier, A.F. (2009). Dampened Hedgehog signaling but normal Wnt signaling in zebrafish without cilia. *Development* 136, 3089–3098.
- Huangfu, D., and Anderson, K. V. (2005). Signaling from Smo to Ci/Gli: conservation and divergence of Hedgehog pathways from Drosophila to vertebrates. *Development* 133.
- Huangfu, D., Liu, A., Rakeman, A.S., Murcia, N.S., Niswander, L., and Anderson, K. V. (2003). Hedgehog signalling in the mouse requires intraflagellar transport proteins. *Nature* 426, 83–87.
- Humke, E.W., Dorn, K. V, Milenkovic, L., Scott, M.P., and Rohatgi, R. (2010). The output of Hedgehog signaling is controlled by the dynamic association between Suppressor of Fused and the Gli proteins. *Genes Dev.* 24, 670–682.
- Iglesias-Bartolome, R., Torres, D., Marone, R., Feng, X., Martin, D., Simaan, M., Chen, M., Weinstein, L.S., Taylor, S.S., Molinolo, A.A., et al. (2015). Inactivation of a Gα s –PKA tumour suppressor pathway in skin stem cells initiates basal-cell carcinogenesis. *Nat. Cell Biol.* 17, 793–803.
- Ingham, P.W. (1998). Transducing Hedgehog: The story so far. *EMBO J.* 17, 3505–3511.
- Ingham, P.W. (2018). From drosophila segmentation to human cancer therapy. *Dev.* 145.
- Ingham, P.W., and Kim, H.R. (2005). Hedgehog signalling and the specification of muscle cell identity in the Zebrafish embryo. *Exp. Cell Res.* 306, 336–342.
- Insel, P.A., Head, B.P., Ostrom, R.S., Patel, H.H., Swaney, J.S., Tang, C.M., and Roth, D.M. (2005). Caveolae and lipid rafts: G protein-coupled receptor signaling microdomains in

- cardiac myocytes. *Ann. N. Y. Acad. Sci.* *1047*, 166–172.
- Irannejad, R., Tomshine, J.C., Tomshine, J.R., Chevalier, M., Mahoney, J.P., Steyaert, J., Rasmussen, S.G.F., Sunahara, R.K., El-Samad, H., Huang, B., et al. (2013). Conformational biosensors reveal GPCR signalling from endosomes. *Nature* *495*.
- Irannejad, R., Pessino, V., Mika, D., Huang, B., Wedegaertner, P.B., Conti, M., and von Zastrow, M. (2017). Functional selectivity of GPCR-directed drug action through location bias. *Nat. Chem. Biol.* *13*, 799–806.
- Ishikawa, H., and Marshall, W.F. (2011). Ciliogenesis: building the cell's antenna. *Nat. Publ. Gr.* *12*, 222–234.
- Jansen, V., Alvarez, L., Balbach, M., Strünker, T., Hegemann, P., Kaupp, U.B., and Wachten, D. (2015). Controlling fertilization and cAMP signaling in sperm by optogenetics. *Elife* *4*.
- Jiang, J., and Struhl, G. (1995). Protein kinase A and hedgehog signaling in drosophila limb development. *80*, 563–572.
- Jiang, J., and Struhl, G. (1998). Regulation of the Hedgehog and Wingless signalling pathways by the F- box/WD40-repeat protein Slimb. *Nature* *391*, 493–496.
- Jiang, J.Y., Falcone, J.L., Curci, S., and Hofer, A.M. (2019). Direct visualization of cAMP signaling in primary cilia reveals up-regulation of ciliary GPCR activity following Hedgehog activation. *Proc. Natl. Acad. Sci. U. S. A.* *116*, 12066–12071.
- Johnson, H.E., and Toettcher, J.E. (2019). Signaling Dynamics Control Cell Fate in the Early Drosophila Embryo. *Dev. Cell* *48*, 361-370.e3.
- Jullié, D., Stoeber, M., Sibarita, J.B., Zieger, H.L., Bartol, T.M., Arttamangkul, S., Sejnowski, T.J., Hosy, E., and von Zastrow, M. (2020). A Discrete Presynaptic Vesicle Cycle for Neuromodulator Receptors. *Neuron* *105*, 663-677.e8.
- Karlstrom, R.O., Tyurina, O. V, Kawakami, A., Nishioka, N., Talbot, W.S., Sasaki, H., and Schier, A.F. (2003). Genetic analysis of zebrafish gli1 and gli2 reveals divergent requirements for gli genes in vertebrate development. *Development* *130*, 1549–1564.

- Kawakami, K., Takeda, H., Kawakami, N., Kobayashi, M., Matsuda, N., and Mishina, M. (2004). A transposon-mediated gene trap approach identifies developmentally regulated genes in zebrafish. *Dev. Cell* 7, 133–144.
- Keely, S.L. (1979). Prostaglandin E1 activation of heart cAMP-dependent protein kinase: Apparent dissociation of protein kinase activation from increases in phosphorylase activity and contractile force.
- Kimmel, C.B., Ballard, W.W., Kimmel, S.R., Ullmann, B., and Schilling, T.F. (1995). Stages of embryonic development of the zebrafish. *Dev. Dyn.* 203, 253–310.
- Kong, J.H., Siebold, C., and Rohatgi, R. (2019). Biochemical mechanisms of vertebrate hedgehog signaling. *Development* 146.
- Kopinke, D., Roberson, E.C., and Reiter, J.F. (2017). Ciliary Hedgehog Signaling Restricts Injury-Induced Adipogenesis. *Cell* 170, 340-351.e12.
- Koschinski, A., and Zaccolo, M. Activation of PKA in cell requires higher concentration of cAMP than in vitro: implications for compartmentalization of cAMP signalling.
- Krueger, D., Izquierdo, E., Viswanathan, R., Hartmann, J., Pallares Cartes, C., and De Renzis, S. (2019). Principles and applications of optogenetics in developmental biology. *Development* 146, dev175067.
- Kwan, K.M., Fujimoto, E., Grabher, C., Mangum, B.D., Hardy, M.E., Campbell, D.S., Parant, J.M., Yost, H.J., Kanki, J.P., and Chien, C.-B. (2007). The Tol2kit: A multisite gateway-based construction kit for Tol2 transposon transgenesis constructs. *Dev. Dyn.* 236, 3088–3099.
- Leaf, A., and von Zastrow, M. (2015). Dopamine receptors reveal an essential role of IFT-B, KIF17, and Rab23 in delivering specific receptors to primary cilia. *Elife* 4.
- Li, W., Ohlmeyer, J.T., Lane, M.E., and Kalderon, D. (1995). Function of protein kinase A in hedgehog signal transduction and *Drosophila* imaginal disc development. *Cell* 80, 553–562.

- Lim, Y.S., and Tang, B.L. (2015). A role for Rab23 in the trafficking of Kif17 to the primary cilium. *J. Cell Sci.* 128, 2996–3008.
- Link, V., Shevchenko, A., and Heisenberg, C.P. (2006). Proteomics of early zebrafish embryos. *BMC Dev. Biol.* 6, 1.
- Low, W.-C., Wang, C., Pan, Y., Huang, X.-Y., Chen, J.K., and Wang, B. (2008). The decoupling of Smoothed from Gai proteins has little effect on Gli3 protein processing and Hedgehog-regulated chick neural tube patterning. *Dev. Biol.* 321, 188–196.
- Marley, A., Choy, R.W.-Y., von Zastrow, M., Bonci, A., and Zastrow, M. von (2013). GPR88 Reveals a Discrete Function of Primary Cilia as Selective Insulators of GPCR Cross-Talk. *PLoS One* 8, e70857.
- Marti, E., Bumcrot, D.A., Takada, R., and McMahon, A.P. (1995). Requirement of 19K form of Sonic hedgehog for induction of distinct ventral cell types in CNS explants. *Nature* 375, 322–325.
- Maurice, D.H., Ke, H., Ahmad, F., Wang, Y., Chung, J., and Manganiello, V.C. (2014). Advances in targeting cyclic nucleotide phosphodiesterases. *Nat. Rev. Drug Discov.* 13, 290–314.
- May, E.A., Kalocsay, M., D'Auriac, I.G., Gygi, S.P., Nachury, M. V., and Mick, D.U. (2020). Time-resolved proteomic profiling of the ciliary Hedgehog response reveals that GPR161 and PKA undergo regulated co-exit from cilia. *BioRxiv*.
- McCormick, K., and Baillie, G.S. (2014). Compartmentalisation of second messenger signalling pathways. *Curr. Opin. Genet. Dev.* 27, 20–25.
- McGrath, J., Somlo, S., Makova, S., Tian, X., and Brueckner, M. (2003). Two Populations of Node Monocilia Initiate Left-Right Asymmetry in the Mouse. *Cell* 114, 61–73.
- Méthot, N., and Basler, K. (1999). Hedgehog controls limb development by regulating the activities of distinct transcriptional activator and repressor forms of cubitus interruptus. *Cell* 96, 819–831.

- Mich, J.K., Payumo, A.Y., Rack, P.G., and Chen, J.K. (2014). In Vivo Imaging of Hedgehog Pathway Activation with a Nuclear Fluorescent Reporter. *PLoS One* 9, e103661.
- Mick, D.U., Rodrigues, R.B., Leib, R.D., Adams, C.M., Chien, A.S., Gygi, S.P., and Nachury, M.V. (2015). Proteomics of Primary Cilia by Proximity Labeling. *Dev. Cell* 35, 497–512.
- Moore, B.S., Stepanchick, A.N., Tewson, P.H., Hartle, C.M., Zhang, J., Quinn, A.M., Hughes, T.E., and Mirshahi, T. (2016). Cilia have high cAMP levels that are inhibited by Sonic Hedgehog-regulated calcium dynamics. *Proc. Natl. Acad. Sci. U. S. A.* 201602393.
- Morin-Kensicki, E.M., and Eisen, J.S. (1997). Sclerotome development and peripheral nervous system segmentation in embryonic zebrafish. *Development* 124, 159–167.
- Mukherjee, S., Jansen, V., Jikeli, J.F., Hamzeh, H., Alvarez, L., Dombrowski, M., Balbach, M., Strünker, T., Seifert, R., Kaupp, U.B., et al. (2016). A novel biosensor to study cAMP dynamics in cilia and flagella. *Elife* 5, 5071–5075.
- Mukhopadhyay, S., and Rohatgi, R. (2014). G-protein-coupled receptors, Hedgehog signaling and primary cilia. *Semin. Cell Dev. Biol.* 33, 63–72.
- Mukhopadhyay, S., Wen, X., Ratti, N., Loktev, A., Rangell, L., Scales, S.J., and Jackson, P.K. (2013). The Ciliary G-Protein-Coupled Receptor Gpr161 Negatively Regulates the Sonic Hedgehog Pathway via cAMP Signaling. *Cell* 152, 210–223.
- Mullershausen, F., Zecri, F., Cetin, C., Billich, A., Guerini, D., and Seuwen, K. (2009). Persistent signaling induced by FTY720-phosphate is mediated by internalized S1P1 receptors. *Nat. Chem. Biol.* 5, 428–434.
- Mykytyn, K., and Askwith, C. (2017). G-Protein-Coupled Receptor Signaling in Cilia. *Cold Spring Harb. Perspect. Biol.* 9, a028183.
- Nachury, M. V (2014). How do cilia organize signalling cascades? *Philos. Trans. R. Soc. B Biol. Sci.* 369.
- Nandagopal, N., Santat, L.A., LeBon, L., Sprinzak, D., Bronner, M.E., and Elowitz, M.B. (2018). Dynamic Ligand Discrimination in the Notch Signaling Pathway. *Cell* 172, 869-880.e19.

- Neves, S.R., Ram, P.T., and Iyengar, R. (2002). G protein pathways. *Science* (80-). 296, 1636–1639.
- Neves, S.R., Tsokas, P., Sarkar, A., Grace, E.A., Rangamani, P., Taubenfeld, S.M., Alberini, C.M., Schaff, J.C., Blitzer, R.D., Moraru, I.I., et al. (2008). Cell Shape and Negative Links in Regulatory Motifs Together Control Spatial Information Flow in Signaling Networks. *Cell* 133, 666–680.
- Niewiadowski, P., Zhujiang, A., Youssef, M., and Waschek, J.A. (2013). Interaction of PACAP with Sonic hedgehog reveals complex regulation of the Hedgehog pathway by PKA. *Cell. Signal.* 25, 2222–2230.
- Niewiadowski, P., Kong, J.H., Ahrends, R., Ma, Y., Humke, E.W., Khan, S., Teruel, M.N., Novitch, B.G., and Rohatgi, R. (2014). Gli Protein Activity Is Controlled by Multisite Phosphorylation in Vertebrate Hedgehog Signaling. *Cell Rep.* 6, 168–181.
- Nonaka, S., Tanaka, Y., Okada, Y., Takeda, S., Harada, A., Kanai, Y., Kido, M., and Hirokawa, N. (1998). Randomization of left-right asymmetry due to loss of nodal cilia generating leftward flow of extraembryonic fluid in mice lacking KIF3B motor protein. *Cell* 95, 829–837.
- Norman, R.X., Ko, H.W., Huang, V., Eun, C.M., Abler, L.L., Zhang, Z., Sun, X., and Eggenschwiler, J.T. (2009). Tubby-like protein 3 (TULP3) regulates patterning in the mouse embryo through inhibition of Hedgehog signaling. *Hum. Mol. Genet.* 18, 1740–1754.
- Nusslein-Volhard, C., and Wieschaus, E. (1980). Mutations affecting segment number and polarity in *Drosophila*. *Nature* 287, 787–790.
- Odenthal, J., Van Eeden, F.J.M., Haffter, P., Ingham, P.W., and Nüsslein-Volhard, C. (2000). Two distinct cell populations in the floor plate of the Zebrafish are induced by different pathways. *Dev. Biol.* 219, 350–363.
- Ogden, S.K., Fei, D.L., Schilling, N.S., Ahmed, Y.F., Hwa, J., and Robbins, D.J. (2008). G

- protein Gai functions immediately downstream of Smoothed in Hedgehog signalling. *Nature* 456.
- Ohadi, D., and Rangamani, P. (2019). Geometric Control of Frequency Modulation of cAMP Oscillations due to Calcium in Dendritic Spines. *Biophys. J.* 117, 1981–1994.
- Pal, K., Hwang, S., Somatilaka, B., Badgandi, H., Jackson, P.K., DeFea, K., and Mukhopadhyay, S. (2016). Smoothed determines β -arrestin-mediated removal of the G protein-coupled receptor Gpr161 from the primary cilium. *J. Cell Biol.* 212, 861–875.
- Patel, N., and Gold, M.G. (2015). The genetically encoded tool set for investigating cAMP: More than the sum of its parts. *Front. Pharmacol.* 6, 164.
- Pazour, G.J., Dickert, B.L., Vucica, Y., Seeley, E.S., Rosenbaum, J.L., Witman, G.B., and Cole, D.G. (2000). Chlamydomonas IFT88 and its mouse homologue, polycystic kidney disease gene Tg737, are required for assembly of cilia and flagella. *J. Cell Biol.* 151, 709–718.
- Pazour, G.J., San Agustin, J.T., Follit, J.A., Rosenbaum, J.L., and Witman, G.B. (2002). Polycystin-2 localizes to kidney cilia and the ciliary level is elevated in orpk mice with polycystic kidney disease. *Curr. Biol.* 12, R378–R380.
- Pennekamp, P., Karcher, C., Fischer, A., Schweickert, A., Skryabin, B., Horst, J., Blum, M., and Dworniczak, B. (2002). The ion channel polycystin-2 is required for left-right axis determination in mice. *Curr. Biol.* 12, 938–943.
- Pierce, K.L., Premont, R.T., and Lefkowitz, R.J. (2002). Seven-transmembrane receptors. *Nat. Rev. Mol. Cell Biol.* 3, 639–650.
- Price, M.A., and Kalderon, D. (1999). Regulation of Ci proteolysis by PKA. *Development* 4331–4339.
- Pusapati, G. V., Kong, J.H., Patel, B.B., Gouti, M., Sagner, A., Sircar, R., Luchetti, G., Ingham, P.W., Briscoe, J., and Rohatgi, R. (2018). G protein-coupled receptors control the sensitivity of cells to the morphogen Sonic Hedgehog. *Sci. Signal.* 11, eaao5749.

- Qi, X., Liu, H., Thompson, B., McDonald, J., Zhang, C., and Li, X. (2019). Cryo-EM structure of oxysterol-bound human Smoothed coupled to a heterotrimeric Gi. *Nature*.
- Rall, T.W., and Sutherland, E.W. (1958). Formation of a cyclic adenine ribonucleotide by tissue particles. *J. Biol. Chem.* 232, 1065–1076.
- Regard, J.B., Malhotra, D., Gvozdenovic-Jeremic, J., Josey, M., Chen, M., Weinstein, L.S., Lu, J., Shore, E.M., Kaplan, F.S., and Yang, Y. (2013). Activation of hedgehog signaling by loss of GNAS causes heterotopic ossification. *Nat. Med.* 19, 1505–1512.
- Reiter, J.F., and Leroux, M.R. (2017). Genes and molecular pathways underpinning ciliopathies. *Nat. Rev. Mol. Cell Biol.* 18, 533–547.
- Reiter, J.F., Alexander, J., Rodaway, A., Yelon, D., Patient, R., Holder, N., and Stainier, D.Y.R. (1999). Gata5 is required for the development of the heart and endoderm in zebrafish. *Genes Dev.* 13, 2983–2995.
- Repina, N.A., McClave, T., Bao, X., Kane, R.S., and Schaffer, D. V. (2019). Engineered illumination devices for optogenetic control of cellular signaling dynamics. *BioRxiv*.
- Riobo, N.A., Saucy, B., Dilizio, C., Manning, D.R., and Bourne, H.R. (2006). Activation of heterotrimeric G proteins by Smoothed. *Proc. Natl. Acad. Sci. U. S. A.* 103, 12607–12612.
- Roelink, H., Porter, J.A., Chiang, C., Tanabe, Y., Chang, D.T., Beachy, P.A., and Jessell, T.M. (1995). Floor plate and motor neuron induction by different concentrations of the amino-terminal cleavage product of sonic hedgehog autoproteolysis. *Cell* 81, 445–455.
- Rogers, K.W., and Müller, P. (2020). Optogenetic approaches to investigate spatiotemporal signaling during development. In *Current Topics in Developmental Biology*, (Academic Press Inc.), pp. 37–77.
- Rohatgi, R., Milenkovic, L., and Scott, M.P. (2007). Patched1 Regulates Hedgehog Signaling at the Primary Cilium. *Science (80-.)*. 317, 372–376.
- Rossi, G., and Messina, G. (2014). Comparative myogenesis in teleosts and mammals. *Cell*.

- Mol. Life Sci. 71, 3081–3099.
- Roth, B.L. (2016). DREADDs for Neuroscientists. *Neuron* 89, 683–694.
- Roy, S., Wolff, C., and Ingham, P.W. (2001). The u-boot mutation identifies a Hedgehog-regulated myogenic switch for fiber-type diversification in the zebrafish embryo. *Genes Dev.* 15, 1563–1576.
- Schou, K.B., Pedersen, L.B., Christensen, S.T., Takeda, S., Kadowaki, S., Haga, T., Takaesu, H., Mitaku, S., Mombaerts, P., Marinissen, M., et al. (2015). Ins and outs of GPCR signaling in primary cilia. *EMBO Rep.* 16, 1099–1113.
- Sigg, M.A., Menchen, T., Lee, C., Johnson, J., Jungnickel, M.K., Choksi, S.P., Garcia, G., Busengdal, H., Dougherty, G.W., Pennekamp, P., et al. (2017). Evolutionary Proteomics Uncovers Ancient Associations of Cilia with Signaling Pathways. *Dev. Cell* 43, 744-762.e11.
- Siljee, J.E., Wang, Y., Bernard, A.A., Ersoy, B.A., Zhang, S., Marley, A., Von Zastrow, M., Reiter, J.F., and Vaisse, C. (2018). Subcellular localization of MC4R with ADCY3 at neuronal primary cilia underlies a common pathway for genetic predisposition to obesity. *Nat. Genet.* 50, 180–185.
- Singh, J., Wen, X., and Scales, S.J. (2015). The Orphan G Protein-coupled Receptor Gpr175 (Tpra40) Enhances Hedgehog Signaling by Modulating cAMP Levels. *J. Biol. Chem.* 290, 29663–29675.
- Stierl, M., Stumpf, P., Udvari, D., Gueta, R., Hagedorn, R., Losi t, A., Gä rtner, W., Petereit, L., Efetova, M., Schwarzel, M., et al. (2010). Light Modulation of Cellular cAMP by a Small Bacterial Photoactivated Adenylyl Cyclase, bPAC, of the Soil Bacterium. *Journal* 286, 1181–1188.
- Sungkaworn, T., Jobin, M.L., Burnecki, K., Weron, A., Lohse, M.J., and Calebiro, D. (2017). Single-molecule imaging reveals receptor-G protein interactions at cell surface hot spots. *Nature* 550, 543–547.

- Taylor, S.S., Ilouz, R., Zhang, P., and Kornev, A.P. (2012). Assembly of allosteric macromolecular switches: Lessons from PKA. *Nat. Rev. Mol. Cell Biol.* *13*, 646–658.
- Taylor, S.S., Zhang, P., Steichen, J.M., Keshwani, M.M., and Kornev, A.P. (2013). PKA: Lessons learned after twenty years. *Biochim. Biophys. Acta - Proteins Proteomics* *1834*, 1271–1278.
- Tillo, S.E., Xiong, W.H., Takahashi, M., Miao, S., Andrade, A.L., Fortin, D.A., Yang, G., Qin, M., Smoody, B.F., Stork, P.J.S., et al. (2017). Liberated PKA Catalytic Subunits Associate with the Membrane via Myristoylation to Preferentially Phosphorylate Membrane Substrates. *Cell Rep.* *19*, 617–629.
- Tischer, D., and Weiner, O.D. (2014). Illuminating cell signalling with optogenetic tools. *Nat. Rev. Mol. Cell Biol.* *15*, 551–558.
- Toettcher, J.E., Voigt, C.A., Weiner, O.D., and Lim, W.A. (2011). The promise of optogenetics in cell biology: interrogating molecular circuits in space and time. *Nat. Methods* *8*, 35–38.
- Tolkovsky, A.M., and Levitzki, A. (1978a). Coupling of a Single Adenylate Cyclase to Two Receptors: Adenosine and Catecholamine. *Biochemistry* *17*, 3811–3817.
- Tolkovsky, A.M., and Levitzki, A. (1978b). Mode of Coupling between the β -Adrenergic Receptor and Adenylate Cyclase in Turkey Erythrocytes. *Biochemistry* *17*, 3795–3810.
- Tschaikner, P., Regele, D., Röck, R., Salvenmoser, W., Meyer, D., Bouvier, M., Geley, S., Stefan, E., and Aanstad, P. (2021). Feedback Control of the Gpr161-G α s -PKA axis contributes to basal Hedgehog repression in zebrafish. *Development* *dev.192443*.
- Tsvetanova, N.G., and von Zastrow, M. (2014). Spatial encoding of cyclic AMP signaling specificity by GPCR endocytosis. *Nat. Chem. Biol.* *10*, 1061–1065.
- Tuson, M., He, M., and Anderson, K. V (2011). Protein kinase A acts at the basal body of the primary cilium to prevent Gli2 activation and ventralization of the mouse neural tube. *Development* *138*, 4921–4930.
- Tyurina, O. V., Guner, B., Popova, E., Feng, J., Schier, A.F., Kohtz, J.D., and Karlstrom, R.O.

- (2005). Zebrafish Gli3 functions as both an activator and a repressor in Hedgehog signaling. *Dev. Biol.* 277, 537–556.
- Ungar, A.R., and Moon, R.T. (1996). Inhibition of protein kinase A phenocopies ectopic expression of hedgehog in the CNS of wild-type and cyclops mutant embryos. *Dev. Biol.* 178, 186–191.
- Varjosalo, M., and Taipale, J. (2008). Hedgehog: Functions and mechanisms. *Genes Dev.* 22, 2454–2472.
- Vuolo, L., Herrera, A., Torroba, B., Menendez, A., and Pons, S. (2015). Ciliary adenylyl cyclases control the Hedgehog pathway. *J. Cell Sci.* 128.
- Walker-Gray, R., Stengel, F., and Gold, M.G. (2017). Mechanisms for restraining cAMP-dependent protein kinase revealed by subunit quantitation and cross-linking approaches. *Proc. Natl. Acad. Sci. U. S. A.* 114, 10414–10419.
- Wan, Q., Okashah, N., Inoue, A., Nehme, R., Carpenter, B., Tate, C.G., and Lambert, N.A. (2018). Mini G protein probes for active G protein– coupled receptors (GPCRs) in live cells. *J. Biol. Chem.* 293, 7466–7473.
- Wang, B., Fallon, J.F., and Beachy, P.A. (2000). Hedgehog-Regulated Processing of Gli3 Produces an Anterior/Posterior Repressor Gradient in the Developing Vertebrate Limb. *Cell* 100, 423–434.
- Wang, G., Wang, B., and Jiang, J. (1999). Protein kinase A antagonizes Hedgehog signaling by regulating both the activator and repressor forms of *Cubitus interruptus*. *Genes Dev.* 13, 2828–2837.
- Wen, X., Lai, C.K., Evangelista, M., Hongo, J.-A., de Sauvage, F.J., and Scales, S.J. (2010). Kinetics of Hedgehog-Dependent Full-Length Gli3 Accumulation in Primary Cilia and Subsequent Degradation. *Mol. Cell. Biol.* 30, 1910–1922.
- Wieschaus, E., and Nusslein-Volhard, C. (2016). The Heidelberg Screen for Pattern Mutants of *Drosophila*: A Personal Account. *Annu. Rev. Cell Dev. Biol.* 32, 1–46.

- Williams, C.H., Hempel, J.E., Hao, J., Frist, A.Y., Williams, M.M., Fleming, J.T., Sulikowski, G.A., Cooper, M.K., Chiang, C., and Hong, C.C. (2015). An in vivo chemical genetic screen identifies phosphodiesterase 4 as a pharmacological target for hedgehog signaling inhibition. *Cell Rep.* *11*, 43–50.
- Wolff, C., Roy, S., and Ingham, P.W. (2003). Multiple Muscle Cell Identities Induced by Distinct Levels and Timing of Hedgehog Activity in the Zebrafish Embryo. *Curr. Biol.* *13*, 1169–1181.
- Wong, W., and Scott, J.D. (2004). AKAP signalling complexes: focal points in space and time. *Nat. Rev. Mol. Cell Biol.* *5*, 959–970.
- Xu, P., Huang, S., Zhang, H., Mao, C., Zhou, X.E., Cheng, X., Simon, I.A., Shen, D.-D., Yen, H.-Y., Robinson, C. V., et al. (2021). Structural insights into the lipid and ligand regulation of serotonin receptors. *Nature* 1–5.
- Ye, F., Nager, A.R., and Nachury, M. V (2018). BBSome trains remove activated GPCRs from cilia by enabling passage through the transition zone. *J. Cell Biol.* *217*, 1847–1868.
- Yoshida, S., Shiratori, H., Kuo, I.Y., Kawasumi, A., Shinohara, K., Nonaka, S., Asai, Y., Sasaki, G., Belo, J.A., Sasaki, H., et al. (2012). Cilia at the node of mouse embryos sense fluid flow for left-right determination via Pkd2. *Science* (80-.). *338*, 226–231.
- Yu, D., Baird, M.A., Allen, J.R., Howe, E.S., Klassen, M.P., Reade, A., Makhijani, K., Song, Y., Liu, S., Murthy, Z., et al. (2015). A naturally monomeric infrared fluorescent protein for protein labeling in vivo. *Nat. Methods* *12*, 763–765.
- Yuste, R., Majewska, A., and Holthoff, K. (2000). From form to function: Calcium compartmentalization in dendritic spines. *Nat. Neurosci.* *3*, 653–659.
- Zaccolo, M., and Pozzan, T. (2002). Discrete microdomains with high concentration of cAMP in stimulated rat neonatal cardiac myocytes. *Science* (80-.). *295*, 1711–1715.

Publishing Agreement

It is the policy of the University to encourage open access and broad distribution of all theses, dissertations, and manuscripts. The Graduate Division will facilitate the distribution of UCSF theses, dissertations, and manuscripts to the UCSF Library for open access and distribution. UCSF will make such theses, dissertations, and manuscripts accessible to the public and will take reasonable steps to preserve these works in perpetuity.

I hereby grant the non-exclusive, perpetual right to The Regents of the University of California to reproduce, publicly display, distribute, preserve, and publish copies of my thesis, dissertation, or manuscript in any form or media, now existing or later derived, including access online for teaching, research, and public service purposes.

DocuSigned by:

Truong, Melissa

981FEF8D26D24B9...

Author Signature

4/7/2021

Date